LEVEL

(12)

DEBRIS DISTRIBUTION AS A PARAMETER IN BLAST/FIRE INTERACTION

Final Report

June 1981

Contract EMW-C-0311
FEMA Work Unit 2564G

Approved for public release; distribution unlimited.

SRI International
333 Ravenswood Avenue
Menlo Park, California 94025
(415) 326-6200
Cable: SRI INTL MPK
TWX: 910-373-1246

UNCLASSIFIED

SECURITY CLASSIFICATION OF THIS PAGE (When Data Entered)

REPORT DOCUMENTATION PAGE

READ INSTRUCTIONS BEFORE COMPLETING FORM

1. REPORT NUMBER

2. GOVT ACCESSION NO. AD-A104 669

3. RECIPIENT'S CATALOG NUMBER

4. TITLE (and Subtitle)

Debris Distribution as a Parameter in the Blast/Fire Interaction

5. TYPE OF REPORT & PERIOD COVERED

Final Report
June 1980 – June 1981

6. PERFORMING ORG. REPORT NUMBER

7. AUTHOR(s)

Rempel, John R.
Center for Planning and Research, Inc.
Palo Alto, CA 94303

8. CONTRACT OR GRANT NUMBER(s)

EMW-C-0311

9. PERFORMING ORGANIZATION NAME AND ADDRESS

SRI International
Menlo Park, CA 94025

10. PROGRAM ELEMENT, PROJECT, TASK AREA & WORK UNIT NUMBERS

11. CONTROLLING OFFICE NAME AND ADDRESS

Federal Emergency Management Agency
Washington DC 20472

12. REPORT DATE

June 1981

13. NO. OF PAGES

96

14. MONITORING AGENCY NAME & ADDRESS (if diff. from Controlling Office)

15. SECURITY CLASS. (of this report)

15a. DECLASSIFICATION/DOWNGRADING SCHEDULE

16. DISTRIBUTION STATEMENT (of this report)

17. DISTRIBUTION STATEMENT (of the abstract entered in Block 20, if different from report)

18. SUPPLEMENTARY NOTES

19. KEY WORDS (Continue on reverse side if necessary and identify by block number)

debris
airblast
building collapse
blast/fire interaction

20. ABSTRACT (Continue on reverse side if necessary and identify by block number)

Improvements in the calculation of over-the-ground transport of solid objects by air blast have been made so that the DIAL-PACK results are satisfactorily simulated with constant parameters over the range of incident pressures 15 to 100 psi. These calculations have then been combined with computational techniques for predicting unreinforced masonry wall collapse to derive an outline scenario for blast impact on an actual building at two incident overpressures, 1 and 30 psi.

DD FORM 1 JAN 73 1473

EDITION OF 1 NOV 65 IS OBSOLETE

UNCLASSIFIED

SECURITY CLASSIFICATION OF THIS PAGE (When Data Entered)

DEBRIS DISTRIBUTION AS A PARAMETER IN BLAST/FIRE INTERACTION

Final Report

June 1981

Prepared by:

John R. Rempel
CENTER FOR PLANNING AND RESEARCH, INC.
PALO ALTO, CA 94303

Prepared for:

FEDERAL EMERGENCY MANAGEMENT AGENCY
WASHINGTON, D.C. 20472

The report has been reviewed in the Federal Emergency Management Agency and approved for publication. Approval does not signify that the contents necessarily reflect the views and policies of the Federal Emergency Management Agency.

Contract EMW-C-0311
FEMA Work Unit 2564G

(SRI International Project HSU-1776)

SUMMARY

INTRODUCTION

The present work is an improvement and application of previous calculational methods for describing building wall failure and movement of wall and other debris by airblast. Both wall reactions and hydrodynamic loading are treated by means of lumped parameters. Classical mechanics using springs friction and viscosity is applied to the simulation of ground interactions. Computerized computations of even large building collapse and subsequent movement of debris requires considerably less time than would be needed by a finite element code and a conventional hydrocode.

The computation system is presently composed of two manually interfacing parts: BRACOB (Blast Response and Collapse of Buildings) which calculates loading and response of one story of a building and DEBRIS which calculates displacement and orientation of the fragment of uniform density. BRACOB supplies failure time, orientation and velocity for each fragment, provided the user defines a fragmentation pattern. The blast loading on the building can be calculated by BRACOB following the classical prototype or can be defined arbitrarily by the user. The blast wind in DEBRIS is presently restricted to the classical form.

THE DEBRIS MODEL AND OVER-THE-GROUND TRANSPORT

The use of a double-valued spring to represent the ground reaction on the fragment corner has been extended to both the vertical and horizontal directions. A double-valued spring constant results in the dissipation of energy apparently more effectively than simple Coulomb friction and velocity-proportional viscosity. It was found friction and/or viscosity without horizontally-acting ground springs led to high speed rotation of the fragment which in turn greatly reduced the relative speed over the ground of each corner and thus also reduced the viscous loss. When the frictional or viscous forces were increased still further in an attempt to compensate, bouncing and loss of the contact with the ground occurred. In any case, when only friction and viscous losses are used, the DEBRIS code calculates transport of some of the lightweight concrete cubes that is excessive when compared to observations at the

DIAL PACK event (23 July 1970).* This lack of agreement between simulations and observations occurs at incident peak overpressures of 50 psi and greater. However, reducing the stiffness of the vertical ground spring and adding a double-valued horizontally acting ground spring has made it possible to simulate the total distance transported by 1 kt blasts over the range of incident pressures from 30 to 100 psi, as can be seen in Figure S-1. (In the Figure, K_{g1} and K_{g2} refer to the two values of the spring constant for the vertically acting ground spring and K_{gh1} and K_{gh2} represent values for the horizontally acting ground spring. The values μ and η stand for the Coulomb friction and viscosity, respectively). Moreover, the simulated motion is a tumbling in which the cube never rises more than 1.5 inches above the ground. The height of rise during tumbling is controlled by the value of the vertical ground spring. Increasing the stiffness by a factor of ten can increase the rise by an order of magnitude. The distance transported is also increased substantially.

Figure S-2 shows the gradual braking action of the DIAL PACK simulation containing both the vertical and horizontal ground springs. The two ordinates show horizontal speed and angular speed of the tumbling cube originally placed at the 50 psi contour.

Over the range of incident over pressure 30 to 100 psi drag or dynamic pressure forces in the blast completely dominate diffraction forces in the transport of the DIAL PACK cube. At 15 psi drag is much weaker than at 30 psi and above so that an estimate of momentum gained through shock diffraction must be added to the simulated cube before agreement with observation is obtained.

The quantity Δt, which is identified in Figure S-2, represents the size of the time mesh and has been found to be important although no quantitative relation has been derived, as yet.

The values of the simulation parameters entered into Figure S-1 are close to the optimum for simulation of the transport of the DIAL PACK cube which was initially resting on the ground surface. Other experiments in which objects are dropped from moving trucks at a height of approximately 2.6 feet above the ground can not be simulated with these "optimum" values. In particular, the horizontal spring must be weakened by two orders of magnitude in order to achieve

---

* Concrete cubes weighing 65 lbs. and measuring 1 foot on edge were placed on the ground at various distances from Ground Zero and total distance moved during the explosion recorded. Explosion yield was approximately 500 tons of TNT.

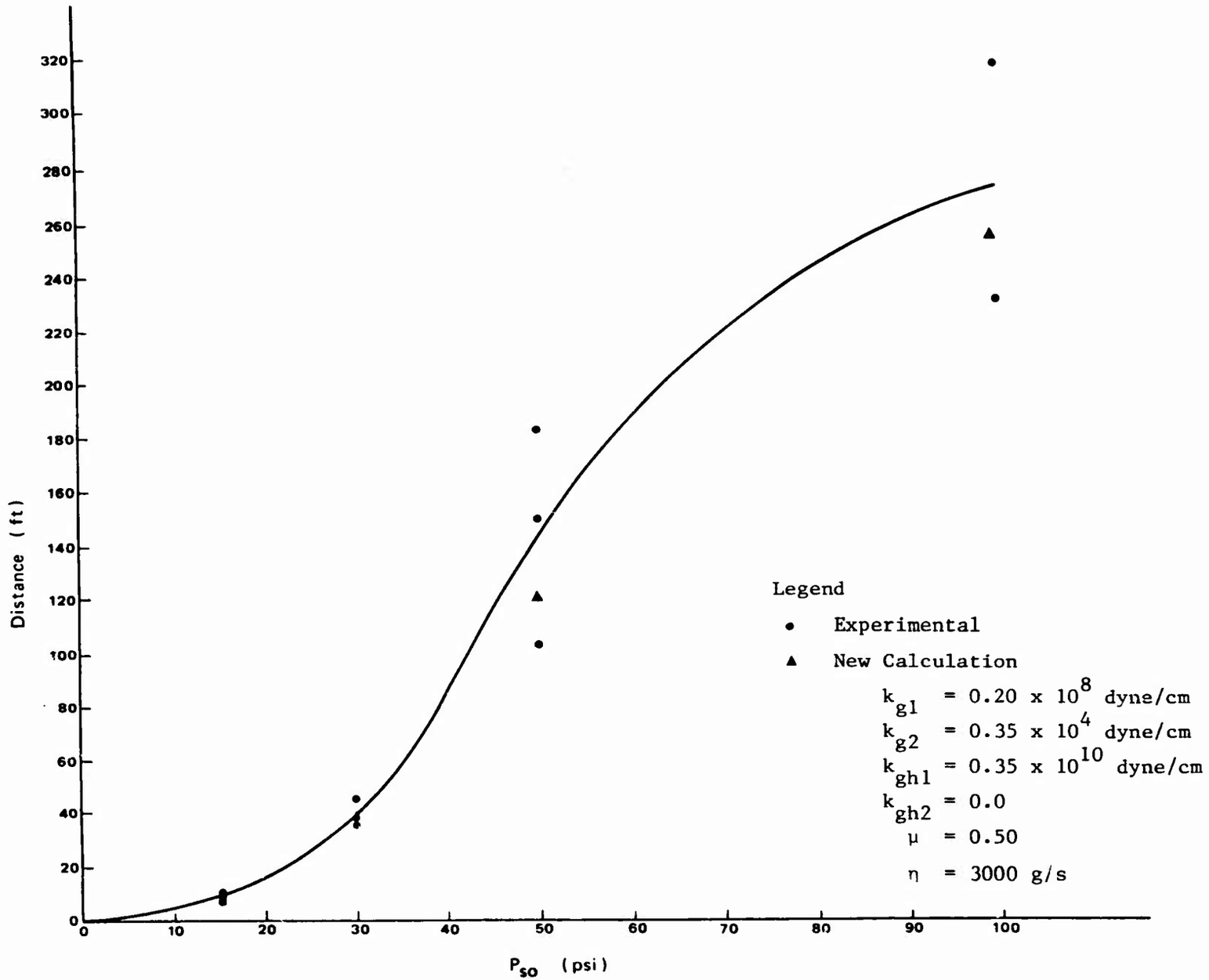

Figure S-1. Simulated and Observed Translation of Concrete at DIAL PACK.

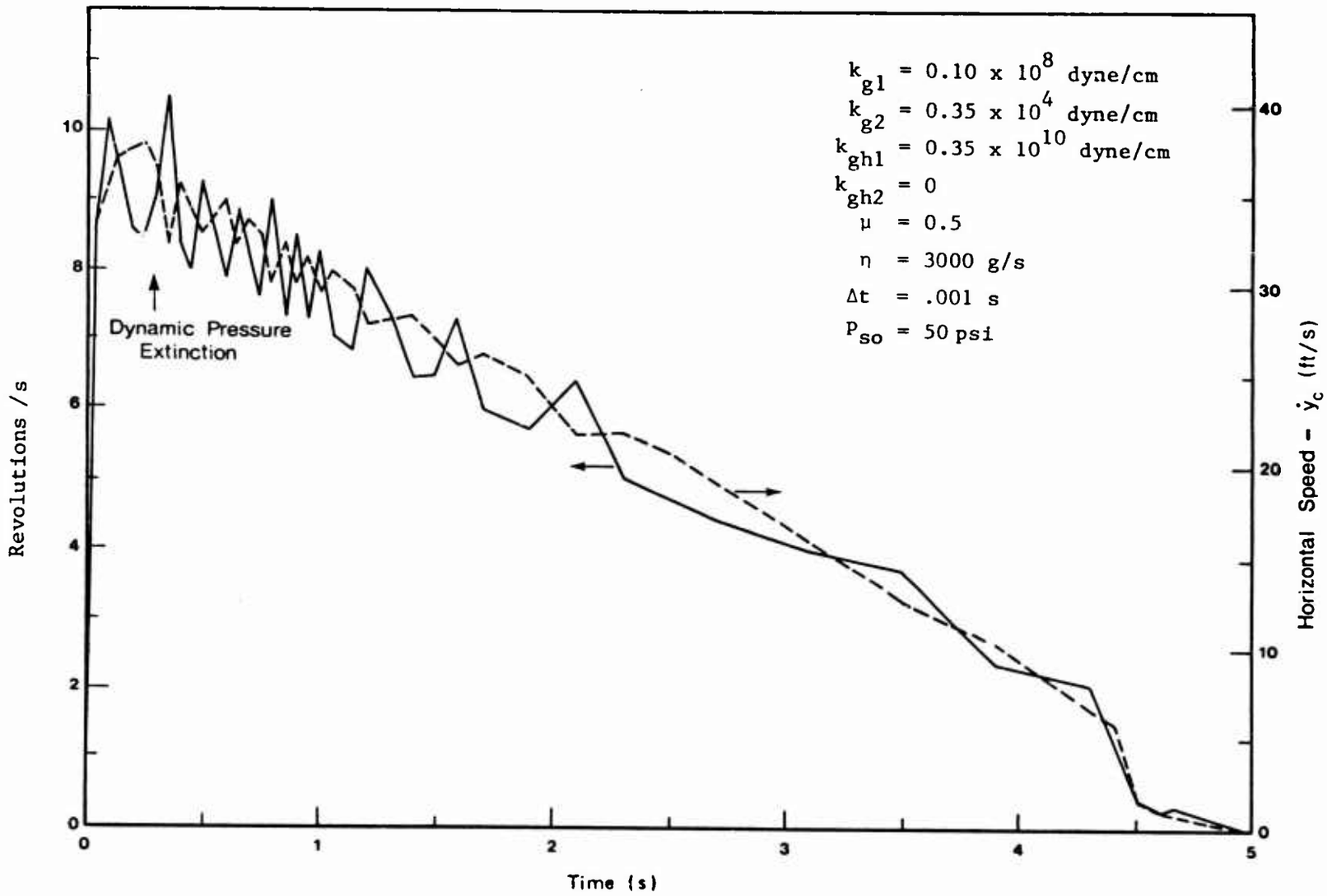

Figure S-2. Braking of Concrete Cube at DIAL PACK.

realistic simulations of distances transported in these experiments from moving trucks. When this change is made however, some of the observations can be simulated, specifically, the distance travelled by the dropped object is independent of object density and is within one standard error of estimate of observed values. Whether or not the need to change the value of the horizontal spring is related to the differences in the surfaces over which the two kinds of experiments were conducted is not known. The photographs from DIAL PACK show a rough surface covered with tufts of grass while the experiments from moving trucks were conducted over a "graded airstrip built on an alluvial plain".

Using the optimum parameter values, as described above, distance the simulated DIAL PACK cubes are transported almost scales with the cube root of yield.

COLLAPSE OF THE LANDIS HOSPITAL

The exterior walls of the Henry R. Landis State Hospital, Philadelphia, one of the buildings in the National Shelter Survey, consist of two tiers of masonry each capable of arching in a nearly rigid frame. A cross sectional view appears in Figure S-3. The outer tier of clay brick arches (one-way) between steel supports; the inner tier of concrete masonry units arches (two-way) in a reinforced concrete frame. In the analysis both frames are treated as rigid. The two tiers respond to air blast in parallel but because of the extreme thinness of each tier the incipient collapse overpressure of the exterior walls in less than 1 psi.* The differences between the simulated behaviors under 1 and 30 psi blast waves are entirely in the debris histories.

Peak Free-Field Overpressure = 1 psi

Interior wall behavior has a small but measureable effect on exterior wall response. Under 1 psi blast wave loading the pressure of interior partitions may delay failure of the front exterior walls by as much as 10 ms and may reduce the departure speed of the fragments from approximately 11 to 6 fps. Figure S-4 is the floor plan that was analyzed in this study. The two coordinates (marked I and J in the Figure) locate corners and openings for the computer calculation. It is estimated that the front or south elevation will fail under 1 psi blast 50 to 60 ms after blast arrival and initial center of mass fragment speed will be in the range 6.2 to 7.8 fps. All interior east-west walls will be breached almost upon blast arrival, except the walls at grid line I = 11, where the build-up of pressure against the surface facing the origin of the blast must await filling of a large volume. However pressure buildups on the opposite (north) face is also slow because the windows in the north elevation of the building lie in the wake of the blast. It is estimated the interior partition line at I = 11 fails sometime between 50 and 70 ms after blast arrival. This failure is the prelude to outward failure of the north exterior walls at 170 ms with a departure speed of approximately 3.4 fps. At this point the blast from a 1 Mt weapon still has several seconds of life left and further downwind trans-

* Collapse overpressure is stated in terms of peak free-field overpressure in a classical blast wave oriented head-on to one facade of the building.

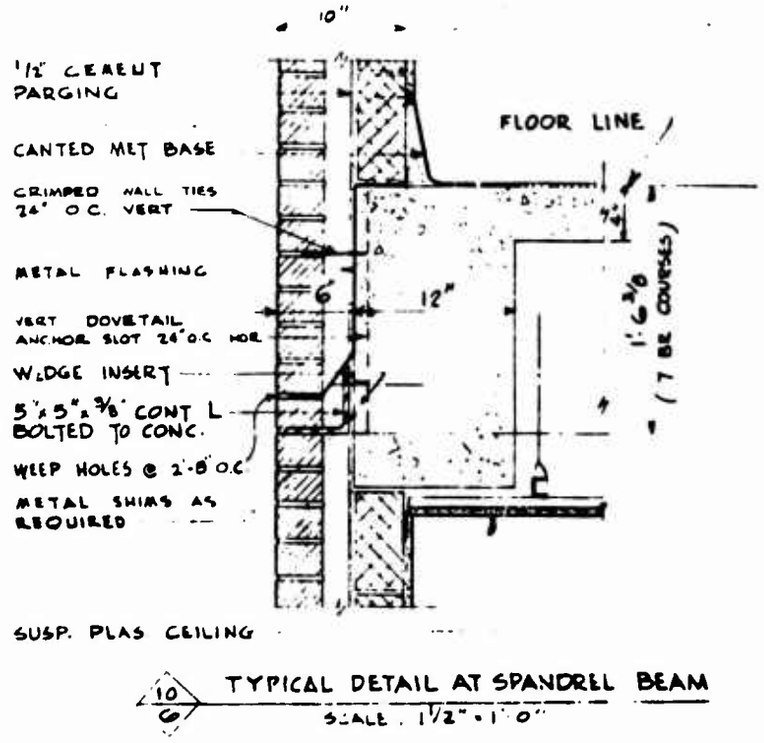

Figure S-3. Outside Wall Detail, Landis Hospital.

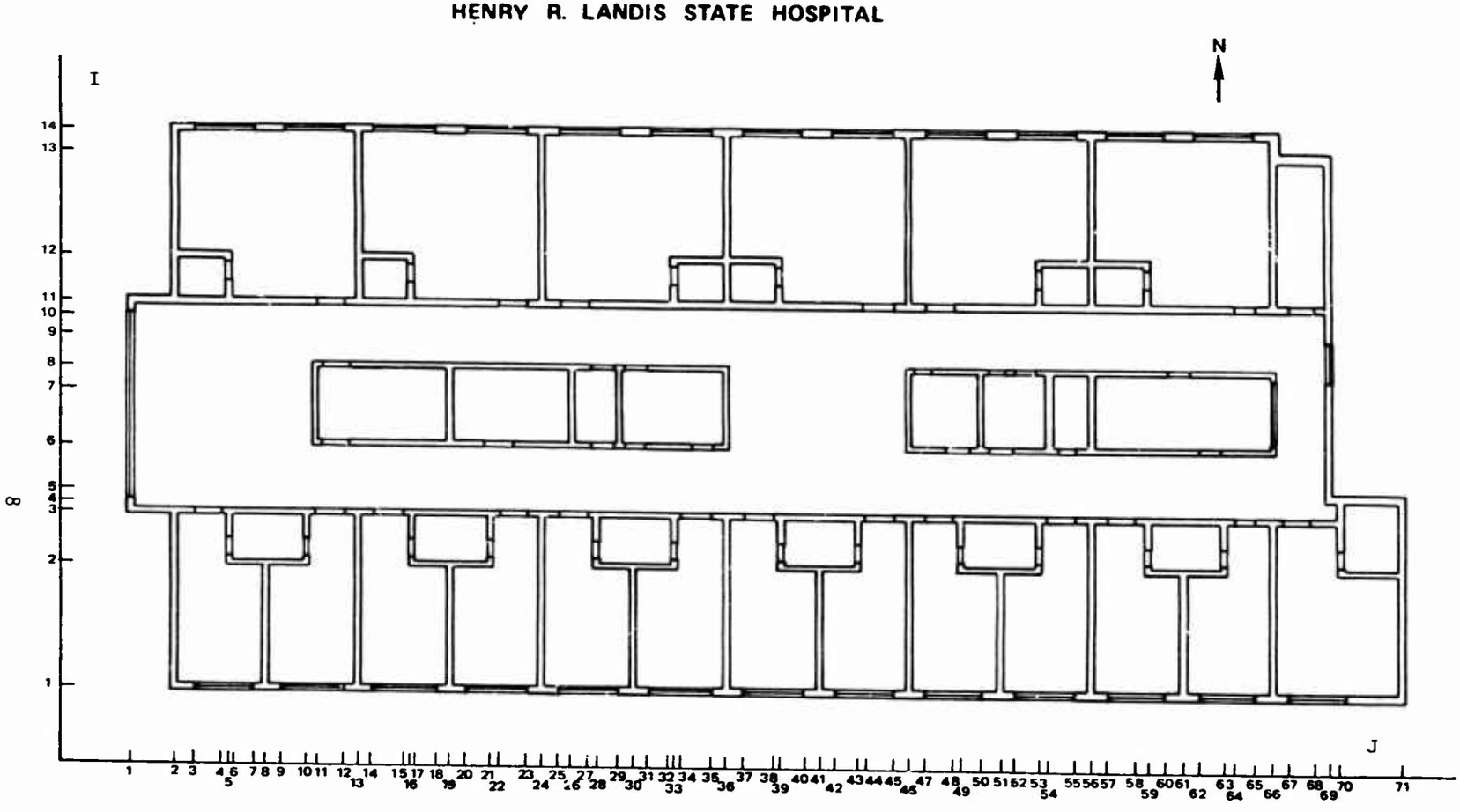

Figure S-4. Simplified Floor Plan, Landis Hospital.

port of debris occurs.

At 1 psi failure of the side (east and west) walls is marginal and results of calculations depend critically on assumptions of behavior of interior partitions. Most probably sidewalls fail inwardly at very low speeds.

Peak Free-Field Overpressure = 30 psi

Under 30 psi blast loading the south exterior walls fail at approximately 6 ms with departure speeds in the neighborhood of 110 fps. Simple room-filling through the south windows quickly breaches the east-west interior partitions in the front tier of rooms and the prompt failure of the south exterior walls insures the presence of loading in excess of 10 psi on the south face of interior partition line I = 11 well before 40 ms when the loading of the north exterior facade begins. Blast filling through the north windows then has no chance of delaying failure of the interior wall line at I = 11. Consequently the north exterior walls fail outward at approximately 62 ms with departure speeds of about 8 fps.

Side walls at 30 psi will most likely fail inward. For example, southernmost sidewalls fail at 23 and 17 ms with speeds of 27 and 40 fps, respectively. Due to the flexure of these walls, however, much of their debris will be deposited outside the building.

FRAGMENT DISTRIBUTION, LANDIS HOSPITAL

Even using loss parameters found to be appropriate for a smooth hard surface the further translation of collapsed wall fragments by the 1 psi blast wind does not appear significant. Fragments from the south exterior wall would appear to be distributed over the floor in an area reaching from 2 to 9 ft. inside the initial wall line. Height of bounce is never more than a few inches, a circumstance related to the relatively slow rotation of the fragments upon their departure from the wall. Fragments from the north exterior wall move even less from their points of impact than does the south wall debris, but since these fragments descend from positions in a six story wall to the ground, the total horizontal transport ranges from 3 to 15 ft.

The fragment disposition at 30 psi is dramatically different. The first fragments from the south wall reach the floor approximately 41 ms after blast arrival at a distance of 3 ft. from the wall line. Assuming these fragments remain intact, they then bounce to a height of approximately 2.5 ft.

above the floor and travel 72 ft. downstream. Such behavior places south wall debris at the north exterior wall line at 370 ms. During this transport collision with interior wall debris will be highly unlikely since such light material as is found in the interior partitions will surely be swept ahead of the masonry material.

After their first impact with the concrete floor north wall fragments may be further fragmented. Treating this debris as individual masonry units moving initially with the speed of the center of fragment mass the horizontal transport is essentially the same as described in the preceding paragraph except the motion is a tumbling. Under this assumption south wall debris reaches the north facade at 340 ms, long after the north wall fragments have departed.

Despite their high initial speed and early departure, the south wall fragments will not necessarily overtake the fragments from the north wall. Trajectories differ markedly. By 170 ms a near classical blast wave is blowing through the building. The rapidly rotating south wall fragments are moved upward or sidewise relatively little. Rear wall fragments, on the other hand, keep for a much longer time an orientation that permits lofting of top wall fragments or side motion in side fragments. The consequence is a far longer trajectory in rear wall than in front wall fragments, as is illustrated in Figure S-5. The small arrows in the Figure show the attitudes of the fragments. In neither case do the fragments travel far over the ground. Fragments from the first (ground) floor of the south wall strike the ground in the wake of the building while blast winds are still blowing, yet travel only 55 ft. after touching down. Comparable fragments from the sixth floor move only 10 ft. after striking the ground.

CONCLUSIONS AND RECOMMENDATIONS

The techniques developed and elucidated in this research are certainly capable of describing gross features of debris distribution from some collapsing building walls; e.g., in the Landis Hospital the dramatic differences between the effects of 1 and 30 psi blast waves, the relative timing of collapse events and debris movements. But some finer points await improvement in the tools themselves; e.g., the conditions for removal of interior partitions must be made more precise and incorporated into the automatic calculations, data to

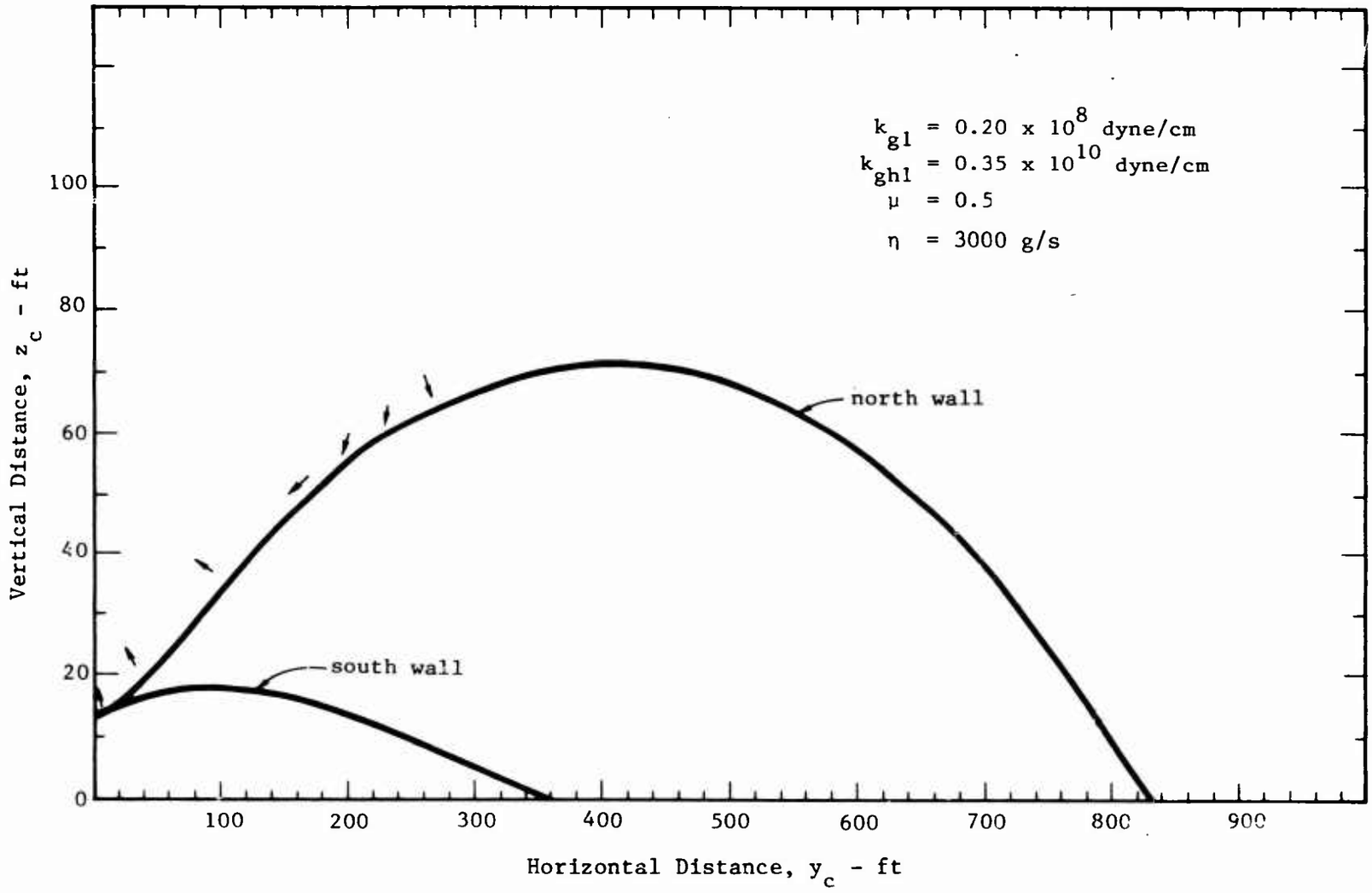

Figure S-5. Lofting of Ground Floor Top Wall Fragments, Landis Hospital, p_{so} = 30 psi.

describe debris transport over a concrete surface must be found before full confidence can be placed in some of the present calculations, and finally it must be pointed out that the case treated in this research, i.e., a weak walled building with a relatively strong frame presents a relatively simple debris distribution problem. Weak frame buildings, tilt-up structures, and certain massive structures supported by load-bearing masonry walls contain complications that may perturb the debris distribution described here.

SRI International

DEBRIS DISTRIBUTION AS A PARAMETER IN BLAST/FIRE INTERACTION

Final Report

June 1981

Prepared by:

John R. Rempel
CENTER FOR PLANNING AND RESEARCH, INC.
PALO ALTO, CA 94303

Prepared for:

FEDERAL EMERGENCY MANAGEMENT AGENCY
WASHINGTON, D.C. 20472

The report has been reviewed in the Federal Emergency Management Agency and approved for publication. Approval does not signify that the contents necessarily reflect the views and policies of the Federal Emergency Management Agency.

Contract EMW-C-0311
FEMA Work Unit 2564G

(SRI International Project HSU-1776)

SRI International®

TABLE OF CONTENTS

ACKNOWLEDGMENTS

The author, a physicist, is indebted to Carl K. Wiehle and James E. Beck for his knowledge of structural engineering, without whose contributions the parts of this study dealing with the conversion of structures to debris would not have been possible. In particular, the author acknowledges the use of computer codes prepared by James Beck in the analysis of the walls of the Henry R. Landis Hospital.

Any errors in the applications of the codes or of structural analysis appearing in this report are, however, solely the responsibility of the author.

ILLUSTRATIONS

TABLES

DEBRIS DISTRIBUTION AS A PARAMETER IN BLAST/FIRE INTERACTION

PART I

INTRODUCTION

Previous civil-defense-inspired work contains estimations of the quantity and distribution of structural debris stemming from the effects of air blast on buildings.[1,2,3,4,5] The estimates were apparently made to determine accessibility and the need for debris clearance. The present research, done in support of studies on the blast/fire interaction, has been designed to provide more detailed descriptions of temporal and spatial debris configurations than have previous civil-defense studies. Previously, rather detailed efforts have determined debris trajectories in connection with U.S. missile defense.[6,7,8] Some of the missile defense work has been most useful to the present research, other parts that deal with small, unrealistically constructed models have not been used.

The present effort by no means provides all the answers required to completely understand the effects of debris on the interaction of blast and fire. The focus is on wall debris, excluding room contents such as furniture. The emphasis is on exterior walls. Other facets of the blast/fire problem are important and can be examined.

The method adopted here is based on two simulation models embodied in the computer codes BRACOB and DEBRIS. BRACOB is a system of codes that compute the simultaneous response of all the walls on one floor of a building. At each step, it determines the net loading on each wall, finds the motion of the wall, and adjusts the loading when wall failures change the geometry of the building. The initial loading may arise in a classical blast wave or in an arbitrarily defined pulse, such as is used in taking into account the blast interference by other buildings.

DEBRIS determines trajectories of single fragments through the air or along the ground in response to classical blast waves. Not treated

in DEBRIS is the impact of one fragment on another and the effects of fragment breakup. Although BRACOB supplies time of wall failure* as well as wall speed and displacement at the moment of failure, the pattern of wall fragmentation must be defined by the system user. Fortunately, a substantial body of observation exists--particularly from atmospheric nuclear weapons tests[9] and from tunnel blasts[10,11,12]--to help define crack patterns.

The single-degree-of-freedom engineering analysis of wall response used in BRACOB is from Wiehle and Bockholt[13,14] and has been applied successfully to civil defense problems.[15,16,17,18,19] The computer simulation, DEBRIS, is drawn from engineering methods of aerodynamics and from classical mechanics.[20] One of the goals of the present research was the continued calibration of the model against the limited data available.

This report falls into two parts: (1) an exposition of further improvements in the computational simulations and (2) simulations of collapse and debris transport within an actual building.

OVER-THE-GROUND TRANSPORT

Any simulation of debris distribution by megaton nuclear blast must accurately estimate the interaction of a moving fragment with the ground or other large surfaces. Except in buildings over three stories in height, wall debris will reach the ground relatively early in the positive dynamic pressure phase. Even in much taller buildings, wall debris will reach the ground with a very high horizontal velocity component. How the ground brakes the blast-driven fragment is crucial to determining the spread of fragments.

Previous Work

Fortunately, observations of blast-driven objects exist. At operation DIAL PACK in July 1970, several (light-weight) concrete-filled plywood cubes were placed on the ground at various ranges from ground zero

*"Failure" is defined as the moment when the component ceases to fulfill its structural function, e.g., support a vertical load. "Collapse" will be used to mean the less well defined point at which the component no longer obstructs air flow.

and driven downrange by the blast from the detonation of approximately 500 tons of high explosive placed on the surface. A postshot photograph of these cubes is reproduced in Figure 1. Incident peak overpressures at the cubes varied from 15 to 100 psi (103 to 689 kPa). The cubes were one foot on an edge[21] and only their displacements by the blast were reported; no information on trajectories has been found, but distances travelled, weights of cubes, and initial peak overpressures are shown in Table 1.[8]

Fletcher and Bowen[22,23] have shown experimentally that the distance required to brake stones and concrete blocks to a stop depends only on the initial speed. In these tests, the objects were thrown out of a moving truck at a height of approximately 2.6 ft above a graded airstrip built on an alluvial plain; results for stones and concrete masonry blocks were reported in two recursion relations:

$$\log_{10} s = -1.4664 + 1.9004 \log_{10} V$$

$$\log_{10} t = -1.1420 + 0.9004 \log_{10} V$$

where s = distance (ft) from point of release to rest position, t = time (s) from time of release to stopping time, and V = horizontal speed (ft/s) of truck at moment of release. These regression relations are nearly equivalent mathematically to the existence of a constant force, F, proportional to the mass, m, and to a fractional power of the initial speed, V:

$$F = 14.63\ V^{.0996}\ m$$

acting through the duration of the motion of the object. The stones weighed from 1.3 to 116 lb; the masonry blocks were both hollow (25 to 32.5 lb) and concrete-filled (55 to 56.5 lb). Standard error in the estimate is $\pm$41.2 percent. The attitude of the object when dropped was randomly varied, and, no doubt, this randomness contributed to the large error of estimate.

Figure 1. Tumbled Block at DIAL PACK

Table 1. Weight and Transport of Tumbling Blocks (from Ref. 8).

Tumbling Block Number	Tumbling Block Initial Overpressure Position (psi)	Actual Weight (Pounds)	Approximate Radial Transport Distance (ft)	
1	15	64.5	6.7	
2	15	65.5	7.3	mean 7.5
3	15	64.0	8.5	
4	30	63.0	36	
5	30	64.0	39	mean 39.3
6	30	61.0	43	
7	50	63.5	103	
8	50	63.5	150	mean 146.0
9	50	61.5	184	
10	100	Destroyed		
11	100	63.5	230	mean 273.0
12	100	61.5	317	

Using aeronautical engineering measurements of wind drag and modeling ground forces by double-valued, vertically acting springs and coulomb friction, the computer code DEBRIS has successfully simulated the data in Table 1 over partial pressure ranges in previous work.[20] A major task of the present effort was to devise satisfactory simulations for the whole range of data stemming from the tumbling cubes. Techniques that produce excellent results at low incident overpressures fail at higher pressures. Because trajectory or displacement versus time information has not been available, we do not know whether the shortcomings of the previous model lie in the acceleration or deceleration phases of the transport. However, while wind drag is a subject for which a great deal of literature exists, relative paucity characterizes the engineering literature of tumbling deceleration. The next section contains the results of the research to find an engineering simulation of ground-fragment interaction.

Improvements in the Model DEBRIS

With a friction force opposing horizontal motion and a two-valued spring exerting vertical ground resistance, simulated air-blast transport of concrete objects generally agrees with observations at peak free-field overpressures of 15 psi and below. The simulated observations were those of the tumbling blocks at 15 psi at DIAL PACK[8] and the collapse of a concrete masonry building situated at the 9-psi contour at PRAIRIE FLAT.[7] The frictional force, F, is proportional to a coefficient of friction, μ, and the force between the object and the ground, i.e.,

$$F_f = \mu F_z$$

where z is the coordinate in the direction perpendicular to the ground and F_z is the force in the ground reaction spring. Force, F_f, is exerted in the opposite direction to the horizontal motion. As the corner of the object moves below the ground surface under the influence of gravity,*

*If the ground and fragment surface were in intimate contact, air blast static pressure would furnish a second downwind force against the vertical spring. However, a real ground surface will probably admit static air blast pressure underneath the fragment. In this case, the net downward air blast pressure is zero.

the ground reaction spring exerts an upward force:

$$F_z = -k_{g1} z, \qquad \text{when } \dot{z} \leq 0 \quad .$$

When the corner is still below the surface but moving upward,

$$F_z = -k_{g2} z$$

so that, if Δz is the maximum downward penetration, the energy loss in a single impact is

$$\Delta E = \frac{1}{2}(k_{g1} - k_{g2})\Delta z^2 \quad .$$

Handbook values of coefficient of friction vary from 0.02 to 4.0, but the majority of values lie in the range 0 to 0.5.[24] None of the materials listed in the handbook resemble masonry on soil in gross physical properties. In simulations of the DIAL PACK tumbling cube, a value of $\mu = 0.4$ predicts nearly the reported transport at 15 psi, but at 50 and 100 psi, the simulated transport distances greatly exceed those observed. From Table 2, increasing the coefficient of friction to 0.5 improves the simulation at the high original overpressures, but results in less than observed transport at low pressures. Furthermore, when $\mu = 0.5$ and when original pressure is 100 psi, the transport is far larger than observed; in fact, at $P_{so} = 100$ psi, the coefficient of friction should be in the neighborhood of 0.75, if reproduction of observed transport is to be achieved.

There is another unrealistic feature of the motion simulated by means of coulomb friction with coefficients in the range 0 to 1. In Figure 2, the angle of tilt of the cube during simulated transport from an initial position at $P_{so} = 100$ psi is plotted as a function of downrange distance, y. The simulated cube never loses contact with the surface over which it moves and never tilts significantly. Such movement can hardly be described as "tumbling." Even from the photograph in Figure 1, it is

Table 2. Total Simulated Displacement y_{max}(ft) of Concrete Cube at DIAL PACK, (friction only).

$k_{g1} = 0.35 \times 10^{9}$ dyne/cm
$k_{g2} = 0.35 \times 10^{5}$ dyne/cm
$\Delta t = .01$ s

p_{so} (psi) \ μ	0.4	0.5	0.75	0.90	1.0	1.2	1.4
15.0	7.54	5.94					
30.0			30.93		△ 28.5*	△ 25.2*	41.2*
50.0	171.0	139.0		79.4			
100.0		503.0		312.			> 524.0+

* Tumbles

△ Initial speed = 4.8 ft/s

\+ Cube still moving at end of calculation

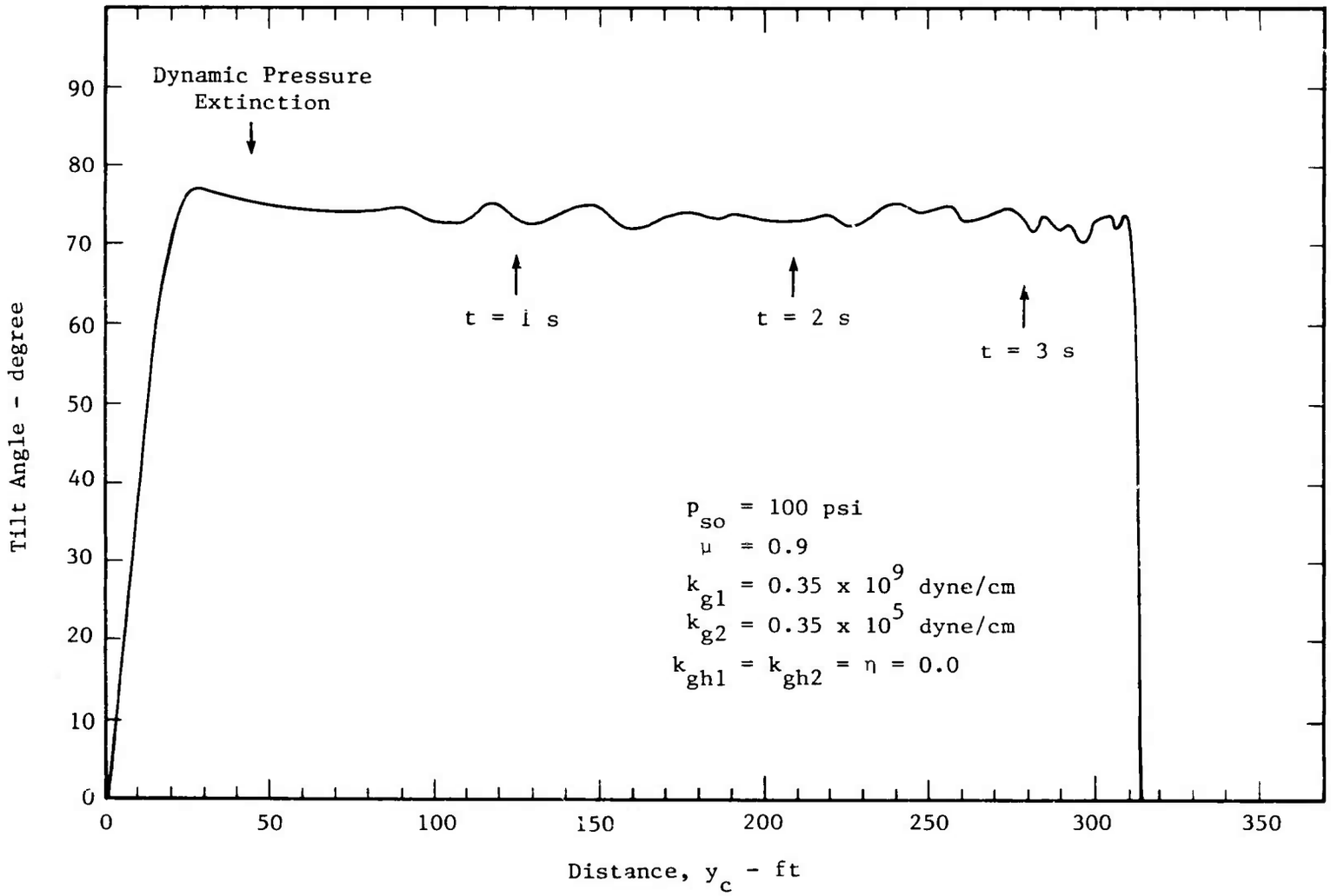

Figure 2. Angle of Tilt of Concrete Cube at DIAL PACK (friction only).

apparent there could have been no purely sliding motion of the concrete cubes over the ground at DIAL PACK.

Simulated tumbling can be achieved by increasing the value of μ. The high frictional force on the bottom of the initially sliding cube causes it to rotate, followed by compression of the ground spring and ending with upward motion of the cube and loss of contact between ground and cube. The subsequent bouncing motion is capable of permitting a much greater transport distance than is achieved by a purely sliding contact. Under these circumstances, the downrange distance moved depends on the value of the vertical spring constant, which will be evident later. Even setting the restoring spring constant, k_{g2}, equal to zero does not prevent upward motion because rotation may cause the corners of the cube to move into the ground at the same time the center of mass is moving upward, and the "braking" spring, k_{g1} may contribute to upward acceleration. Some results of high value for the coefficient of friction are shown in Table 2 for an initial location at the 30 psi contour. The asterisk in the table indicates that the corresponding motion includes airborne segments or tumbling. Thus, increasing μ from 1.0 to 1.2 shortens the distance transported, but increasing μ still further allows for greater transport than when μ is small. Some other characteristics of the motion of this simulation at p_{so} = 30 psi are represented in Figures 3 and 4, i.e., height of center of mass above ground and angle of tilt, both as functions of the downrange distance transported. Although the total transport in the case of μ = 1.4 and p_{so} = 30 psi appears nearly correct, the same value of μ in the case of p_{so} = 100 psi yields a distance transported that is much larger than observed. Hence, even though tumbling motion may be simulated with friction only, the coefficient of friction must still be varied with incident overpressure.

Viscosity. A viscous force, i.e., resistance proportional to speed or some power of speed, seems to provide braking that increases with peak overpressure. It is easy to estimate a value of a coefficient of viscosity, η.

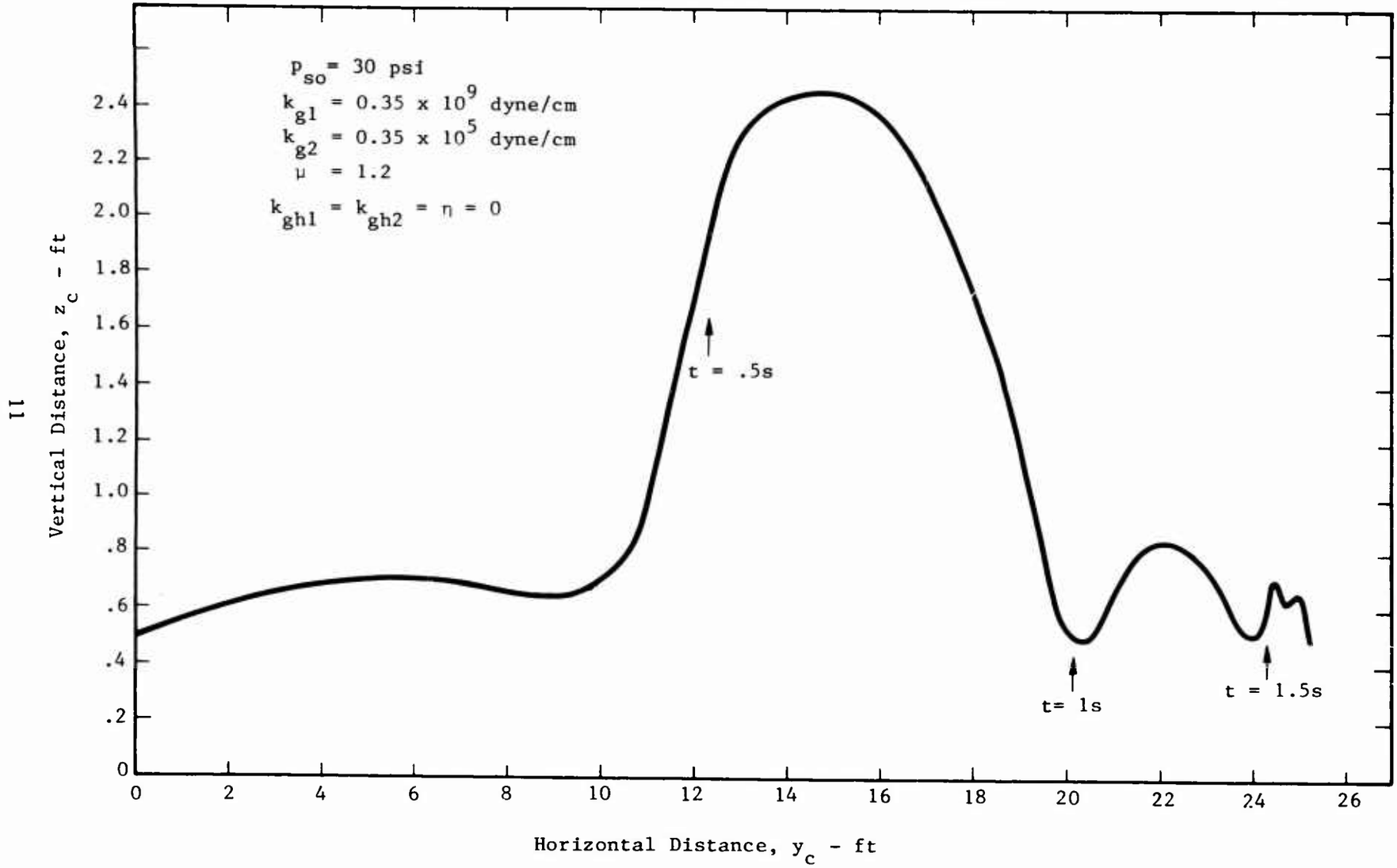

Figure 3. Simulated Trajectory of Center of Mass of Concrete Cube at DIAL PACK (friction only).

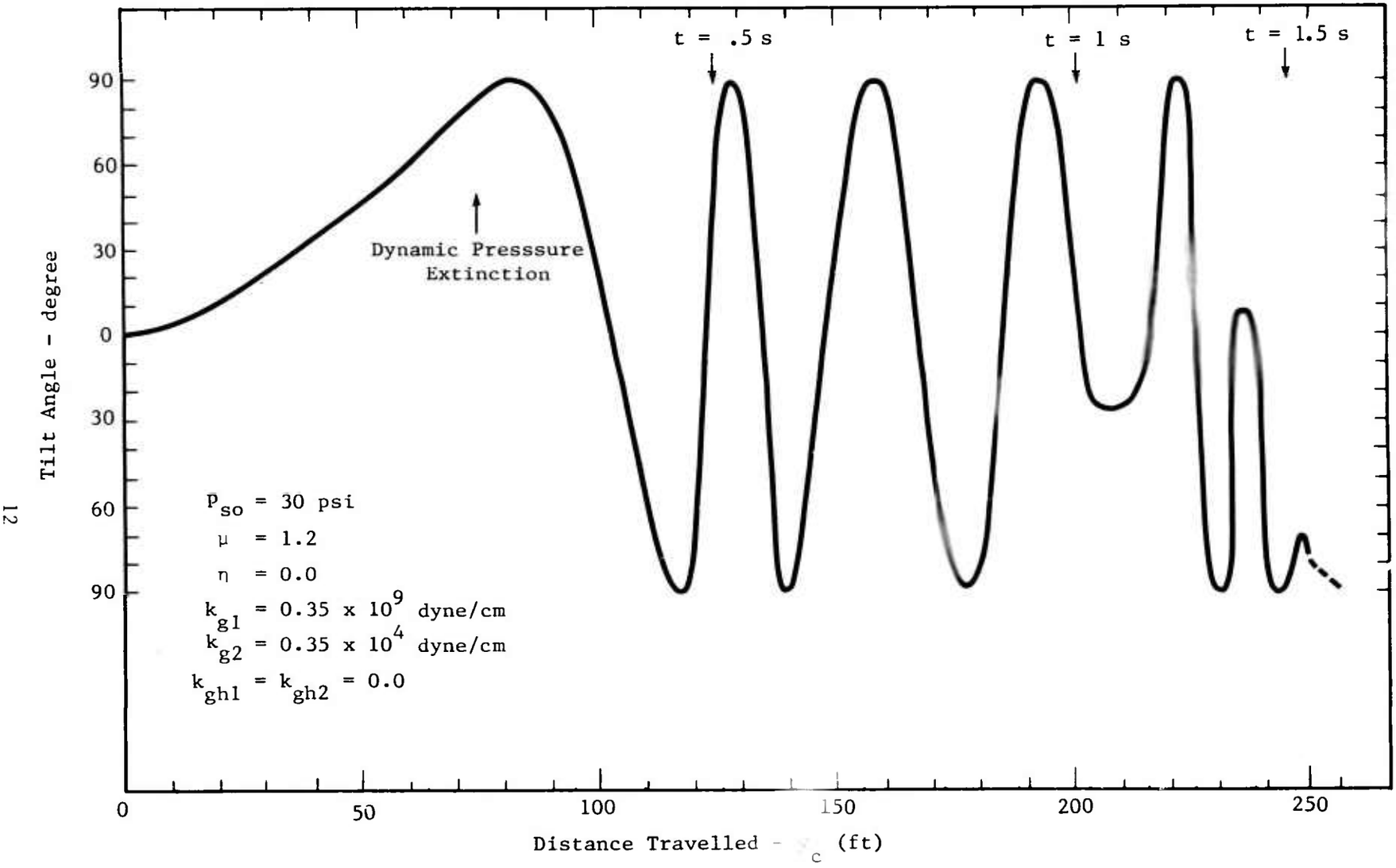

Figure 4. Simulated Rotation of Concrete Cube at DIAL PACK (friction only).

$$F = \eta \dot{y}$$

where F is the force resisting horizontal motion and $\dot{y}$ is the time derivative of the horizontal component of the object's motion.

A zeroth order numerical approximation to η can be found by treating the viscous effect as a correction:

$$y_c = \int \dot{y}_o \, dt + \int \int a \, dt \, dt - \frac{\eta}{M} \int \int \ddot{y} \, dt \, dt$$

in which y_c represents the observed displacement of the center of mass, acceleration, a, is calculated from wind and friction forces only, $\dot{y}_o$ is intial fragment speed (if any), and M = cube mass. At DIAL PACK $\dot{y}_o$ = 0, mass M = 65 lb and the second term on the right can be estimated from Table 2. The equation can be solved as follows:

$$\eta = \frac{y \text{ (calculated)} - y \text{ (observed)}}{\int y dt} \times M \quad .$$

Table 2 shows for overpressure of 100 psi that the calculated value of y is 503 ft when $\mu = 0.5$ and no viscosity is used. The difference, therefore, between calculated and observed distances on the right side of the equation above is estimated to be 230 ft; and the duration of simulated motion is the integral representing the area under the calculated displacement curve is approximately 1901 ft-s. Because the mass of the cube is reportedly 65 lbs, the first estimate of η becomes 7.86 lbs/s or 3567 g/s.

When the displacement history is recalculated using η = 3000 g/s, the plot of the trajectory in a plane perpendicular to the ground (i.e., in the y-z plane) is presented in Figure 5. Total displacement is overly large, but the reason is clear from the illustration: the cube bounces so much that it is seldom in contact with the ground where the viscous and frictional forces operate.

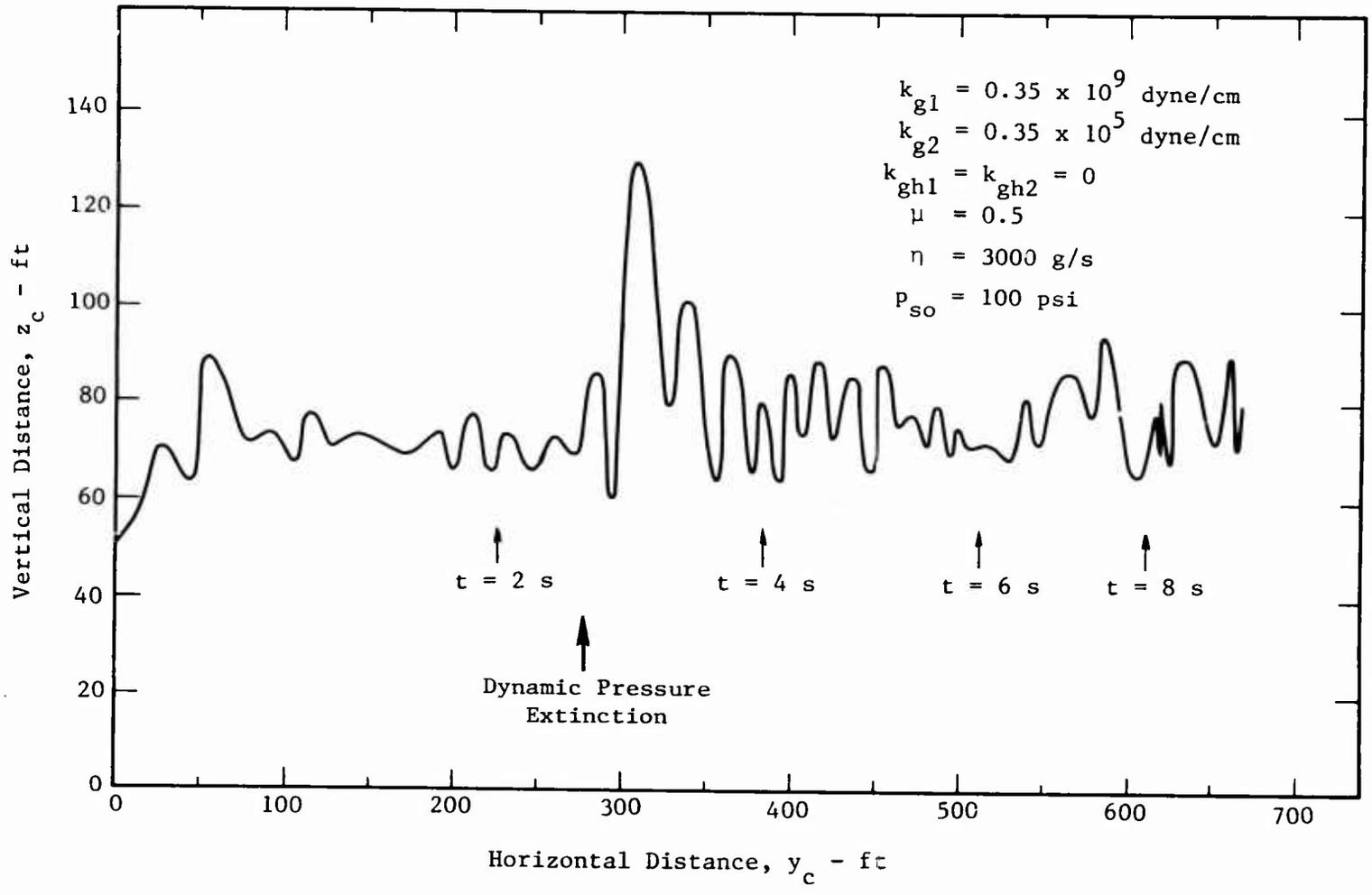

Figure 5. Simulated Trajectory of Concrete Cube at DIAL PACK (friction only).

Another revealing feature of the simulation with η = 3000 g/s is demonstrated in Figure 6, a plot of tilt angle against downrange distance, y_c. Clearly, the cube is spinning at a high rate (~18 rps). In fact, detailed examination of the computer output shows that the over-the-ground speed of the lower corners is much less than the downrange speed of the center of mass. Inclusion of the viscous force appears to be self-defeating: the net result has been to reduce the braking force.

The general validity of this observation may be verified by computing a trajectory without permitting a torque about the internal α-axis. Figure 7 is two such displacement histories corresponding to two different values of viscosity for an original location on the 100-psi contour. (Originally the internal α-axis coincides with the external x-axis; the blast direction is in the positive y-direction, so that rotation caused by contact with the ground is about the α-axis.[20]) Clearly, the successive approximations outlined above will converge on a successful value of η as long as no torque caused by ground forces are allowed. Such a restriction is unrealistic.

Although it is meaningless to continue the series of successive approximation using the results of the simulation with η = 3000 g/s, trial and error using several values of η, but without the restriction on torque, produce the results tabulated in Table 3. In all these cases coefficients of friction, μ, is 0.5, but three different values of η are represented. With two exceptions, all simulated motions slide, including usually slight rocking back and forth, as illustrated by a plot of tilt versus ground range in Figure 8. When P_{so} = 100 psi and η = 1500 g/s, transport is not by sliding; rather the simulated cube bounces. The height of the center of mass is drawn in Figure 9 as a function of ground range. In this case, as well as the case shown in Figure 5, the cube is spinning (reaching a maximum rate of approximately 3 rps), but the rate of spin of the cube represented by Figure 9 is not high enough to reduce the viscous force to a negligible quantity.

Displacements reported in Table 3 suggest that the viscous force appropriate to this simulation may not be proportional to the first power

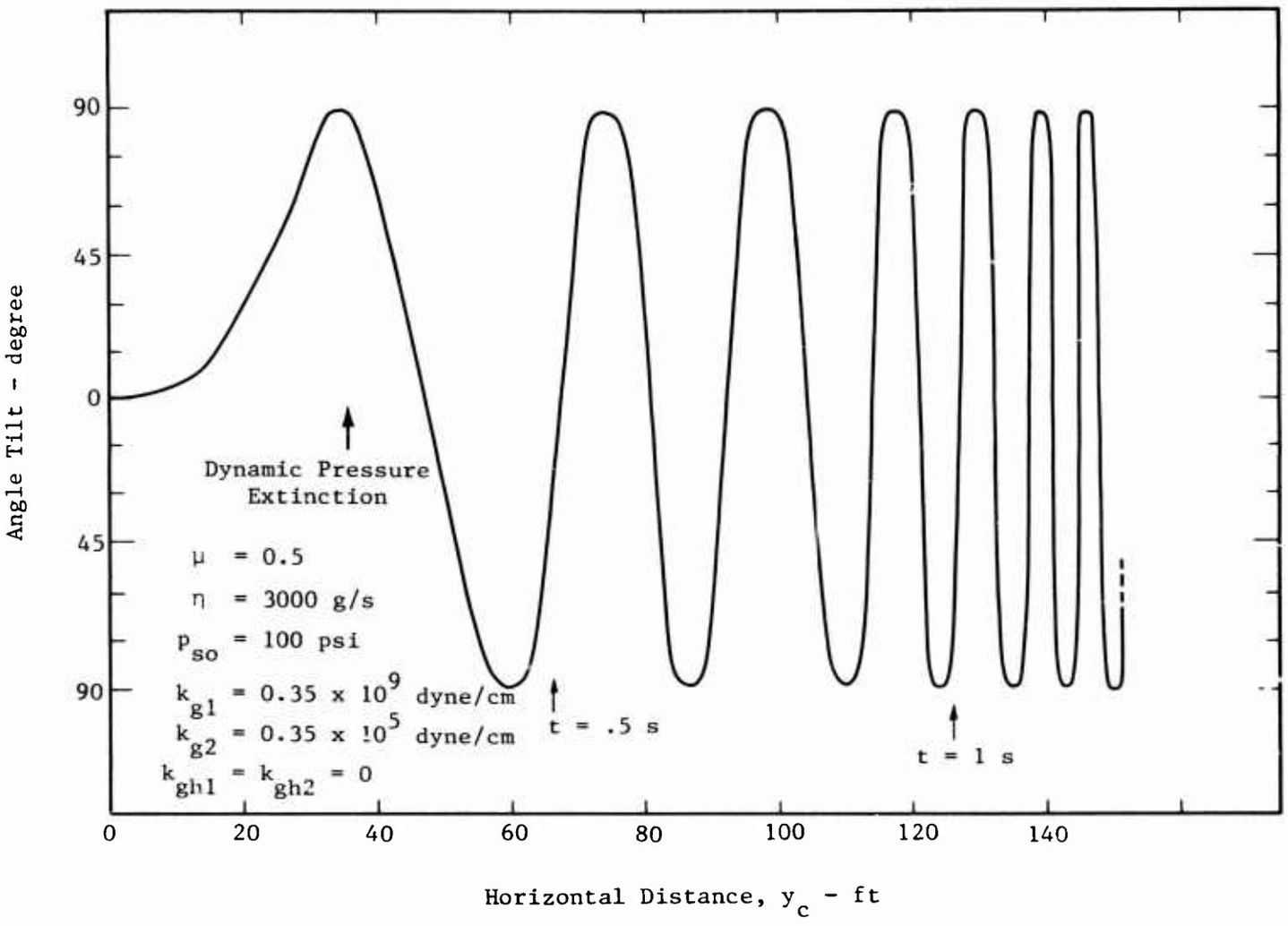

Figure 6. Simulated Tilt of Concrete Cube at DIAL PACK (high viscosity).

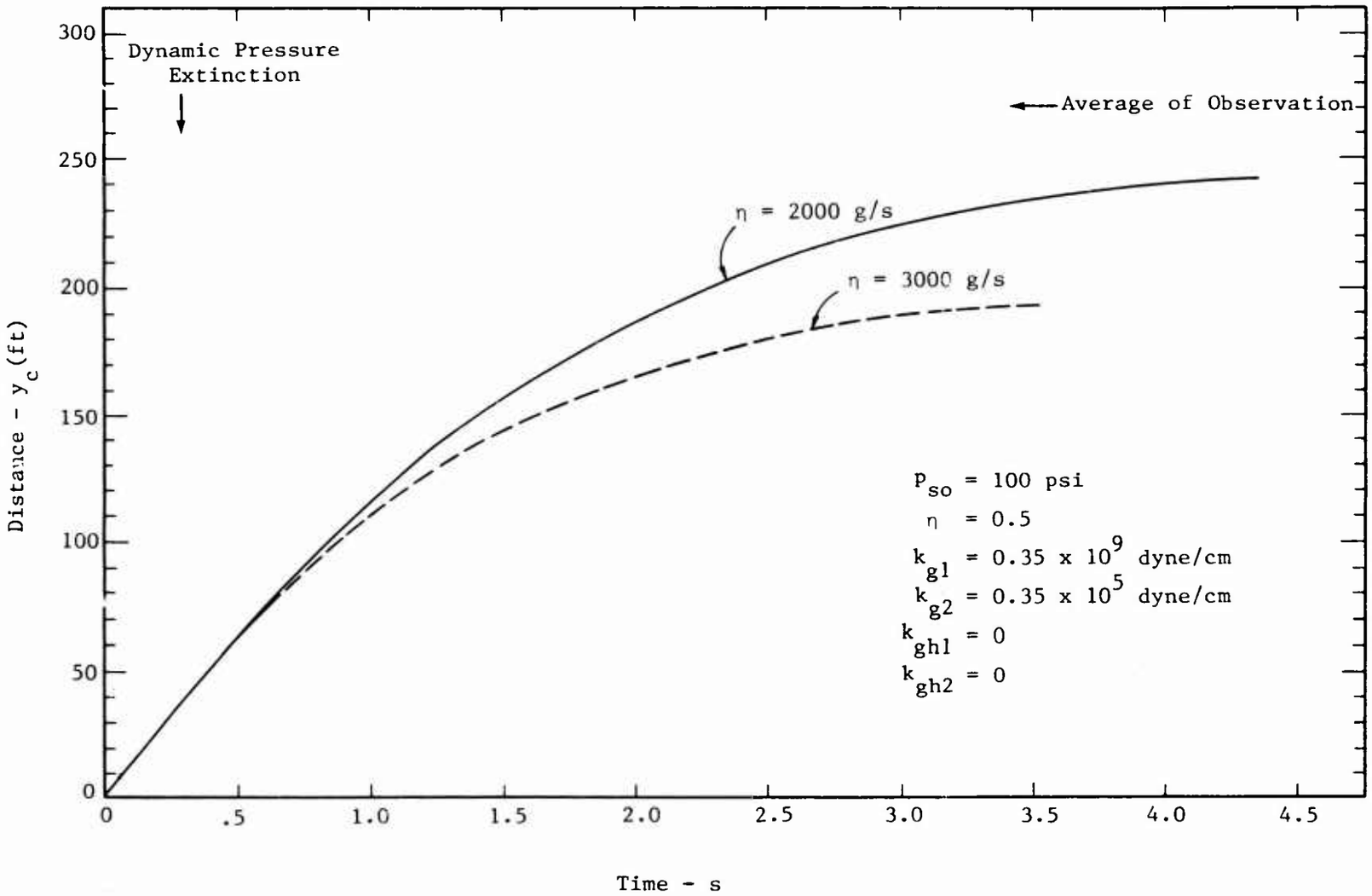

Figure 7. Simulated Displacement Histories of Concrete Cube at DIAL PACK, α-component of Ground-Induced Torque Set to zero.

Table 3. Effect of Viscosity on Total Distance Transported (ft)
$\mu = 0.5$, $k_{g1} = 0.35 \times 10^9$ dyne/cm, $k_{g2} = 0.35 \times 10^5$ dyne/cm.

p_{so} (psi) \ η (g/s)	0	300	1000	1500	3000
15	5.94				
30		39.4	34.8	32.2	
50					
100	503.0	430.0	332	407.0*	668.0*

* tumbling motion

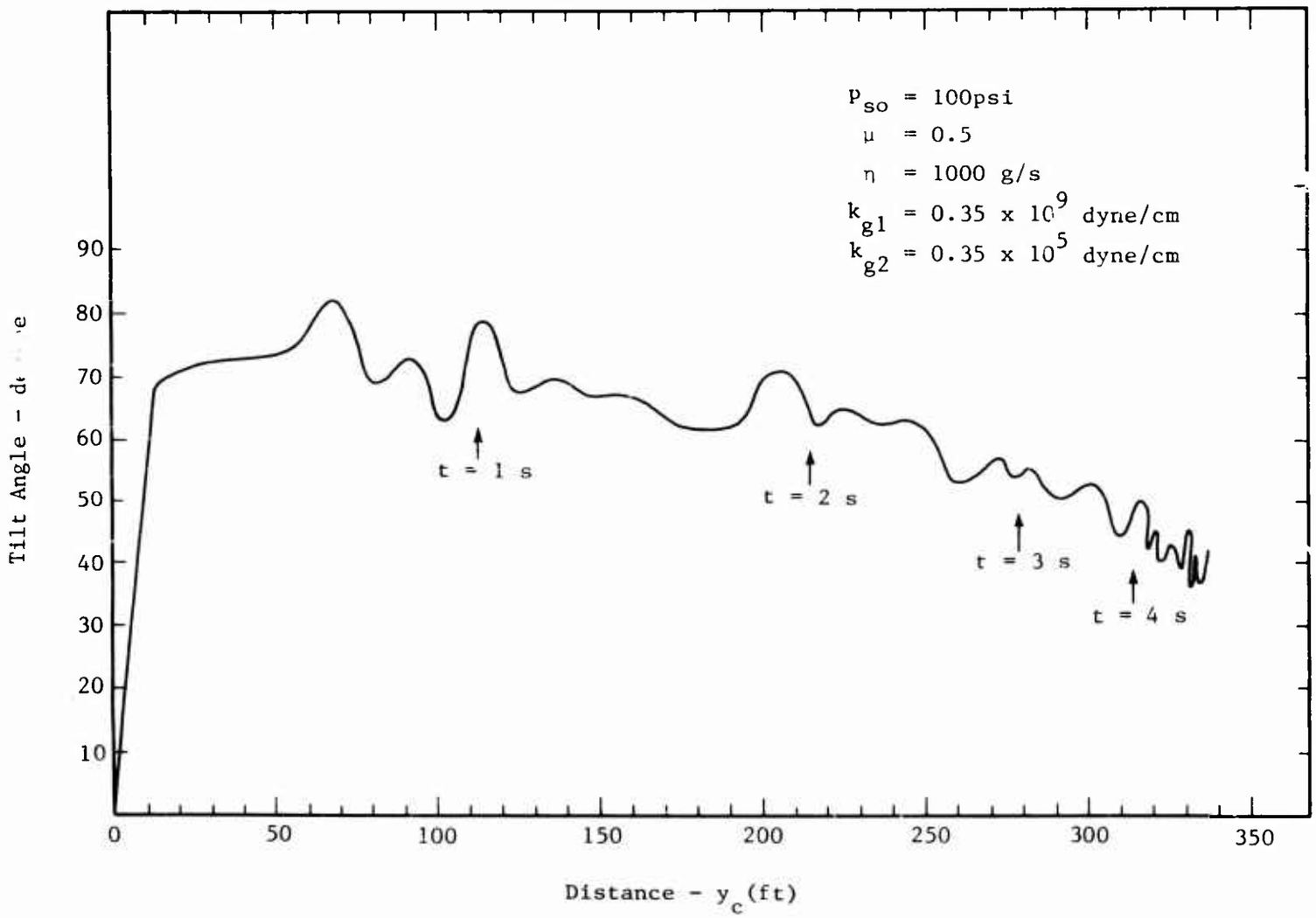

Figure 8. Simulated Tilt of Concrete Cube at DIAL PACK (low viscosity)

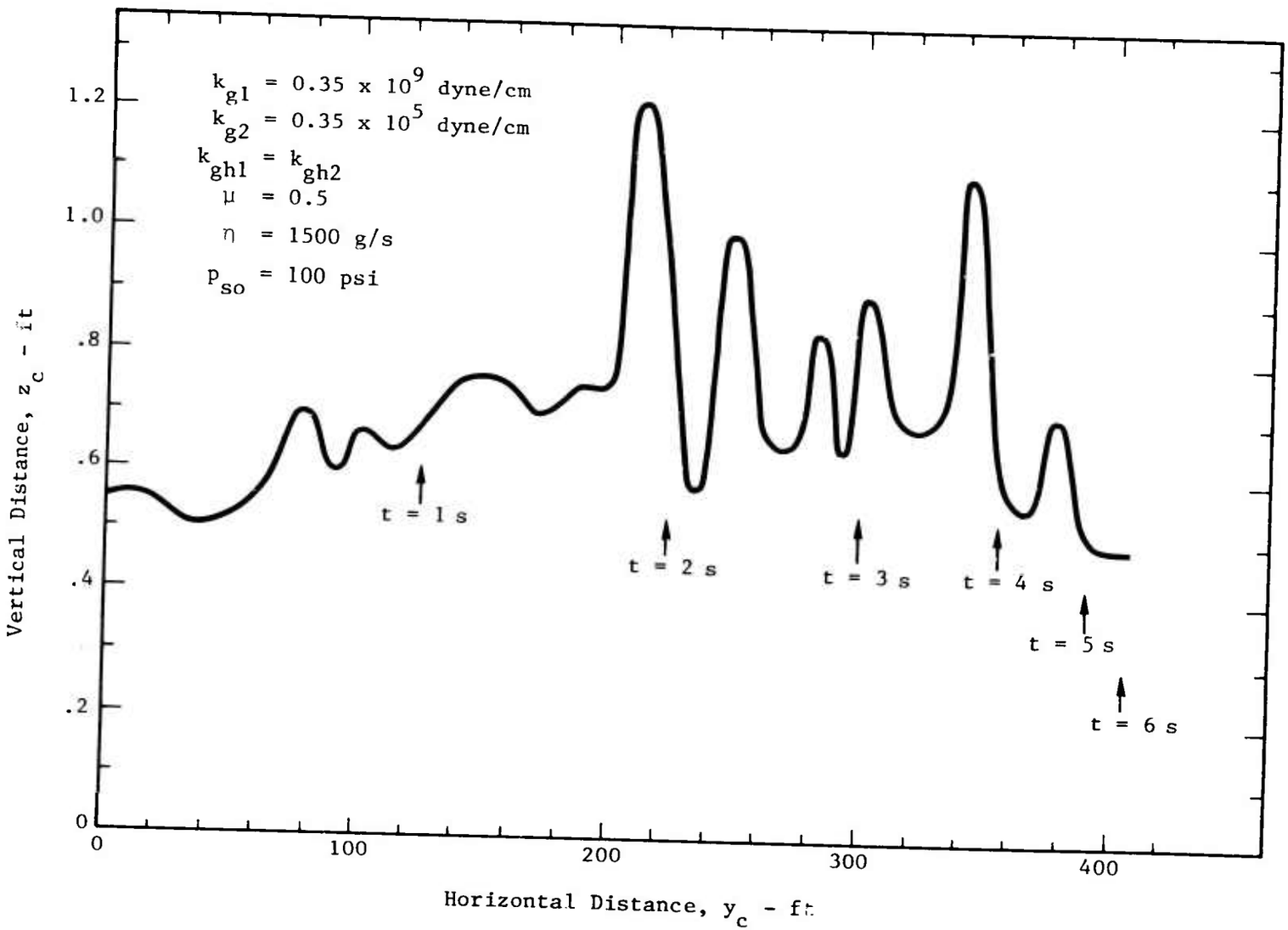

Figure 9. Simulated Trajectory of Concrete Cube at DIAL PACK (medium viscosity).

of object speed. Restricting consideration to only those simulations resulting in sliding transport, Table 3 indicates that less viscosity is needed at low overpressure than at high, since η = 300 g/s appears to be adequate for a cube originally at 30 psi; at P_{so} = 100 psi, however, a value of η >1000 seems required. However, another approach to the braking problem appears more fruitful.

Horizontal Ground Spring. The bouncing mode of blast transport appears realistic for most object-soil interactions. It does not seem at all likely, for example, that the grassy surface shown in the photograph contained in Figure 1 would allow a sliding motion of even a heavy, relatively smooth object such as the concrete-filled plywood cube observed at DIAL PACK. The torque, therefore, that tends to tumble a blast-driven object appears to be a desirable feature of the model. To be able to keep tumbling transport, yet get enough braking on ground contact to simulate experimental results, a horizontally-acting spring has been added to the ground-object interaction. Like its vertical counterpart, this spring is double valued to dissipate energy, but the double valuedness also serves to reduce spinning.

In the simplified flowchart of DEBRIS presented in Figure 10, the box marked with the star has been added to provide notice to the program when one or more corners of the debris fragment first come into ground contact, at which time logical variable GNDHIT is set equal to .TRUE. At the same time GNDOFF is set to .FALSE. so that on the next time-cycle, GNDHIT may be set to .FALSE. These logical operations permit subroutine CORNER to record the coordinate of the point and the direction of horizontal motion of most recent contact and to measure horizontal spring compression from that point. Subroutine CORNER has also been modified to apply the horizontal spring forces to fragment corners below ground.

As with the vertical ground spring, horizontal spring constant takes a high value at compression and a low value at release. During release, however, should the corner pass through the point of most recent touchdown, horizontal spring compression may begin again, the direction of horizontal motion noted, and the high value of spring constant be applicable. In this way, considerable energy can be dissipated upon a single

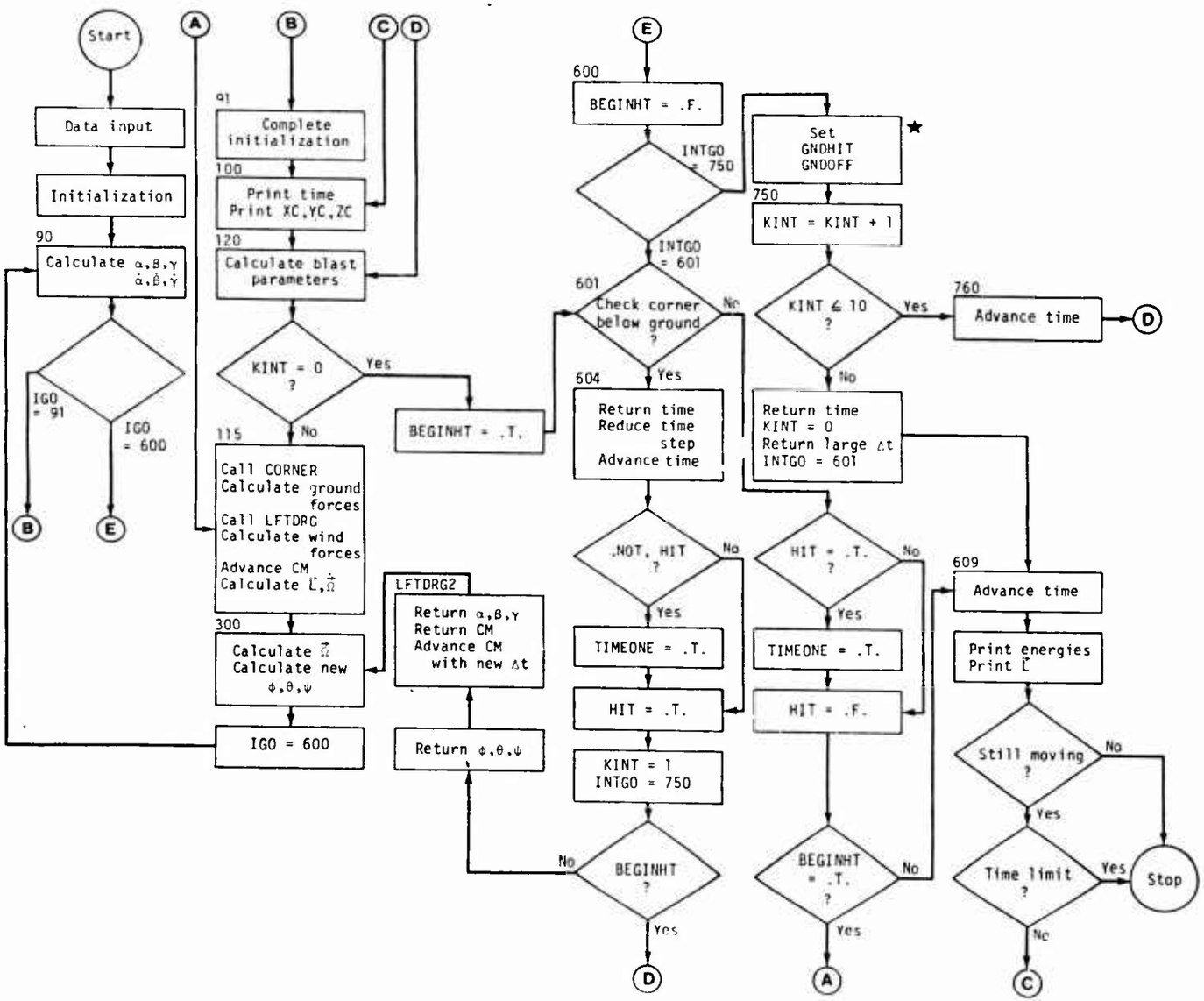

Figure 10 Summary Flowchart of the DEBRIS Program.

ground contact--provided the fragment remains in contact and does not immediately bounce off. The direction of horizontal spring force is always pointed toward the point of first touchdown. The action of the ground springs is sketched schematically in Figure 11.

Although pure friction is capable of inducing bouncing motion in the blast-transported cube, to simulate the observed transport distance, the coefficient of friction must vary with incident overpressure and increasing the coefficient does not always reduce distance travelled. From the limited number of trials performed so far, it appears that using horizontal ground springs in conjunction with the vertical the same behavior may be achieved while the values of all the arbitrary parameters are held constant. These parameters must, however, be changed with the soil. They probably also depend on the nature of the transported object. In the work to date, constant values of friction $\mu = 0.5$ and of viscosity $\eta = 3000$ g/s have been left in the calculations throughout. Spring constants have been varied, however, and it is clear that the two springs, the horizontal and the vertical, must cooperate in producing the desired motion. Two simulated partial trajeccories shown in Figures 12 and 13 demonstrate this. Horizontal constant, k_{ghl}, is held constant in the two calculations, but the vertical constant, k_{gl}, is changed by a factor of ten. The stiffer vertical spring causes much higher bounce than the weaker spring and the greater ground contact present with the weaker spring causes increased loss of horizontal speed. When $k_{gl} = 0.35 \times 10^8$ dyne/cm,distance moved during the first second after blast arrival is approximately 85 ft; increasing k_{gl} by a factor of ten raises the transported distance in the same time interval to nearly 95 ft. The loss of forward momentum might be caused by any or all of the three mechanisms: friction, viscosity, or the double-valued horizontal spring. Further research is required to untangle these effects.

With the parameter values unchanged the simulations represented in Figures 12 and 13 have been completed and two aspects of these calculations are shown in Figures 14 and 15. Incident peak overpressure is 50

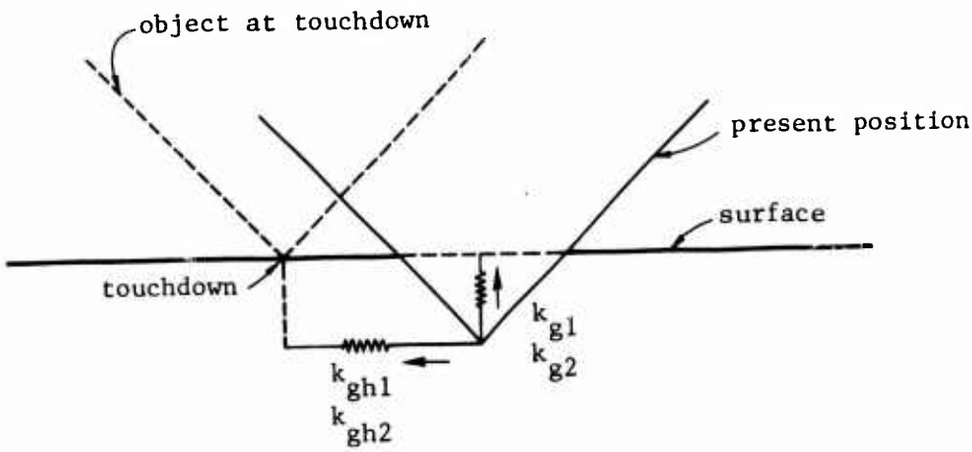

Figure 11. Schematic Illustration of Ground Reaction Springs in DEBRIS.

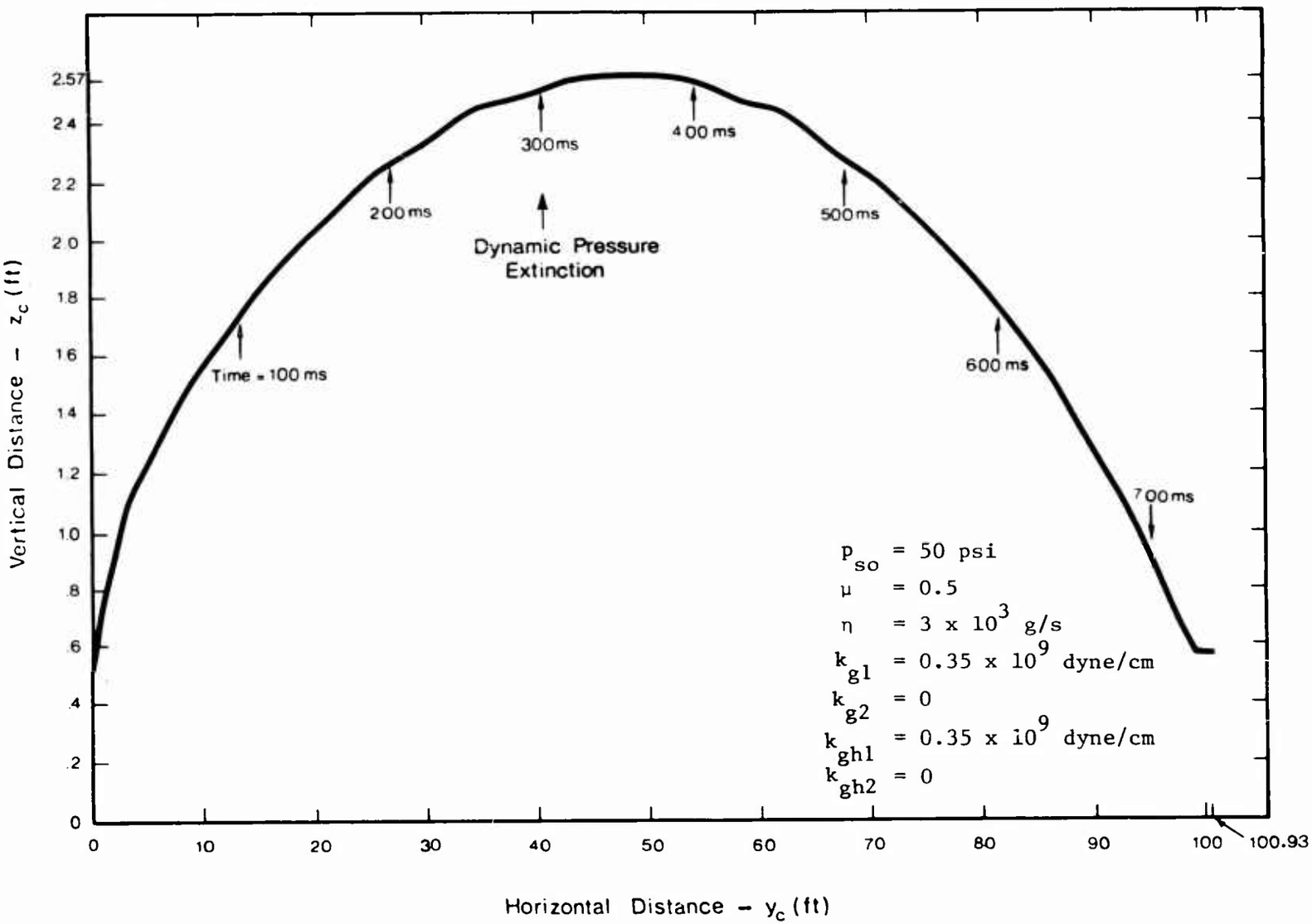

Figure 12. Simulated Trajectory of Center of Mass of Concrete Cube at DIAL PACK (strong vertical spring).

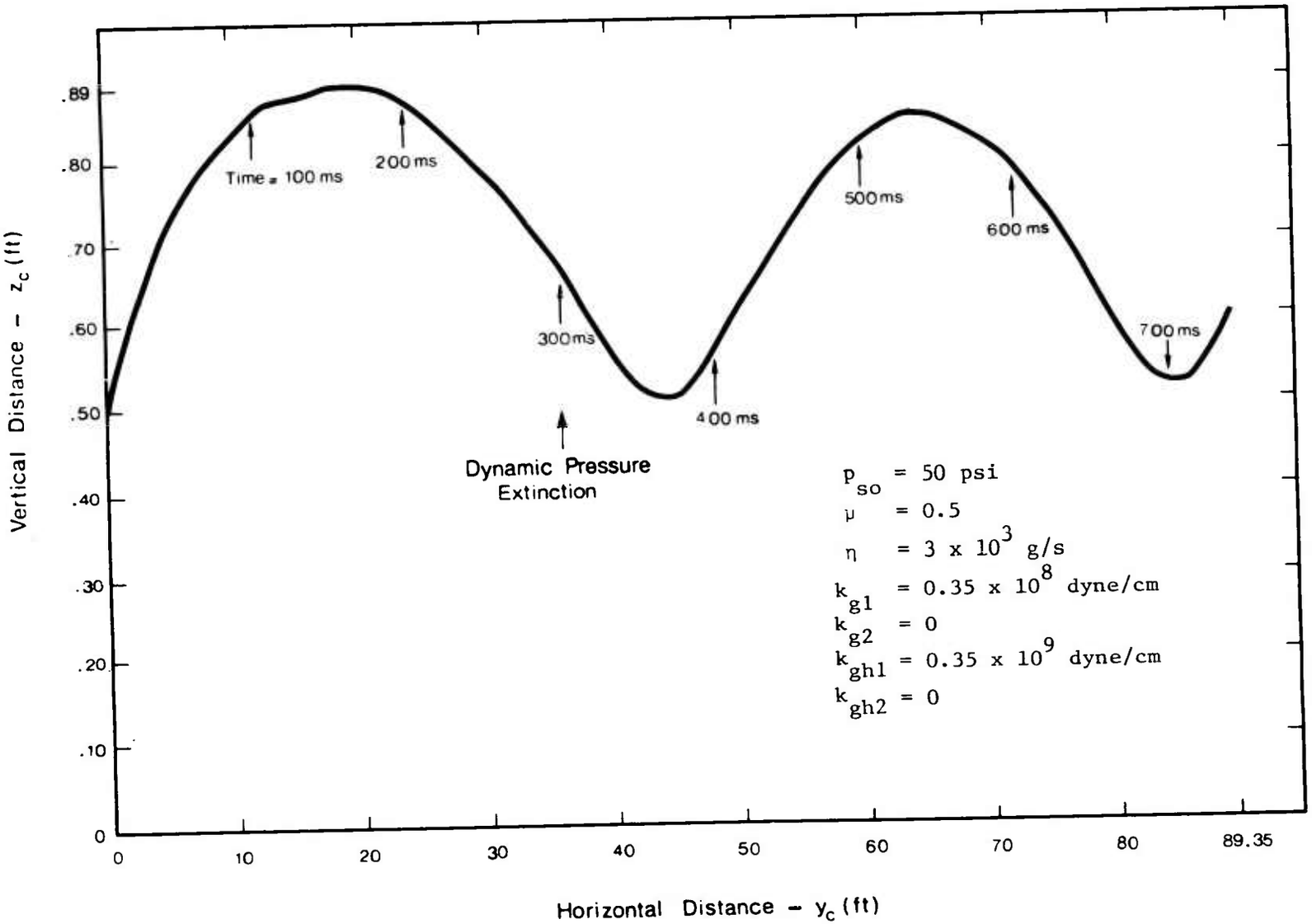

Figure 13. Simulated Trajectory of Center of Mass of Concrete Cube at DIAL PACK (weak vertical spring).

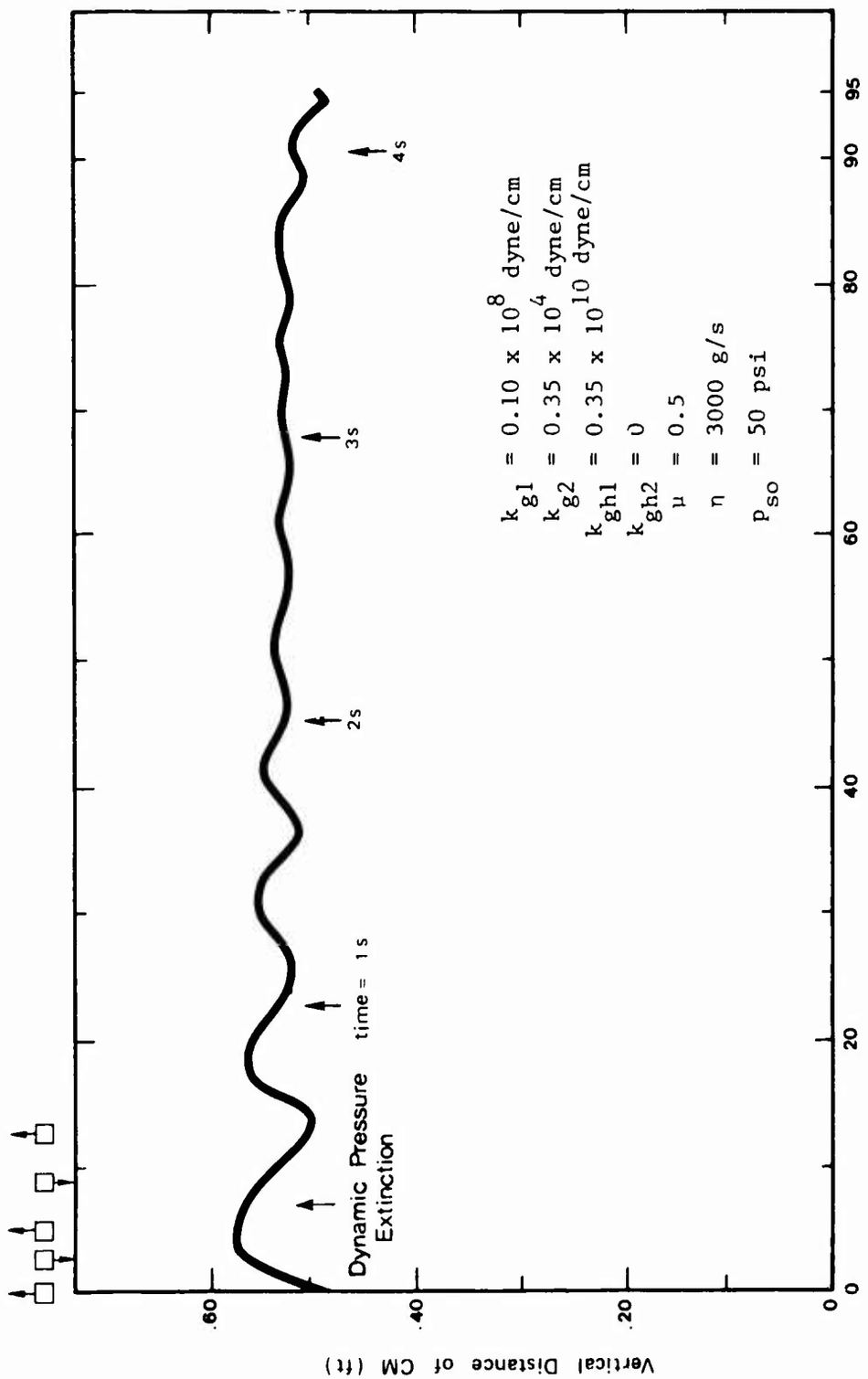

Figure 14. Trajectory of Center of Mass of Concrete Cube at DIAL PACK.

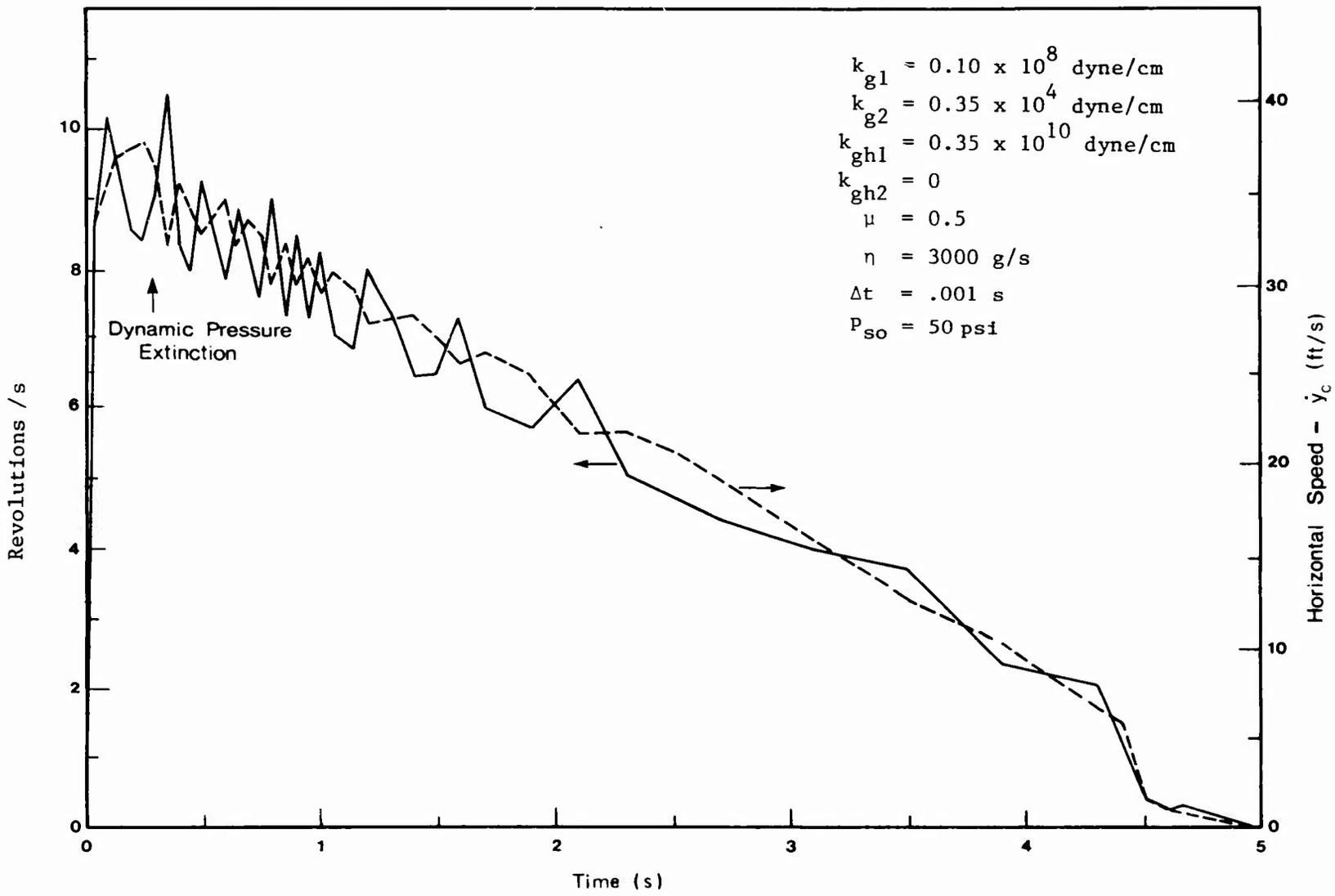

Figure 15. Braking of Concrete Cube at DIAL PACK.

psi. Figure 14 is a trajectory of the center of mass downrange from which it is seen that the center of mass never rises above approximately 1.5 in. from its original height. The small squares along the top of the figure are meant to represent the approximate orientation of the cube at the locations shown; the simulated cube turns completely over once before reaching the top of its first bounce, but the rate of tumbling declines rapidly after two bounces. (This is in contrast to behavior in simulations with friction or viscosity or both and without the horizontal spring.) Plotted in Figure 15 are two aspects of the motion illustrating braking of the rotary motion and of the translation. The peak speeds are reached very early in the travel under the influence of the dynamic pressure; most of the transport is during the braking phase. Maximum rotary speed is approximately 9 rps and maximum horizontal speed is approximately 38 ft/s. These values depend on the parameter values and it is not known from the experimental data whether or not the tumbling motion in the simulation is an accurate representation of the actual motion. The sharp fluctuations of the speeds during the trajectory are not real and the discontinuities of first derivatives are due mostly to the lack of detailed computer printout; fluctuations in angular and translational speeds no doubt actually occur. Also no attempt has been made as yet to simulate the fluctuation in transport caused by variation of ground surface conditions. In the DIAL PACK data, for example, there is a 50 percent variation in observed transport at 50 psi.

Figures 14 and 15 list the value of the integration tone step Δt. In these simulations, when the transport depends critically on ground contact during bounces, the fineness of the time mesh is important. The value of Δt entered in the figures is 0.001 s, but during the time any part of the cube is in contact with the ground, the code automatically reduces the preset time step by a factor of ten in size so that during most of the motion simulated in Figures 14 and 15 the time integration was performed with steps of 0.0001 s. For example, increasing the nominal value of Δt to 0.01 s can increase calculated transport significantly in some over-the-ground translations.

By trial and error, the parameter values

$$k_{g1} = 0.20 \times 10^{8} \text{ dyne/cm}$$

$$k_{gh1} = 0.35 \times 10^{10} \text{ dyne/cm}$$

$$\mu = 0.5$$

$$\eta = 3000 \text{ g/s}$$

were successful in simulating distance transported in the range of incident pressures 30 to 100 psi.* The values of the recovery spring constants are very small or zero and do not seem to be critical to the distance travelled. Distances transported in simulations with these values are plotted as triangles in Figure 16 along with the reported observations.

At least in this pressure range, "tuning" of the model may most easily be accomplished by adjusting the constant, k_{g1}. The strong influence of the vertical compressive spring, k_{g1}, on braking is demonstrated by the distances transported reported in Table 4.

Effect of Yield

Because the DIAL PACK event was a surface explosion of approximately 500 tons of high explosive, the equivalent nuclear explosion has been simulated by airblast arising in a 1-KT surface burst. To explore the influence of yield on the translation model, airblast parameters corresponding to a 1-MT surface burst have been used in one simulation with the result that total travel from a location on the 100-psi contour was 2060 ft. Simulation parameter values were the optimum values noted above.

---

*At 15 psi, the diffraction phase is relatively more effective than at higher overpressures. Allowing for diffraction by starting the cube at t = 1 ms with a speed of 1.84 ft/s increases displacement by approximately 1 ft; also changing k_{g2}, the recovery ground spring constant, from 0.35×10^{4} to 0.35×10^{6} dyne/cm raises transport at 15 psi to 6.26 ft, which is close to the observed average 7.5 ft. See appendix for a calculation of diffraction momentum.

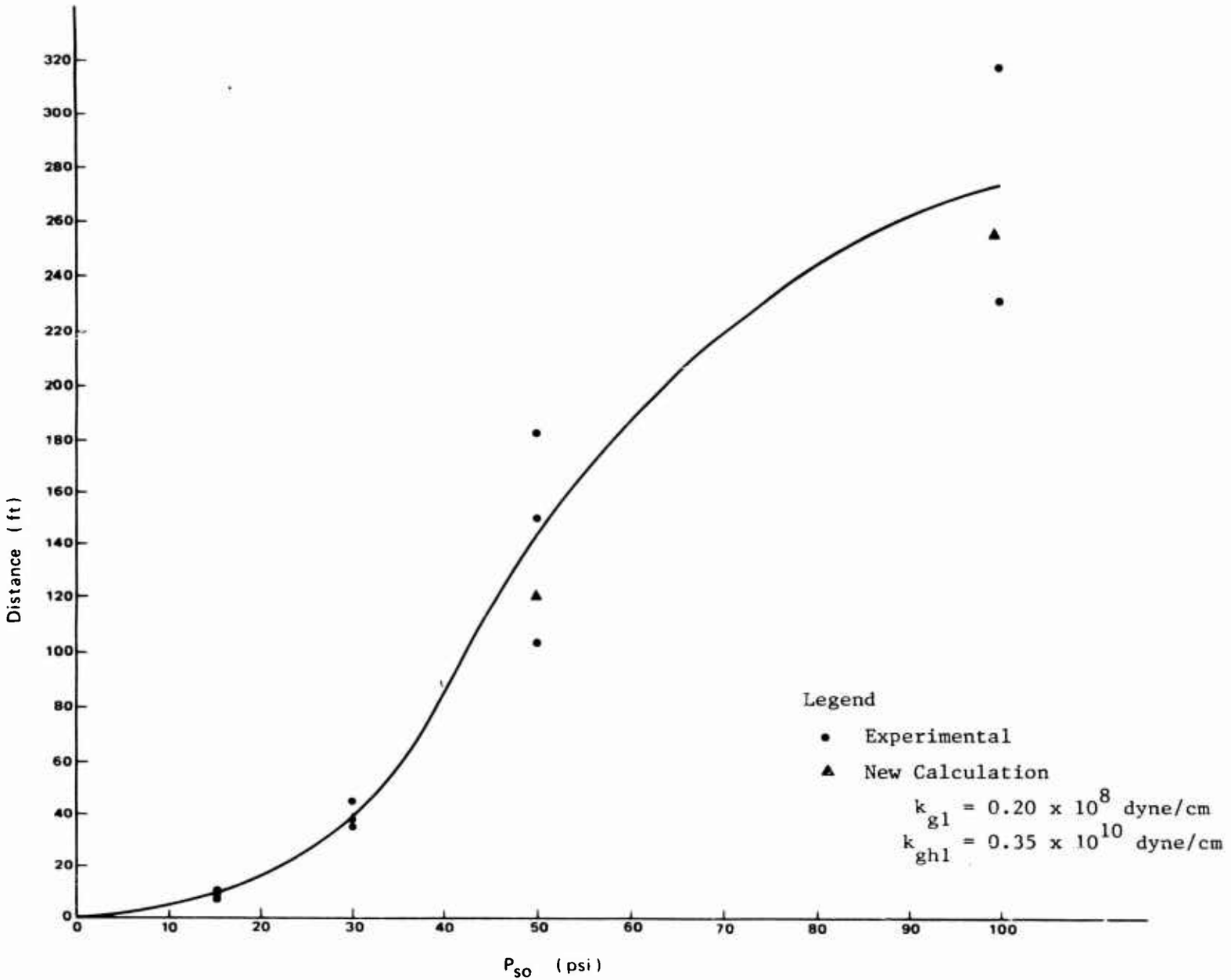

Figure 16. Simulated and Observed Translations of Concrete Cube at DIAL PACK.

Table 4. Effect of Compressive Vertical Spring Constant of Concrete Cube at DIAL PACK.
$\mu = 0.5$, $\eta = 3000$ g/s, $k_{ghl} = 0.35 \times 10^{10}$ dyne/cm.

Distance Transported (ft)			
p_{so} (psi) / k_{gl} (10^7 dyne/cm)	30	50	100
0.35	—	32.5	—
0.90	44	—	187
1.00	—	96.7	—
2.00	72	118.4	255.0

This value of transport is about the average of the DIAL PACK observations scaled from 1 KT to 1 MT. However, to save computation costs, the time step for the megaton calculation was increased to 0.01 s. This change probably introduced error.

Comparison with Other Data

The model DEBRIS can simulate the translation experiments described by Fletcher and Bowen[22,23] by the choice of the initial conditions in the calculation. When the height of the bottom surface of the dropped object is 2.6 feet, the initial speed is 38 ft/s, and the departure time later than the positive dynamic pressure phase duration, the calculated motion with the optimum simulation parameters noted above for DIAL PACK does not agree with the described behavior of the stones and masonry blocks dropped from the moving truck. In fact, the strong horizontal spring appears to throw the object backward toward the point of origin. However, when the horizontal spring constant is reduced by two orders of magnitude or more, the computed motion is more realistic. The trajectory of the center of mass according to a simulation of the drop from a moving truck for the concrete cube of DIAL PACK is drawn in Figure 17. The total distance travelled after release is 44.6 ft. According to Fletcher and Bowen,[22,23] the distance travelled in this manner is independent of the mass of the object dropped. This is borne out by DEBRIS, when a cube identical to the DIAL PACK cube, but having a density of 0.08391 lb/in^3 (which is the density of normal concrete), is simulated with DEBRIS. In the case of the heavier cube, total transport is 44.0 ft. The trajectory (Figure 18) is again realistic, and, in fact, quite similar to that appearing in Figure 17 for the much lighter cube. Whether or not the similarity of the trajectories is accurate is not known.

In any case, the distance and time of transport provided by DEBRIS with the parameter values discovered so far do not agree with the predictions of the empirical formulas given by Fletcher and Bowen.[22,23] If the initial speed, v, is 38 ft/s, these formulas yield distance, s = 34.3 ft and time to stop, t = 1.907 s. In the case of the heavy cube DEBRIS estimates stopping time t = 3.27 s and for the DIAL PACK density,

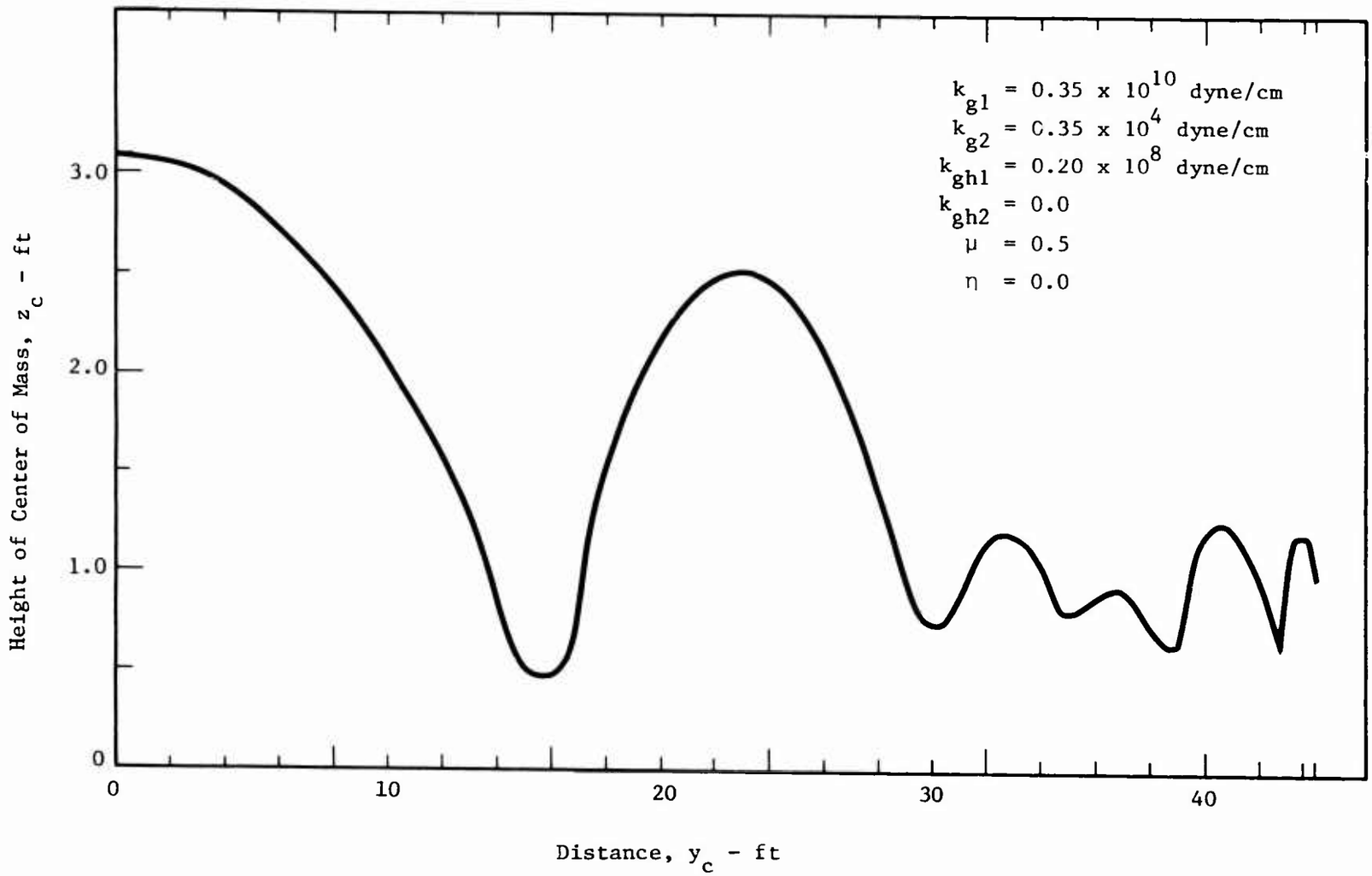

Figure 17. Simulated Trajectory of Center of Mass of Concrete Cube Thrown from Moving Truck, Density = .03704 lb/in^3

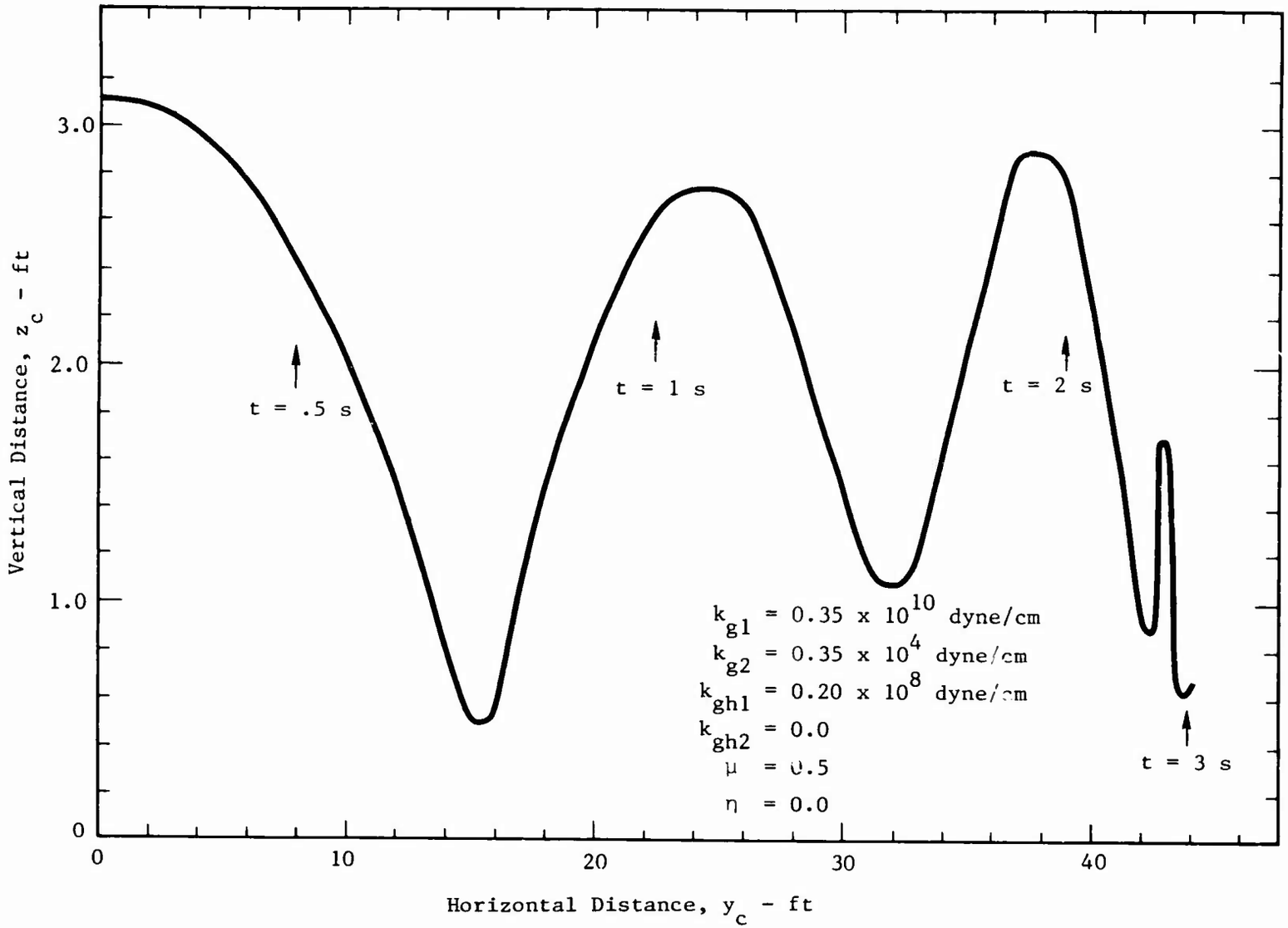

Figure 18. Simulated Trajectory of Center of Mass of Concrete Cube Thrown from Moving Truck, Density = .08391 lb/ft^3

t = 3.62 s. Again t is nearly independent of mass, as forecast by Fletcher and Bowen,[22,23] but the quantity differs from their forecast. The prediction of DEBRIS as to distance falls within one standard error of estimate of the value predicted by Fletcher and Bowen's formula; the detailed printout shows the light and heavy cubes cease downrange progress at 2.7 s and 3.3 s, respectively.

PART II

BLAST RESPONSE AND COLLAPSE OF BUILDINGS (BRACOB)

An early version of the BRACOB system of computer programs has been described in Rempel and Wiehle[25] and a then current listing published in Rempel.[26] The system accepts information about the floor plan in terms of a user-defined rectangular coordinate system, engineering parameters for walls and airblast specification either in terms of a classical blast of user-chosen pressure and angle of impact, or in terms of arbitrarily specified pressure histories. The program itself computes loadings against all walls as functions of time, response of walls up to the point of collapse, at which time the program will adjust the loading on other walls if necessary. Because only simplified physical principles are used, i.e., structural response is deduced from a single degree of freedom model and airblast loading is computed with the help of concepts of clearing time and room filling, the computer time required for a complete history is much less than time ordinarily taken for finite element or hydrodynamic calculations.

The single degree of freedom (SDOF) model provides histories of velocity and the displacement of a mass equivalent to the effective mass of the wall, which is assumed to bend or flex under an airblast load. Load-mass factors have been chosen so that these displacements and speeds correspond to observed motions of central points in the responding walls.[27,28] Further evidence of the applicability of the SDOF model to estimates of deflection are expected from the upcoming MILL RACE event,* particularly in regard to unreinforced masonry. Failure of an unreinforced wall, according to the model, takes place when deflection has reached the extent that the wall is unable to support overburden, i.e.,

---

*Particularly, the FEMA Experiments 5401, 5402, and 5403.

when deflection of the central point is equal to the thickness of the wall itself. At this point BRACOB ceases to compute the wall movement. In fact, these final conditions of speed and deflection become initial conditions for the code DEBRIS; provided the fracture pattern is known as well, then all required input information is available for a calculation of the continued motion of the wall fragments as free bodies.

A previous study[20] suggests that even at pressures as high as 30 psi, unreinforced masonry fails in flexure, i.e., that shear walls provide support of some degree even when they themselves are strongly disturbed by the blast. (Again, experiments to be conducted in 1981 at MILL RACE should give more information on this question.) During the present research, then, exterior unreinforced walls have all been assumed to fail in flexure, demonstrating typical failure patterns, such as the classical pattern exhibited in Figure 19, or patterns observed during Shot ENCORE.[9,20] The ENCORE walls were made of baked clay masonry units within steel frames and were exposed in the range from 4 to 9 psi. Portions of the centers of these walls punched out, as illustrated in Figure 20.

Published reports from the URS blast tunnel* tests of masonry walls[10,11,12] do not show the failure patterns of Figures 19 and 20. In these experiments the test walls generally filled or nearly filled the entire cross section of the large walk-in gallery that was used as a blast tube; furthermore, support conditions at wall edges were often unusual. Failure in walls without windows appears to have been generally by a more or less horizontal crack the full width of the panel, suggesting that vertical edge support may not have been present, or not effective.

In addition to wall speed and time of failure, the DEBRIS code takes as input the kind of hinging before collapse or assumes none. The subsequent trajectory is determined in large measure by the initial conditions, including the kind of hinging or its absence.

---

*Located at Fort Cronkhite, Marin County, California.

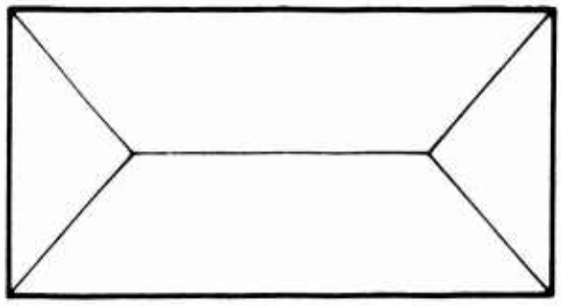

(a) Wall Without Window

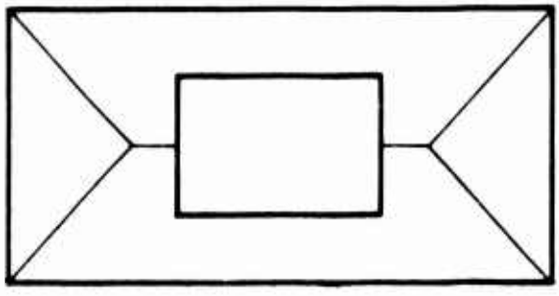

(b) Typical Yield Line For Wall With Window

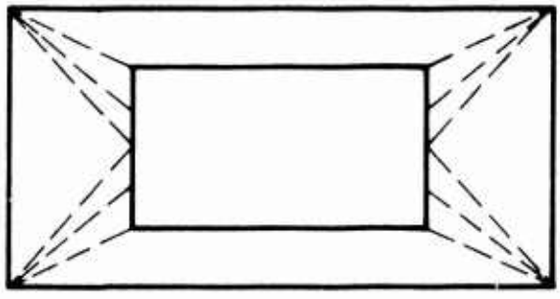

(c) Yield Line For Wall With Wide Window

source: Ref. 14

Figure 19. Yield-Line Patterns for Rectangular Wall Panel.

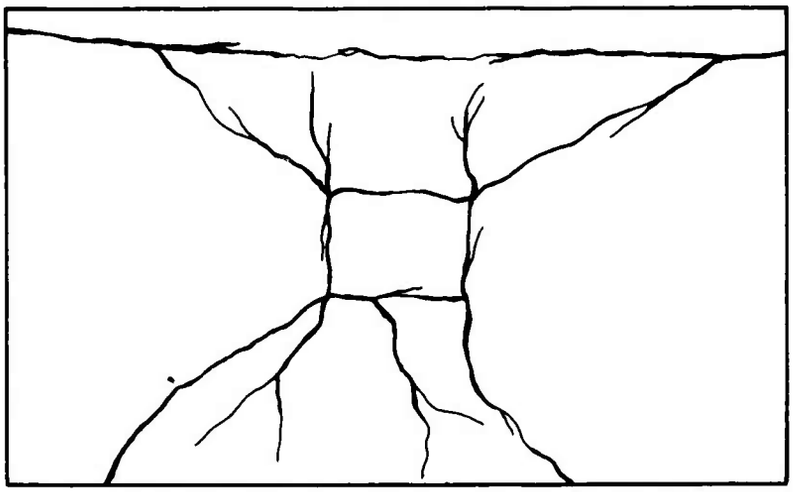

Panel No. 5

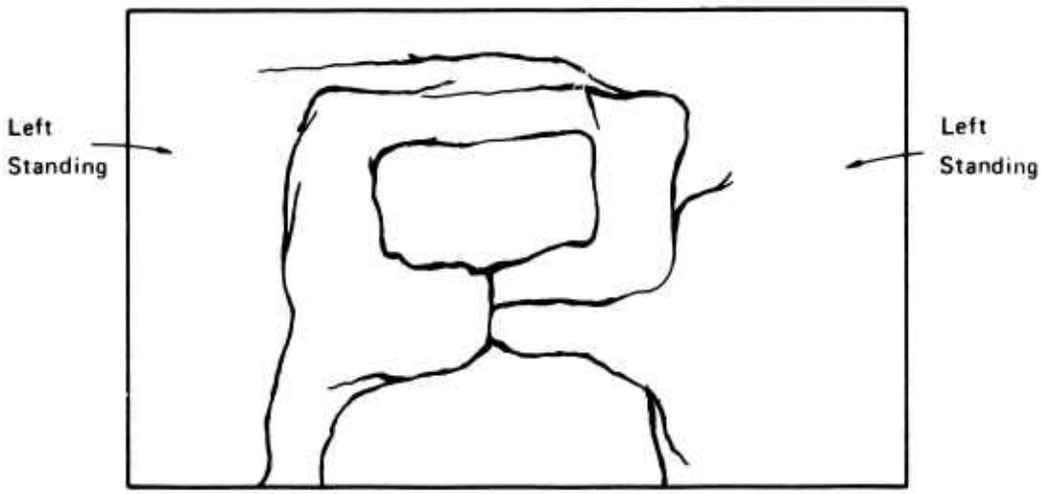

Panel No. 9

Figure 20. Wall Crack Patterns, Shot ENCORE.

At the present time BRACOB does not calculate the response of interior walls, but it will treat them as "collapsed" as of a certain preset time during the problem, at which time the pressures in adjoining rooms are recalculated by means of thermodynamic principles. When exterior walls collapse, the then existing outside pressure against the wall is transferred to what were interior walls after a preset time (to allow for pressure buildup behind the collapsed wall). The same kind of arbitrary delay is imposed on the room-filling process to allow for (1) breakage of windows and doors, and (2) interior pressure to buildup throughout the room. After this delay on room filling, BRACOB calculates an average interior pressure resulting from the air streaming in from outside high pressure regions.

Because reinforced wall panels seldom support overburden (except in earthquake zones), the "failure" criterion for these walls is different from that for unreinforced load-bearing walls. Failure of reinforced concrete walls, for example, is defined to occur when a certain degree of plastic deformation of the reinforcement has occurred. Exactly at what point in their response to air blast such panels become "debris" is not known at this time, but FEMA Experiment 5402 at MILL RACE should provide some insight on this question.

Because of the greater degree of understanding of unreinforced wall behavior after collapse, attention during this research has focussed on unreinforced masonry walls.

Improvements in BRACOB

In preparation for systematic studies of debris formation and scatter in cities, BRACOB has been enhanced to handle all angles of impact, 0 to 2π; necessary restructuring of the data base when incidence is from the rear is now accomplished automatically.

Better use of the powerful computing system at the Stanford Center for Information Processing is now made possible by a system of independent compilation of subroutines. Data bases also--for specifying airblast and for describing the building--have been individualized, as have output

for various kinds of output information. Although computation remains in the batch mode to take advantage of reduced costs, operation of the system, including disposition of files, may be interactive.

Multiply-connected spaces in floor plans formerly caused an error termination from BRACOB; this shortcoming has been corrected. Storage specifications have been changed to permit calculation of blast response of larger buildings than before.

Another enhancement to facilitate application of BRACOB to large urban buildings is the creation of "loading multipliers" that enable the program to calculate clearing times from geometric data pertaining to a single floor of a multiple-story building. Clearing time, t_c, for reflected pressure against a facade of any building may be found from the formula[29]:

$$t_c = \frac{n\,(A_{wall} - A_{opng})}{aP}$$

where A_{wall} is the total area of the facade and A_{opng} is the area of openings in the wall, a = sound speed in the reflected zone in front of the facade, and P = the total perimeter in the facade from which clearing relief waves may originate. (Window and facade edges are treated as equal despite the fact that room interiors may contain a higher pressure than found at the edge of the building.)

The quantity n is 3 if incident overpressure is below 12 psi, and n = 4 if incident overpressure is >12 and <25 psi. There are three multipliers: one for wall area, another for window or opening area, and a third for perimeter. Were all multipliers unity, the calculation of clearing time would be correct for a single-story building. A six-story building with six identical floors would require all multipliers to be equal to 6 because the roof is claimed as free perimeter only once, i.e., the perimeter multiplier is applied only to the length of vertical edges. In the case of oblique incidence, the vertical facade edge is a free perimeter for only one of the two adjoining facades.

Certainly one of the major enhancements accomplished during this period of research has been the incorporation into the subroutine RESIST (which determines the parameters of the resistance function for each exterior wall) of provision for Support Conditions 9 and 10.[28] Walls so supported are unreinforced and arch in a flexible or rigid frame, a condition common among large urban buildings in the United States outside California or other earthquake-prone areas. Support Condition 9 refers to one-way arching in a frame and Condition 10 describes two-way arching. The arching code was originally written to calculate the blast response of half-timbered walls, i.e., bricks inside a wooden frame, in which case the yielding of the frame was important to the result. In steel frame or even reinforced concrete frame buildings, yielding of the frame is not usually significant. For the present research the frame has been considered rigid.

LANDIS HOSPITAL

The Henry R. Landis State Hospital, Philadelphia, Pennsylvania, is one of the buildings in the National Shelter Survey inventory. An elevation view of one wing, taken from blueprints received from Research Triangle Institute appears in Figure 21 and a simplified typical floor plan in Figure 22 showing the orthogonal grid required by BRACOB as the basis for geometric input data. The computer program BRACOB has produced the schematic drawing in Figure 23. The drawing corresponds to a time 0.01 s after blast arrival; the current location of the blast front is shown by the dashed line across the first tier of rooms. Openings are represented by short lines that parallel the walls. As can be seen from the figure, BRACOB now accepts cases in which rooms are entirely surrounded by other rooms; that is, artificial walls are not necessary to connect the inner core of rooms to the surrounding rooms. In Figure 23, the blast front parallels the long axis of the floor and travels from the bottom to the top of the page.

As can be seen from the structural detail of the outer walls reproduced in Figure 24, there are two tiers of masonry, each arching in a nearly rigid frame. The outer tier of red brick is framed top and bottom

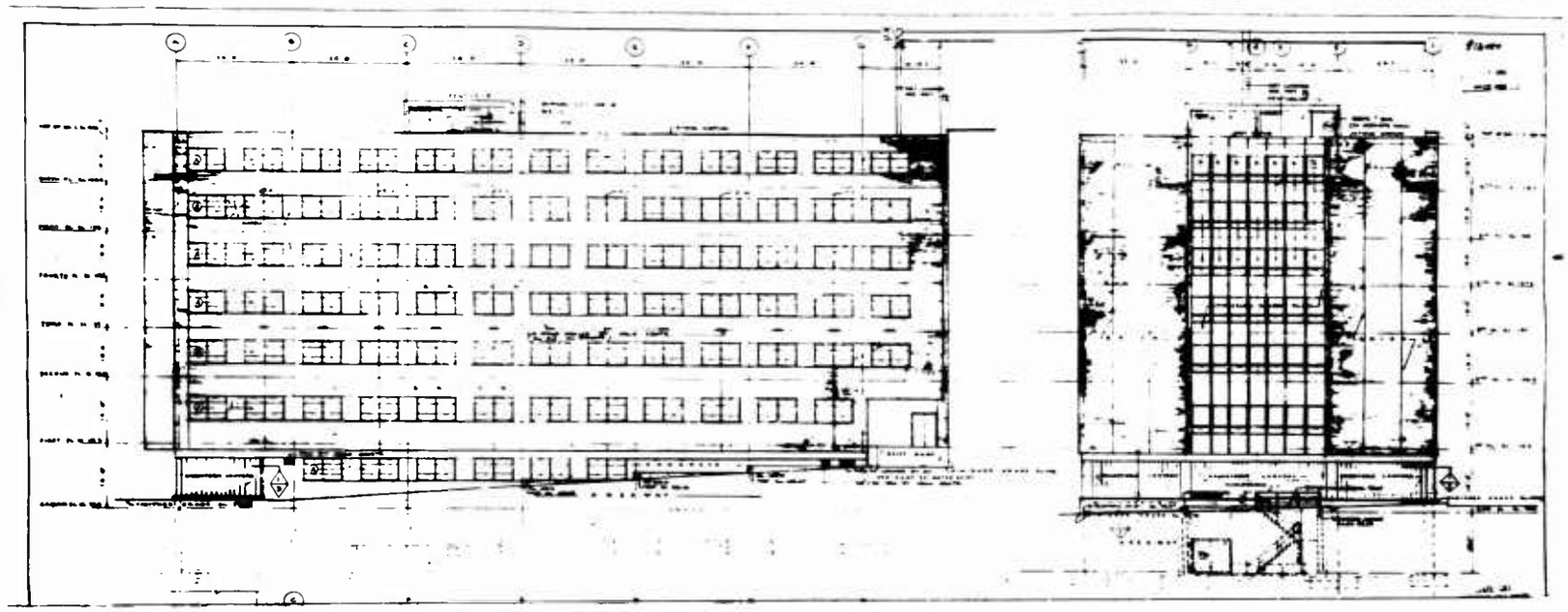

South Elevation

West Elevation

Figure 21. Henry R. Landis State Hospital, Philadelphia, South and West Elevation.

HENRY R. LANDIS STATE HOSPITAL

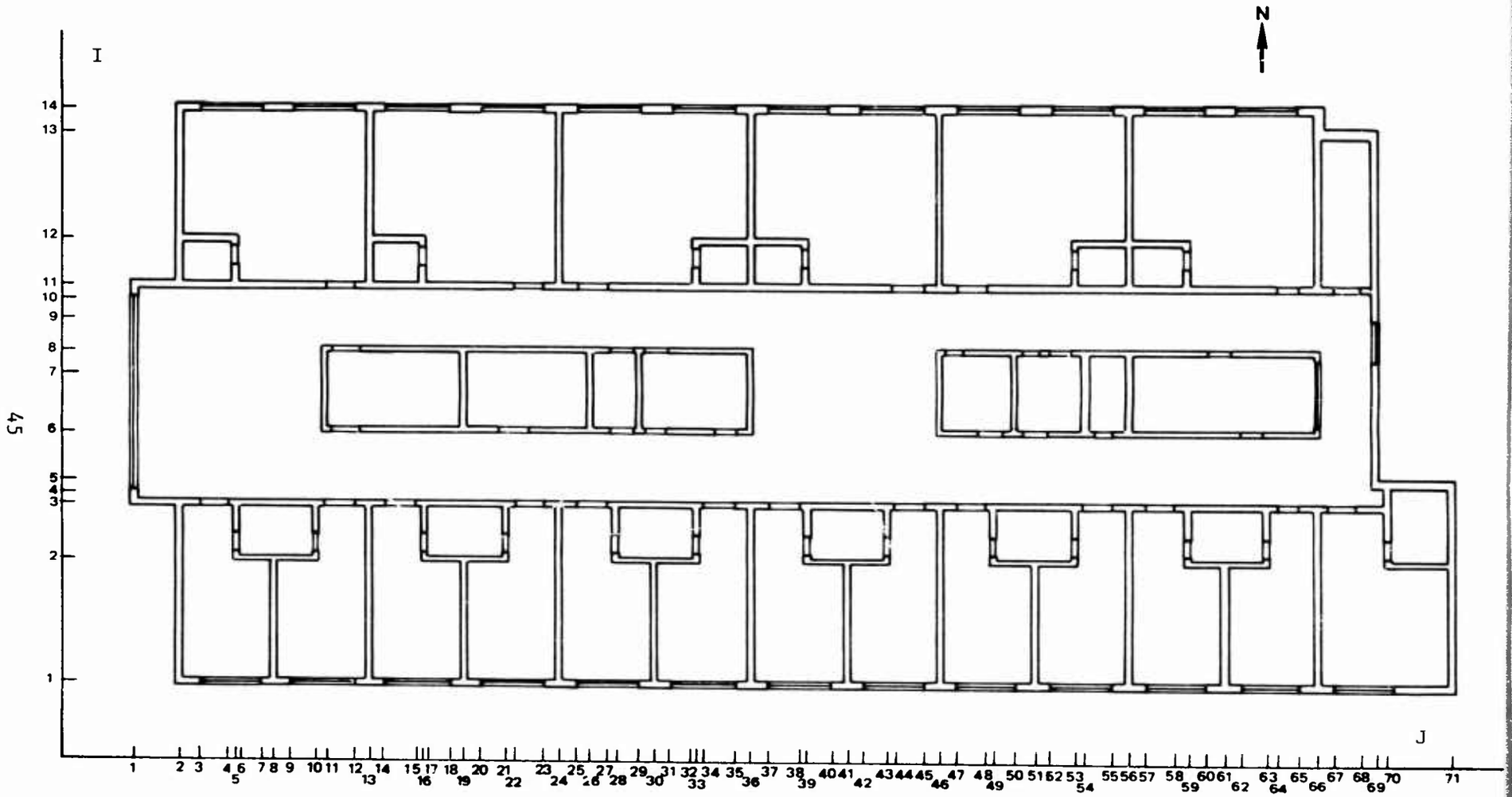

Figure 22. Orthogonal Grid for Landis Hospital.

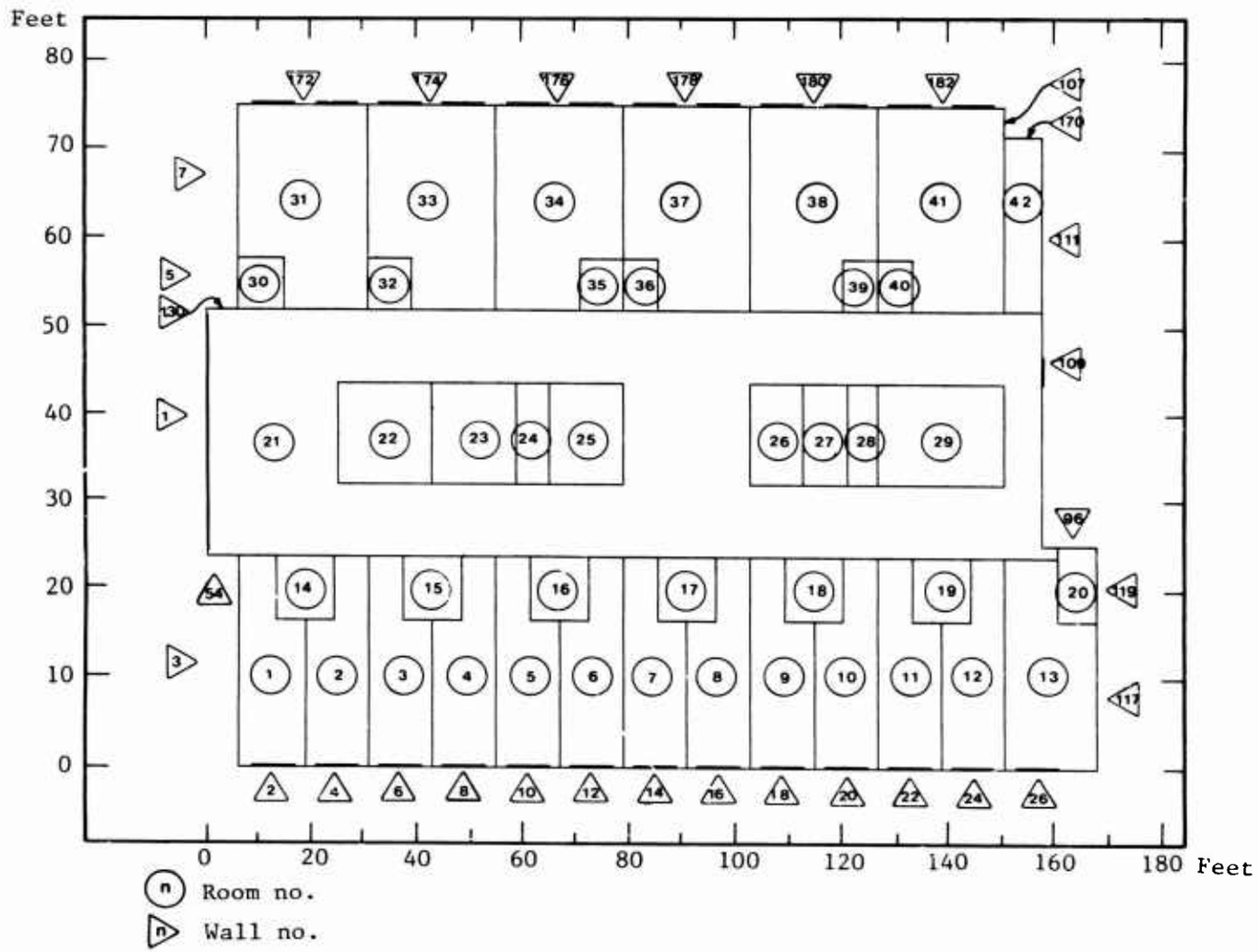

Figure 23. BRACOB-Generated Floor Plan, Landis Hospital.

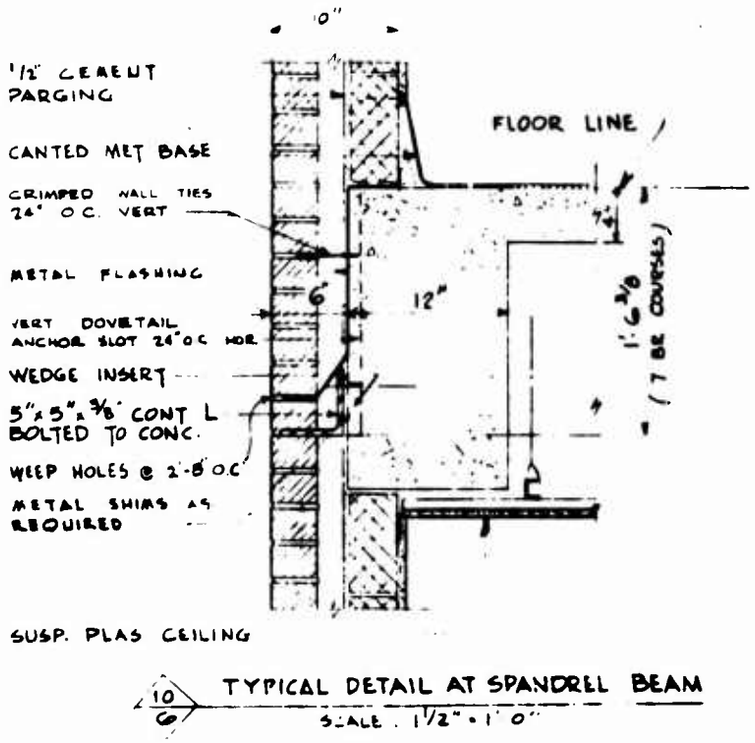

Figure 24. Outside Wall Detail, Landis Hospital.

by metal angles embedded in the reinforced concrete spandrel beam; the inner tier of concrete masonry units arches at top and bottom within the R/C frame itself. There are vertical frame members only at every other cross partition along the "front" outside wall, i.e., the wall at the bottom of the page in Figures 22 and 23. The nonstructural interior partitions offer strong initial support to the outer wall, but arching is not assumed there; hence, the exterior front walls are treated in the analysis of blast response as "one-way arching" in a rigid frame. Figure 24 shows metal ties 24 in. on center vertically between the two tiers of the outer walls; this is not regarded as enough to transfer shear forces, and the two wythes are treated analytically as independent or additive; that is, the resistance to deflection is the sum of the two acting independently. Because both wythes are the same thickness, "failure" is equated to a deflection of the center of the wall equal to a brick width, i.e., 3.625 in.

The crushing or compressive strength for the outside walls, which, when arching within a rigid frame, determines the ultimate resistance of the wall to flexure, has been chosen to be that of type S field-prepared mortar, i.e., 1600 psi.[28] (This value is also approximately that for the concrete masonry unit itself, but the clay brick is stronger in compression than mortar.) Except for the variations in window sizes, all the outside walls are the same structurally. Because most of the windows occupy such a relatively large portion of the wall areas, the walls themselves have been treated as one-way, i.e., the support given to the walls by adjacent edges is not considered. The resistance function of an outside wall of the Landis building is computed as the sum of the individual resistances of two identical tiers, each 3-5/8 in. thick, 1600 psi in compressive strength, modulus of elasticity 1×10^6 psi, and density equal to the sum of brick and concrete masonry units, i.e., 109.2 pcf, plus 48.3 pcf or 157.5 pcf. (Taking wall thickness equal to that of a single tier ensures that the collapse criterion will be correct during calculation and adding the densities of the two tiers then makes the inertial mass correct. Were the two tiers capable of bending as a unit, i.e., were the metal ties capable of transmitting shear forces

between tiers, then the total resistance of the wall to flexure would be considerably higher than merely the sum of the resistance of each wall singly. Using the sum is equal to considering the two tiers as SDOF systems in parallel, i.e., that the ties maintain the distance between the tiers fixed, so that the deflection of the two SDOF systems are equal.)

Inside Walls

To some extent the behavior of the outside walls depends on the response of the interior walls. Should the inside walls remain in place long enough to hold the backfilling pressure against the inner surfaces of the outside walls for an appreciable time, then the outside walls will appear stronger than if the interior walls disappear immediately and open up the whole interior space to blast pressure. In its present form, BRACOB will remove the interior walls at any preset time after blast arrival at the wall, but it cannot now analyze the inside walls for response to airblast. In the case of the Landis Hospital, it does not appear that the interior partitions have significant structural strength, except as shear walls (i.e., in resisting loads applied in the direction of their long axes) and except insofar as they have mass to be moved out of the path of the airblast. Therefore, building response has been analyzed two different ways: first, all interior walls remain intact throughout the calculation, and second, interior walls are removed instantly at blast arrival. The corresponding difference in response of the outside walls is measureable, but not large. Although no attempt has been made to pinpoint it exactly, the "incipient collapse overpressure" under the first assumption is higher than under the second. When interior walls are kept in place, the front walls reach failure deflection at a loading applied by a 1-psi head-on blast between 48 and 50 ms after blast arrival; furthermore, they are at that time being pushed weakly outward by the slightly higher inside pressure; on the other hand, without the presence of the interior walls, but with the same incident blast conditions, the front walls fail at 39 ms, when they are still accelerating inwardly. Departure speeds of the center of mass of the front wall fragments vary somewhat from room to room, depending

on wall span, room volume, and window area, but under the first assumption these speeds vary from 6.04 to 7.15 fps (1.84 to 2.18 m/s). Under the second assumption about the behavior of the interior walls, the variation is from 11.45 to 12.4 fps (3.49 to 3.79 m/s).

Because each window in the front wall occupies such a large portion of its wall, the failure pattern will be close to that sketched in Figure 25. The four fragments will most likely be temporarily "hinged" at their outer edges, that is, will tend to rotate initially about the edge. Under such circumstances, their trajectories will take them into collision with a ceiling, sidewall, or floor, all of which structural elements are very likely to be still in place at the time of collision with the front wall debris. The effect of this debris mass on these surfaces is not clear at this time. The impacts represent transient loadings in excess of design capacities.

Collapse Scenarios

The collapse of walls and creation of wall debris in the Landis Hospital are described by means of the foregoing techniques.

The Landis Hospital is regarded as a typical large urban building found outside the earthquake zones of the United States. With small changes in details, the scenarios presented here are expected to be similar to the airblast responses of nearly all buildings of this class.

Two observations about the Landis Hospital are appropriate, however. First, the exterior walls are relatively weak. Even the assumption of full arching in a rigid frame does not raise their strength significantly because each tier is so thin. A 4-in. thick, unreinforced masonry wall does not resist airblast; even adding two of them together does not create a good blast shelter. Second, the relatively large windows in the south and north elevations* permit a rapid buildup of interior pressure in the first tier of rooms, but the relatively large open spaces on the

*Airblast approaching from either the south or north will have almost the same effect on Landis Hospital.

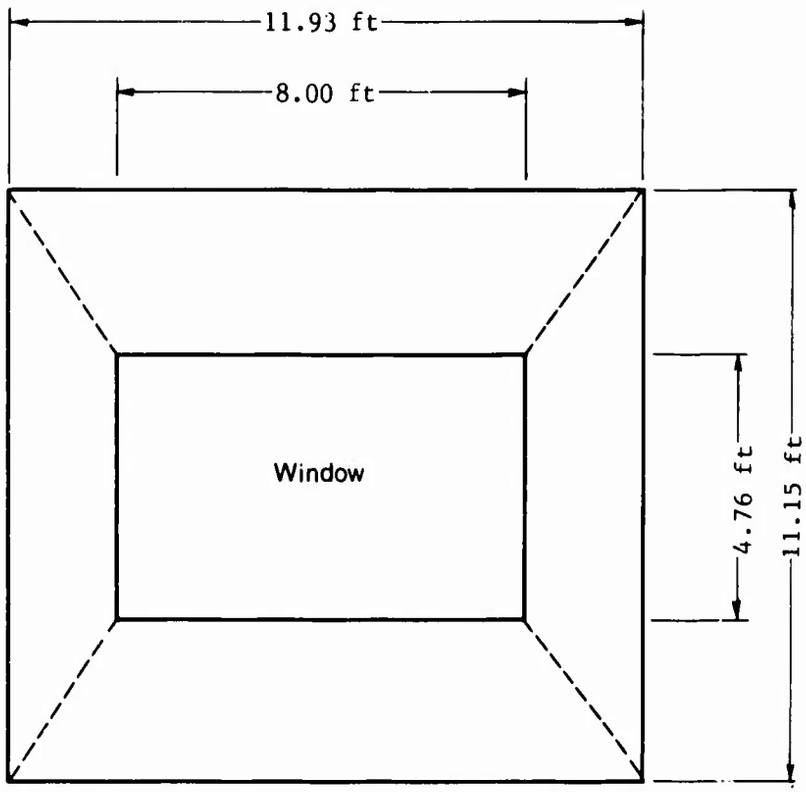

Figure 25. Assumed Failure Pattern of Typical Wall, South Elevation, Landis Hospital.

far side of the first tier of rooms means that net pressure on some of the interior walls becomes large enough to break their connections to the frame and convert them into debris, although the interior walls themselves may remain intact for some time (as described in Gabrielsen et al.[11]) The interior walls are similar both in method of anchorage and in construction to interior walls exposed to low-pressure airblast in the URS shock tunnel during the early 1970s.[11] Figure 26 is taken from the construction drawings for Landis Hospital to illustrate the interior walls.

The most nearly comparable panels tested in the URS tunnel were made of metal studs covered with 4-in. sheetrock, fastened to the rock tunnel wall with explosively driven studs. These examples were tested at only two peak incident overpressures, 1.7 and 3.5 psi. The results were reported in the form of photographs before and after and measured displacement histories. These walls apparently travelled outward from their original positions as single units, at least for several feet. Displacement histories for the two pressures are shown in Figure 27 (Gabrielsen et al.[11]). Figure 27 also contains two conjectural histories for 1 and 30 psi, calculated from the reported data by simple interpolation (a procedure that essentially neglects the strength of the fasteners). The conjectural curves in Figure 27 will be used later in the analysis.

Certain major events and conditions are predicted as a nuclear-derived airblast impinges directly against the south elevation, reflects and diffracts around the structure, and finally sweeps through the interior. For the purposes of this discussion, the airblast originates in the explosion of 1 MT on the surface. Incident pressures are restricted to 1 and 30 psi, providing two extremes in response.

The influence of backloading on the collapse of the outside walls of the south elevation is clarified by Figures 28 and 29. In both figures the exterior-reflected pressure as a function of time is shown by Curve A. In Figure 28 the interior pressure within the first tier of rooms (e.g., Room Number 2 in Figure 23), shown by Curve B, rises to its peak in approximately 30 ms at which time inside room pressure surpasses outside pressure slightly. However, enough momentum is imparted to the wall by the short-lasting blast impact that the wall fails later

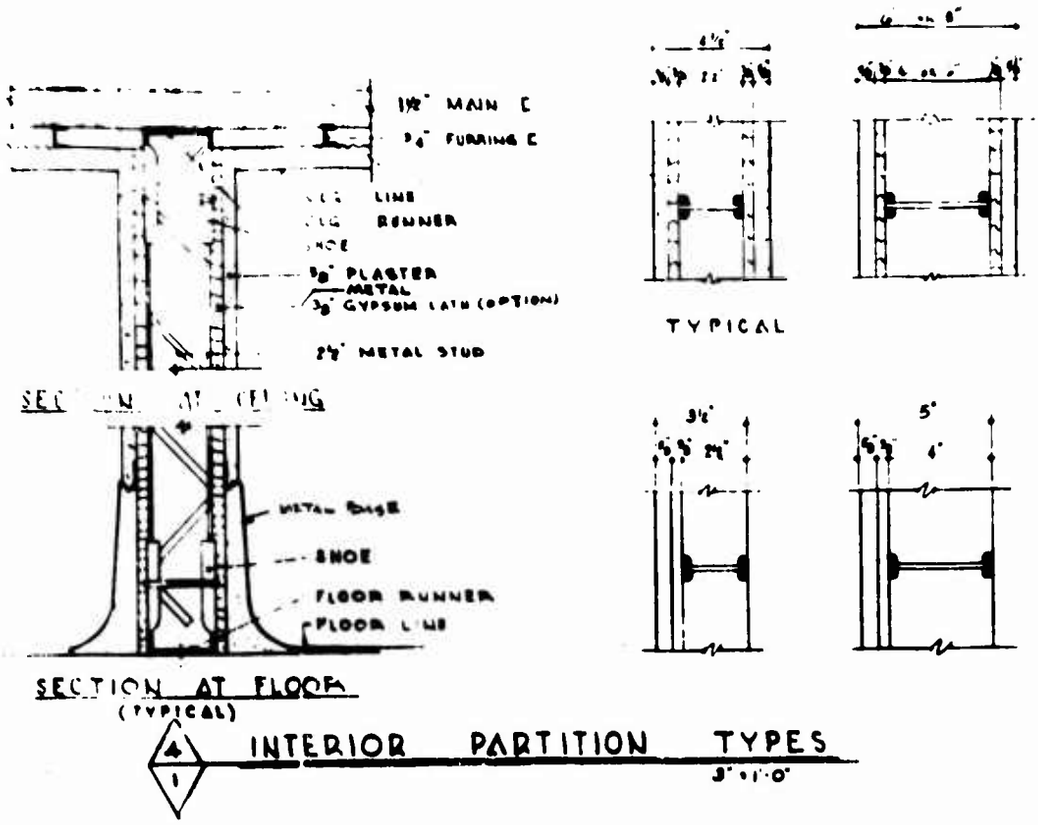

Figure 26. Interior Wall Detail, Landis Hospital.

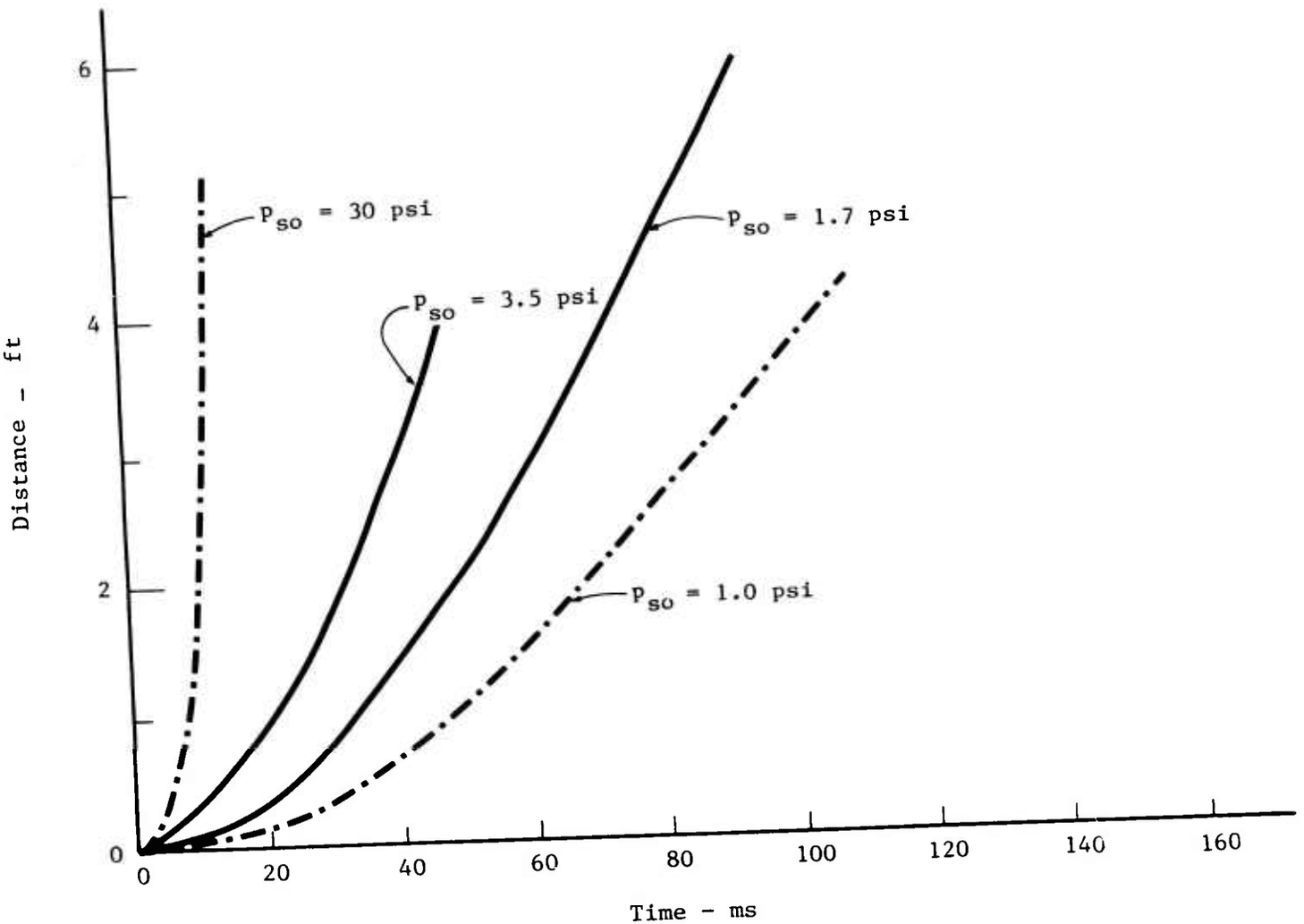

Figure 27. Displacement of Interior Partition as a Function of Time.

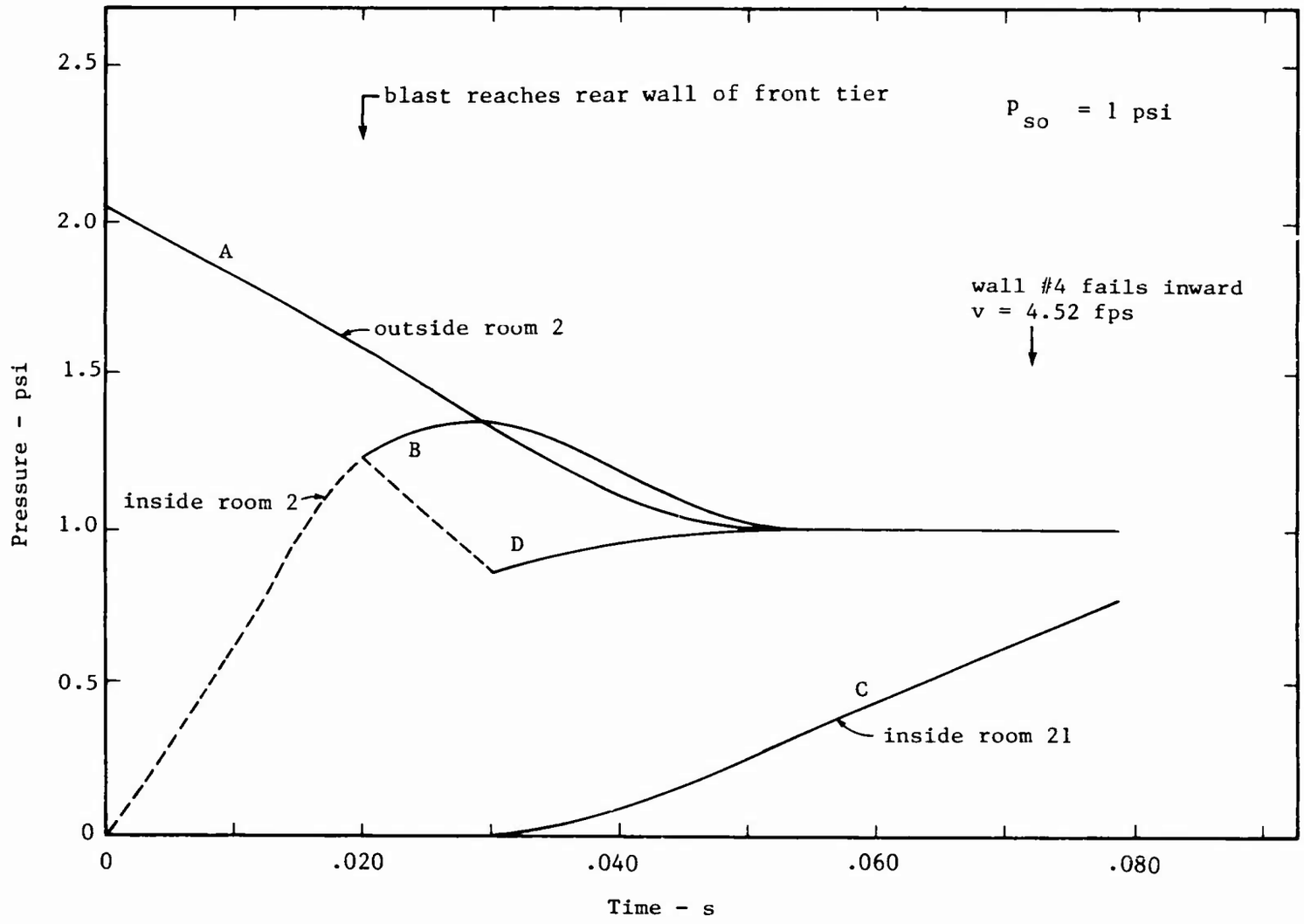

Figure 28. Interior and Exterior Pressures, Landis Hospital, All Walls Present, P_{so} = 1 psi.

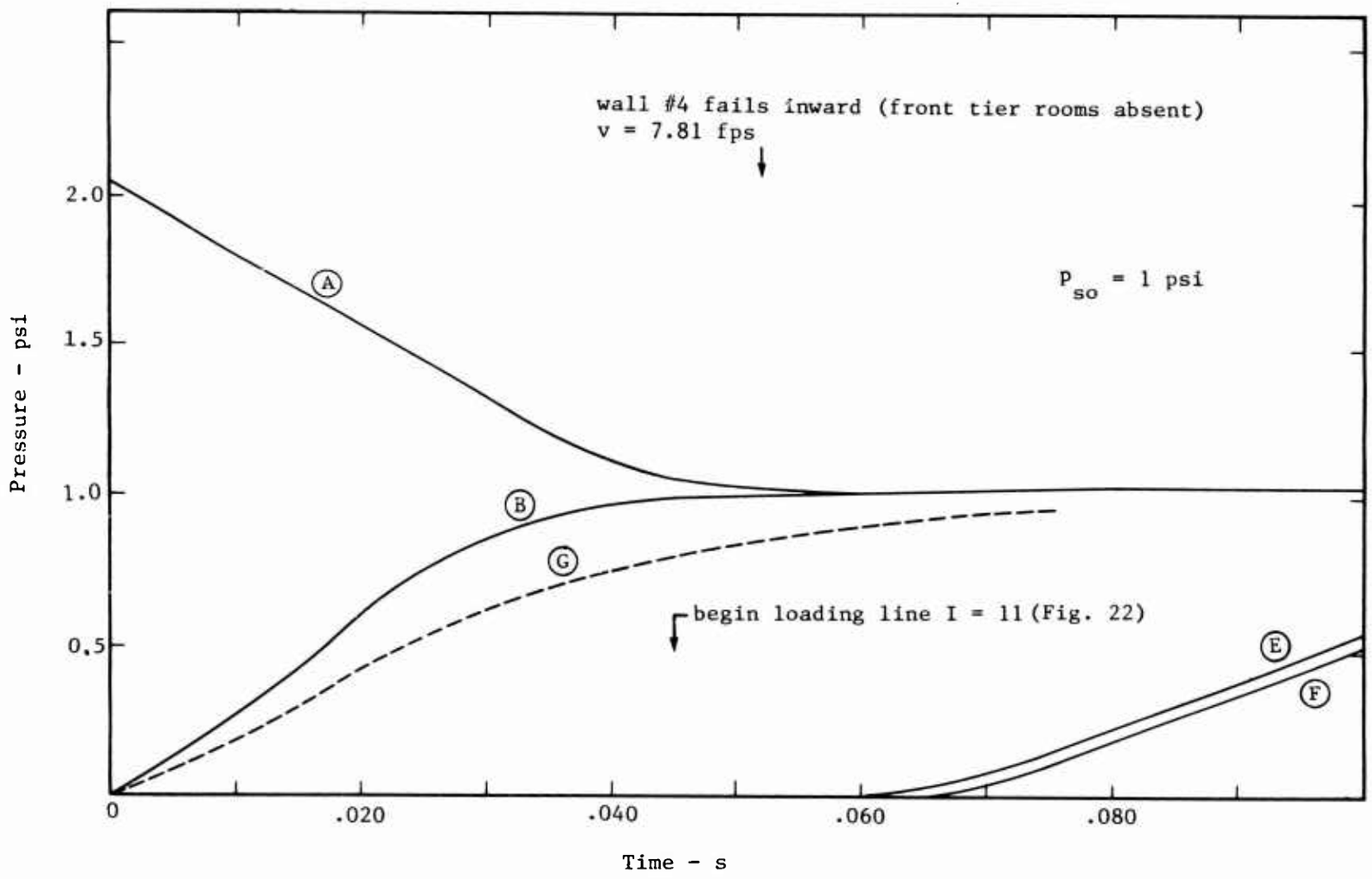

Figure 29. Interior and Exterior Pressures, Landis Hospital Front Rooms Removed, P_{so} = 1 psi.

at approximately 72 ms with an inward speed of 4.52 fps. In Figure 29 the interior pressure has been calculated for the case of no interior walls in the front tier of rooms. The initial floor plan for this calculation is represented in Figure 30. Under these conditions the backloading is still rising as late as 55 ms, and the high net pressure (i.e., Curve A less Curve B) collapses the outside walls in the south facade at approximately 52 ms and imparts speeds of 7.81 fps. Probably neither of the two Curves B is correct because of the presence of the interior walls in the front rooms for a portion of the time during exterior loading. It is conjectured, based partly on the work reported in Gabrielsen et al.,[11] that the interior partitions break their anchorages at least as soon as the pressure differential across them reaches 1 psi and that at that moment equalization of air pressure between the front tier of rooms and the open spaces behind them begins. In Figure 28, the computed pressure in this open space (designated as Room 21 in Figure 23) calculated by assuming the presence of all interior walls is shown by Curve C. Clearly, backfilling into Room 21 does not occur fast enough to prevent failure of most of the interior walls in the front tier of rooms (Numbers 1 through 20 in Figure 23).

Curve D in Figure 28 represents the backloading against the front exterior walls under the assumptions that at approximately 20 ms the exposed interior walls start to move out of the way of the air last entering through the front windows, and that at 30 ms the pressure is equalized throughout the area indicated as Room 1 in Figure 30. (The shear walls supporting the 13 individual front walls in the south elevation are replaced by pilasters in the calculations based on Figure 30.) Using a net load equal to Curve A less Curve D, response of the front walls can be calculated. It is clear the calculation will predict the conditions of exterior front wall collapse between those given in Figures 28 and 29. In estimating debris formation and distribution, an average will be used, i.e., failure at 62 ms and fragment speed* equal to 6.16 fps.

---

*The speed of the center of mass of the fragments.

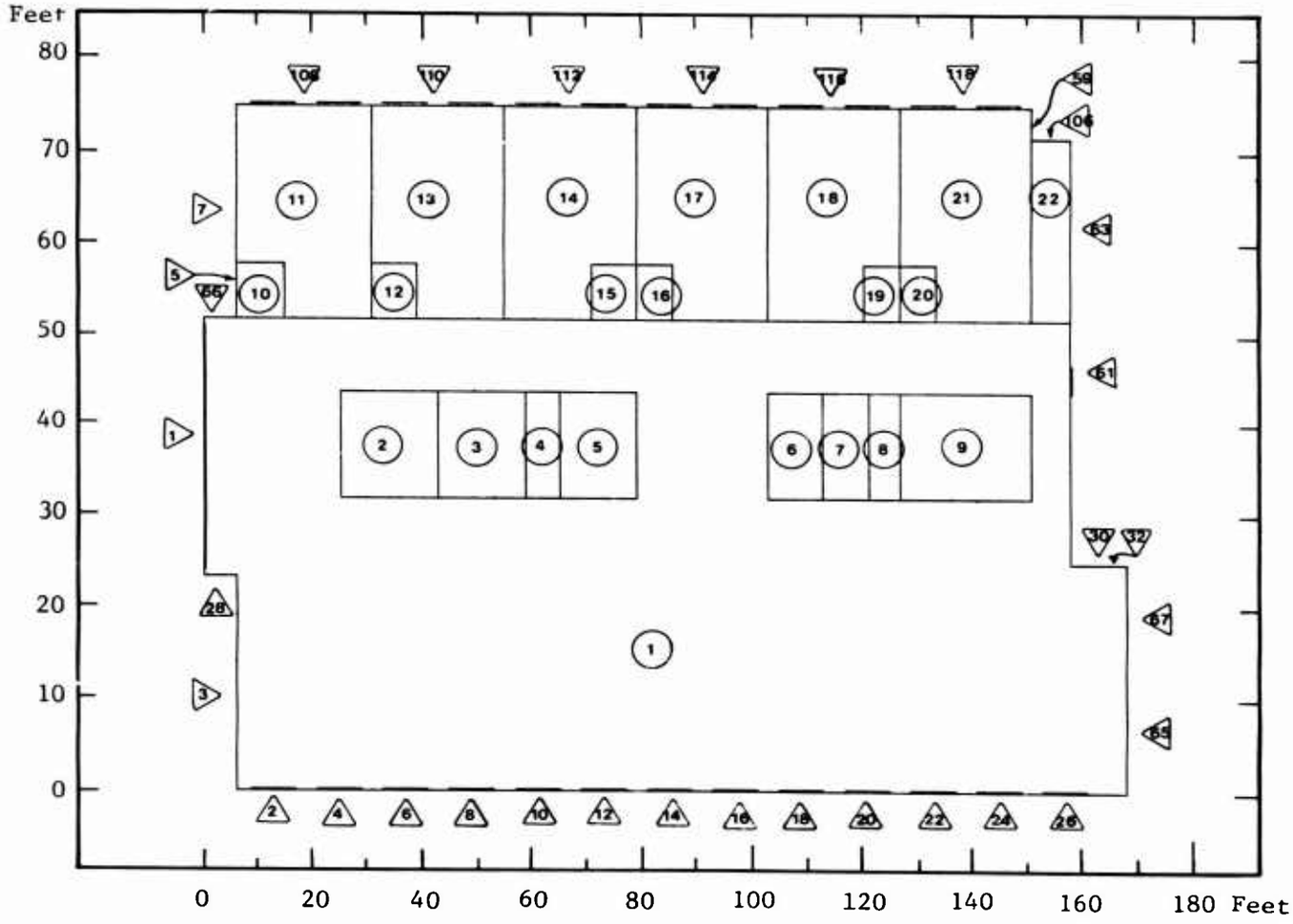

Figure 30. Special Initial Floor Plan, Landis Hospital.

The rooms in the central core (Numbers 2 through 9 in Figure 30) will most likely disappear soon after the blast reaches them, unless there are large openings in the walls, in which case they may survive the diffraction phase to perish in the later drag phase.

No loading of an interior wall can begin before the blast wave can reach it; hence, the earliest any load can be expected against the interior walls defining the rear tier of rooms (along Line I = 11 in Figure 22) is 45 ms. However, after this time, the pressure builds up much faster on the south side of this line of partitions (facing the oncoming blast) than it does on the north side, facing downstream. This is shown in Figure 29 by the two Curves E and F, which represent the outside and inside* pressures, respectively, in the rear tier of rooms (Numbers 10 through 21 in Figure 30). Evidently the interior and exterior pressures remain nearly in equilibrium because of the relatively slow outside buildup and the large windows in the north facade. It is presumed that the interior partitions separating the rear tier of rooms from the rest of the floor will fail at a time between 60 and 70 ms, and pressure within those rooms will rise to the values given in Figure 29 by Curve G. Under these conditions, the outside walls of the north facade are predicted to collapse outward at time equal to 170 ms with a departure speed of approximately 3.4 fps. The floor is thus completely opened to airblast at a time when the free-field static pressure still has 95 percent of its peak value. Further downrange translation of wall debris can be expected.

Because of the temporary shielding of the interior offered by the front tier of rooms, under certain conditions some side walls may fail as well as the forward and backward facing walls. For example, Wall Number 5 (Figure 30), will not be backloaded until the partition line I = 11 ceases to block blast pressure. Calculations show that Wall Number 5, without backloading, fails inward at 103 ms. However, as noted above, Wall Line 11 may well become ineffective before 103 ms, in which case the motion of Outside Wall Number 5 will be slowed, if not reversed. At 1 psi incident pressure, all exterior sidewalls either do not fail during

* Assuming inside pressure rises due to filling through windows in the north facade.

the period covered by calculations to date, or do so marginally, as Wall Number 5.

The comparable analysis for an incident overpressure of 30 psi presents a much faster moving version of the same picture as the analysis for p_{so} = 1 psi. The pressures responsible for the destruction are depicted in Figure 31. Curves A and F represent the two exterior pressure histories, A against the south facade and F against the north facade. The remainder of the curves in Figure 31 show interior pressures calculated under various assumptions. Curve B is the backloading against the south facade, assuming all the interior walls are in place and act as effective barriers to rapid pressure rise. The insignificant level of the backloading pressure contrasted to the exterior pressure means almost instantaneous collapse of the south facade; in the south facade, calculation shows failure 6 ms after blast arrival and a speed of departure of the center of mass of the wall fragments equal to 111 fps. The interior walls defining the front tier of rooms disappear within a few milliseconds because they are significantly loaded by simple room filling through the windows in the south facade; the advent of the high reflected pressure against the south facade upon failure of that facade at approximately 16 ms will shear the connections of the interior panels within much less time than the same task required during the URS tunnel tests.[11] The conjectural displacement history corresponding to p_{so} = 30 psi in Figure 27 suggests a separation from the frame equal to 1 ft within 10 ms of blast arrival at the partition. Because the exterior blast front reaches the grid line I = 11 at approximately 25 ms, the surge of high pressure resulting from the failure of the south facade may be expected at the interior partition line I = 11 about 10 ms later or at time equal to 35 ms. This is before any backfilling of the north tier of rooms can begin (shown by Curve D in Figure 31) and after average interior pressure in the remainder of the floor has reached approximately 10 psi (Curve E). Again, the interior partition line at I = 11 will cease acting as a pressure barrier within 10 ms, admitting high pressure at that time to the rear tier of rooms. This high pressure is between values given by Curves A and C, that is, an order of magnitude higher than the backfilling pressure entering through the windows in the north facade. The exterior walls of the north facade then

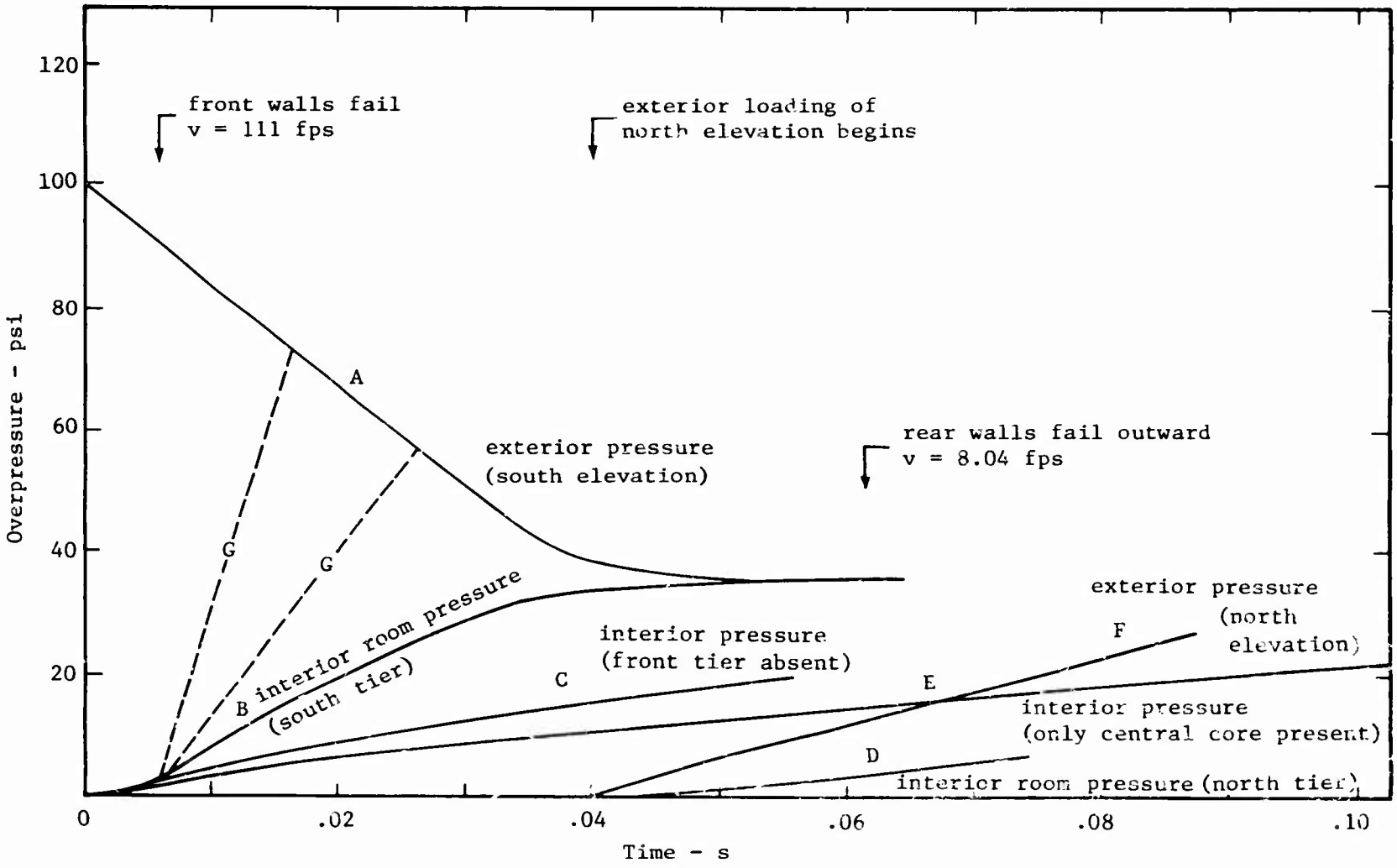

Figure 31. Pressures, Landis Hospital at p_{so} = 30 psi

begin their response to the 30-psi blast by moving inward as the blast engulfs the building, but almost immediately their acceleration is reversed because of the rapid buildup of interior pressure and these exterior walls ultimately collapse outward. Current estimates place the time of failure in the north facade at 62 ms and outward speed of the fragments at 8 fps.

North and south exterior wall failure data are summarized in Table 5.

The behavior of the shear walls at 30 psi is not so clear. Under the influences of ordinary room filling through the windows in the south facade and blast loading as the front passes down its length, the two first-loaded shear walls (Numbers 3 and 117 in Figure 23) move inward and fail at 23 and 17 ms, respectively, and with speeds of 27 and 40 fps, respectively. However, the front wall opens up after 6 ms and interior pressure in the front tier of rooms rises more rapidly than shown in Curve B; in fact, the effective pressure increase is probably similar to that suggested by the two Curves G in Figure 31. However, even the steeper of the two Curves G will not reverse the ultimate inward failure of the shear walls in the fron tier of rooms, although the wall speed at failure will depend on the exact assumption regarding interior pressure.

Calculation suggests that the behavior of the front outside shear walls is typical of their class at p_{so} = 30 psi. Unless it becomes evident from further experimentation, interior blast loading does not appear rapid enough to halt the strong inward motion imparted to outside shear walls by the initial blast impact. Walls Number 1 and 109 fail inwardly, for example, at 32 ms with computed speeds near 45 fps. Such a computation admittedly is based on ordinary room-filling and does not allow for blast removal of exterior walls; but the time of failure is so early and the speed so high that it is not likely to be reversed.

Inward failure of shear walls does not necessarily imply inside deposition of shear wall debris,[20] a subject that will be discussed later.

Table 5

FAILURE OF EXTERIOR WALLS, LANDIS HOSPITAL

Yield = 1MT HOB = 0

Peak Free-field Pressure (psi)	South Elevation	North Elevation
1	Inward	Outward
	v_1 = 6.16 fps	3.4 fps
	t_c = 62 ms	170.0 ms
30	Inward	Outward
	v_1 = 111. fps	8.0 fps
	t_c = 6 ms	62. ms

v_1 = speed of departure of fragments

t_c = time of structural failure

Fragment Distribution, p_{so} = 1 psi

After the failure of the exterior walls in the south elevation there is continued flow into the building as the blast finds its way deeper into the interior. Such flow helps carry the fragments of the failed walls, but the major contributor to their momentum at this time is still the previous impact of the air blast.

The flow stream has been established around the structure. There are only weak or short-lasting pressure differentials within the building itself. However at some time a flow path is opened up through the building; this will occur after the failure of the north exterior walls at 170 ms makes a connection between the high pressure on the south and the relatively low pressure on the north. Gradually a flow pattern through the building will be established. This extremely complicated process will be represented in these simplified calculations by a hiatus of zero flow immediately after the failure of the southern external facade followed by free-field flow beginning after the failure of the northern facade is communicated to the upstream facade of the building by a sound signal. At 1 psi under standard conditions sound speed is 1150 fps; the building is 76 feet wide; so that the delay in establishing flow after failure of the northern facade will be assumed to be 66 ms. Thus the front wall fragments will travel for 170 + 66 - 62 = 174 ms without acquiring momentum from air flow. Fragments at the northern facade will do the same for twice 66 ms or 132 ms after failure. Upon expiration of the hiatus classical air blast flow appropriate to the adjacent free-field environment will be assumed to translate the fragments.

Calculation with DEBRIS shows that during the hiatus the south wall fragments translate approximately 0.6 ft downstream, fall approximately 0.5 ft toward the floor and rotate 40 degrees. Since the fragments will soon strike interior structures such as the floor, shear walls and ceiling, the precise orientation at any time is not important, and the translation distances during the hiatus are clearly negligible. In calculation of the further displacement of the fragments from the front wall the greatest uncertainty lies in the choice of parameters characterizing

the concrete floor for the purposes of the DEBRIS code. No experimental data are known from which to deduce values for the spring constants, viscosity and friction. Since the horizontal ground spring seems to be most useful in representing rough terrain rather than smooth surfaces, it will not be incorporated into the calculations of front wall debris transport. The vertical spring should presumably be stiff; thus k_{gl} will be set equal to 0.35×10^9 dyne/cm. Friction and viscosity will be unchanged from the values $\mu = 0.5$ and $\eta = 3000$ g/s. Initially, no consideration will be taken of the presence of other debris within the building nor of the possible further breakup of the four individual fragments into which the wall is assumed to have broken by the blast impact. (The fragmentation pattern is that of Figure 25.)

Detailed results of calculations with DEBRIS show that, after resumption of classical air blast flow through the building, the south exterior wall fragments fall into the concrete floor 4 to 7 ft inside the wall depending on origin* and that none of these fragments under the present assumptions advances further than 2 ft from the point of impact. The fragments of the northern exterior wall fall directly into the ground outside the building and even under the assumptions used for the simulation of the concrete surface these fragments do not bounce more than a few inches. This behavior appears to be due to the simultaneous absence of strong rotation and strong dynamic pressure at the time of impact. (A fragment rotating into a surface has, as noted before, the opportunity to be propelled upward by the compressive ground spring after which it may be caught and rotated further by blast wind, if any exists at that time.) Downrange transport from the sixth floor varies from 6 to 15 ft; from the ground floor, 3 to 6 ft.

---

* the top fragment in Figure 25 travels a foot or so farther than the others.

Fragment Distribution, p_{so} = 30 psi

The disposition of the south and north exterior wall fragments resulting from the impact of a 30 psi blast is quite different from what is described above for a 1 psi blast.

The time scale of events is compressed approximately an order of magnitude and wall debris is carried completely out of the building. Flow through the building is established early and the interior partitions being much lighter than but offering the same area as the heavy masonry exterior walls are swept ahead.

The southern external walls fail structurally at approximately 6 ms.

Each fragment, top, side and bottom, is immediately driven into a boundary of the room, i.e., the floor, a partition or the ceiling. The bottom fragment, for example, is flat on the floor 41 ms after blast arrival and after travelling only 3 ft downrange. The calculations with DEBRIS show the fragment bouncing up to reach within 370 ms a height at which the center of mass is approximately 2.5 ft above the floor. During the upward motion the fragment turns over slightly more than two times and travels downstream 72 ft. Such behavior is not realistic for the fragment as a whole because it will almost certainly break up on violent contact with the concrete floor. Whether or not the individual masonry units composing the fragment will tend to bounce that high or not is not known at this time. However at the peak of the bounce the center of mass has a speed of 41 fps and the blast wind is still blowing strongly. Considerable further downrange translation is to be expected, although the fragment has travelled almost to the north exterior wall line during the single bounce.

At p_{so} = 30 psi sound speed is 1375 fps so that simulated time to establish throughflow at the south facade after failure of the north exterior walls is 55 ms. Translation of south wall fragments in a classical blast will commence at 61 ms; and at the north exterior wall such movement will begin at 172 ms.

It is probably more realistic to calculate the transport of the bottom south wall fragment as due to the sliding of individual masonry units over the concrete floor; surprisingly, when this is done from the point of first fragment impact with the floor, and attributing the speed of the fragment to the individual unit, the net horizontal transport is essentially the same, that is, the individual units reach the north wall line at approximately 340 ms. Their motion is a tumbling.

The top south wall fragment may strike the ceiling and be deflected downward into the floor; that possibility has not been examined in a DEBRIS simulation as yet. In the absence of a ceiling the simulated transport of the top fragment takes it well past the northern facade, as shown in Figure 32. From the sixth floor, the fragment hits the ground (at time equal to 2.75 s) after the end of the positive phase of dynamic pressure, and travels less than 10 ft after impact. The total downrange transport in this example is 677 ft. Surface parameters supposedly appropriate to earth have been used, e.g., $k_{gl} = 0.20 \times 10^{8}$ and $k_{ghl} = 0.35 \times 10^{10}$ dyne/cm. The comparable fragment in the south wall of the first floor hits the ground outside the north facade at approximately 1.5 s, which is before the dynamic pressure positive phase ends at 2.67 s, but again, this fragment travels over the ground only a comparably short distance. The first floor top fragment travels approximately 300 ft through the air before striking the ground and comes to rest 355 ft from its origin (Figure 32). In these cases of limited post-impact transport it is probably not important to know how the fragment breaks up on impact.

Trajectories of the top exterior wall fragments from the first and sixth floors of the north wall are depicted in Figure 33.

The great contrast between Figures 32 and 33 is surprising. The north wall fragments depart later with a slower speed than the south wall fragments (Table 5), yet the total downrange transport shown in Figure 33 is twice that in Figure 32. The more slowly moving fragment is lofted higher and carried farther than the initially fast moving fragment. The explanation lies in the initial rotation assumed for these arching

exterior wall fragments. The piece of wall that breaks away early with a high speed rapidly rotates out of the attitude which is optimal for lofting in the blast wind. The small arrows in Figure 33 indicate the attitude of the fragment in the locations shown. In Figure 32 the angular speed is 13 times its value in Figure 33. The realism of the simulation in this case remains to be demonstrated.

As suggested above, the behavior of the exterior shear walls is speculative at this time. If, as seems likely, they fail during the initial inward motion and if they subsequently do not arch during the sharp increase in interior pressure, they will be flexed inward at the time classical flow is established through the structure. Such an initial posture will result in translation of most wall debris downstream and outward.

The progress of debris movement in the Landis Hospital at 1 and 30 psi is described in Table 6. Since at p_{so} = 30 thermal irradiation is still underway during events tabulated, there is a column to show the fraction of total irradiation received at each time at the 30 psi contour.

Table 6. Timing of Blast Events, Landis Hospital (ms)

Event	Incident Overpressure (psi) 1	30	Fraction of Total Thermal Irradiation at 30 psi
Blast at south facade	0.	0.	.350
South exterior wall fails	62.	6.	.351
Blast at I = 3*	20.5	17.	.353
Blast at I = 11	45.	25.	.355
Collapse at I = 11	55.	35.	.357
South exterior frags on floor		41.	.358
Blast at north facade	65.	55.	.360
North exterior fail	170.	62.	.362
South exterior frags @ I = 3		170.	.382
South exterior frags @ I = 11		270.	.401
South exterior frags @ I = 14		337.	.414
South exterior top frag on floor	1000.	—	
South exterior bottom frag stop		—	

* See Figure 22.

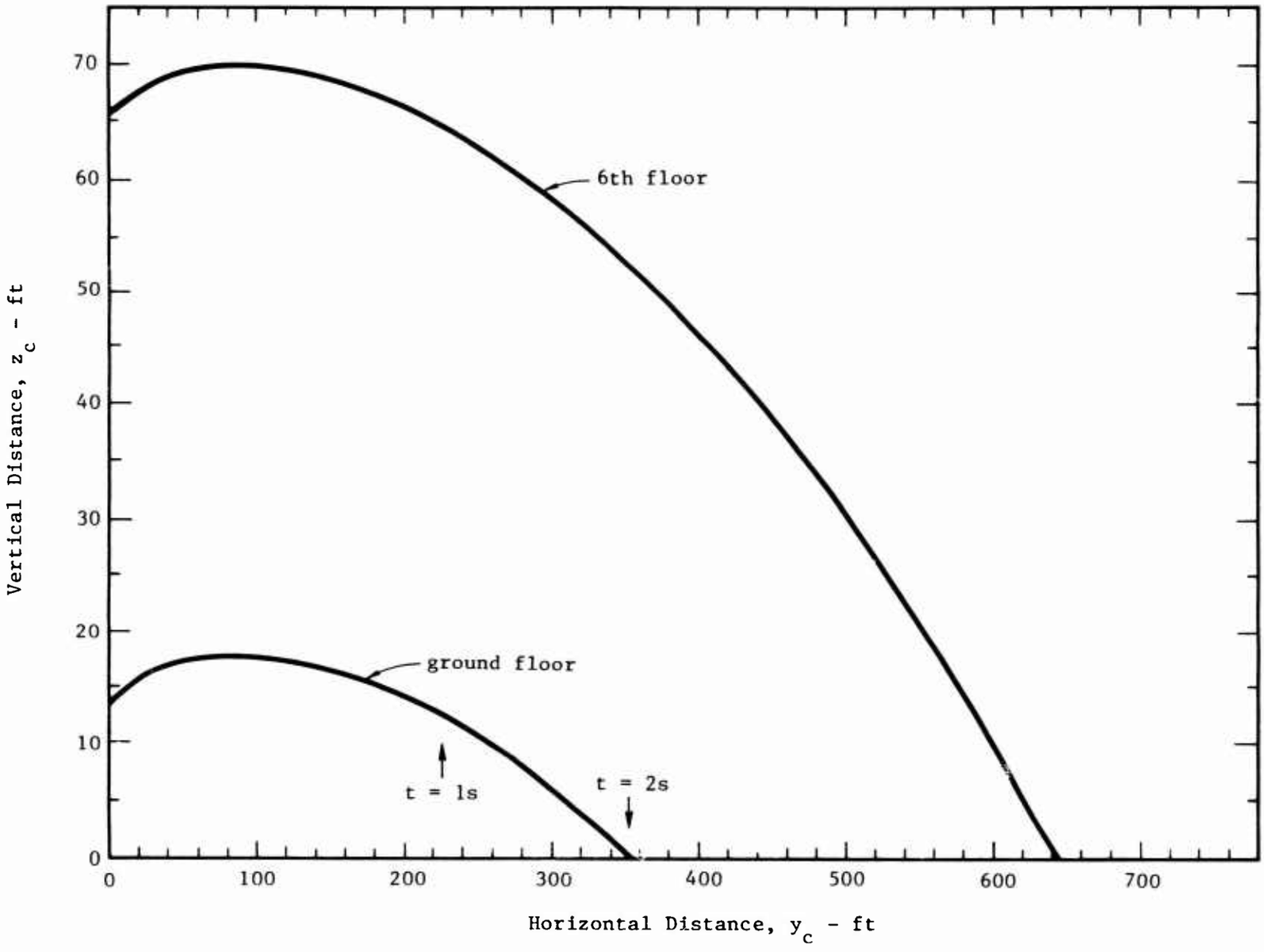

Figure 32. Trajectories, Top South Wall Fragments, p_{so} = 30 psi.

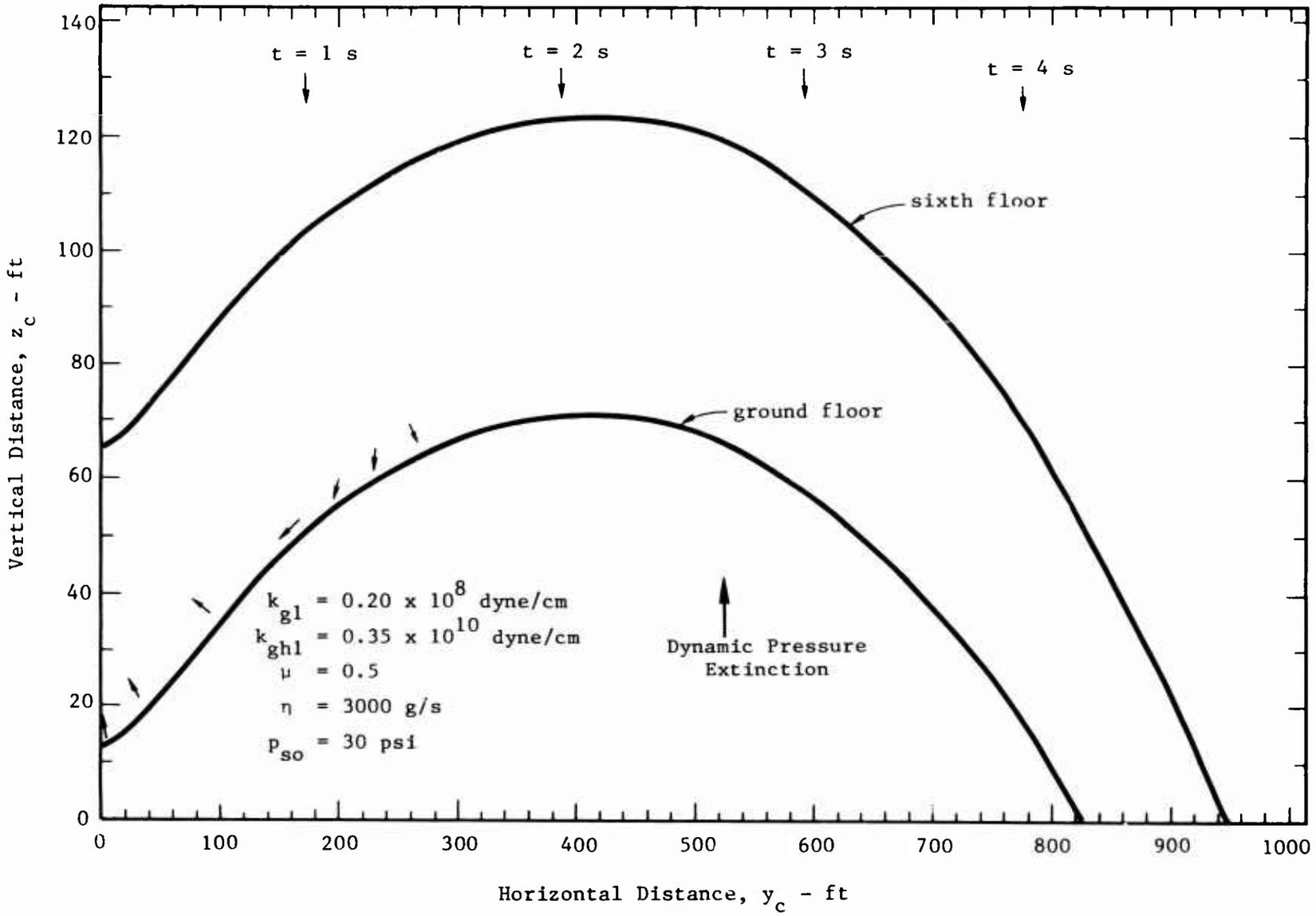

Figure 33. Trajectories, Top North Wall Fragments, p_{so} 30 psi.

CONCLUSIONS AND RECOMMENDATIONS

Over-the-ground transport of heavy objects by blast can be successfully simulated by calculation provided different parameter values are chosen for the three different kinds of motion, i.e., bouncing, tumbling and sliding. In bouncing transport the object strikes the ground from a height and is carried further downwind; by tumbling motion is meant a rolling movement from a position initially on the ground. In sliding motion the object does not rotate or lose contact with the ground. The first two kinds have been quantitatively observed in experiment and simulations are in satisfactory agreement with observations, although there is insufficient data to develop a relation between the nature of the ground surface and parameter values.

The simulation BRACOB has been enlarged and adapted to apply to a large urban building with only modest increases in running time on the IBM 3033 computer, and the system has been organized into separately compilable modules so that changes can be introduced with a minimum of recompilation. Capability to treat walls arching in a frame has been added. When combined with the debris transport simulation and applied to a weak walled building, it appears to provide the temporal and spatial resolution required by fire researchers.

Just to accurately describe the debris field in a collapsing building requires improvements in the simulations, but perhaps more importantly at this juncture attention needs to be given to defining the elements of the debris environment of special importance to the incidence and development of fire. Wall debris is certainly one of the important elements but so, very likely, are debris arising in furnishings and special air flow patterns within the collapsing building. This may be a good point in this research to introduce these considerations.

Both DEBRIS and BRACOB require improvement. It was originally intended that fragments be of any shape and there is provision in the DEBRIS code for defining arbitrary shapes but this feature has never been implemented and tested. This is most urgent in satisfactorily treating the so-called "side" wall fragment, the trapezoidal shape of which may be important. Also the code does not handle without error blast impact from the side, i.e., an angle of 90 degrees. Some debugging is needed in existing code. But the most pressing deficiency is further data for adjustment of the simulation parameters, particulary to describe the interaction with concrete surfaces. Some further attention should also be devoted to additional checking of the airborne phase of the transport against existing data, such as the small scale Bell Laboratories models at PRAIRIE FLAT.

BRACOB is in need of enhancement with regard to the removal of interior partitions which should be automatic when the pressure differential across the partition reaches a certain preset value.

After the data from MILL RACE have been examined, both DEBRIS and BRACOB might be enhanced to take into account new understanding on reinforced concrete wall debris, establishment of flow through a collapsing building and the behavior of exterior shear walls at high pressures. BRACOB presently drops calculation of wall response after it "fails" structurally; this may be premature from the point of view of debris distribution. High internal pressures within a room may bend or flex a "failed" wall, in which case its disposition as debris may differ from the present treatment.

Finally, before the effects of debris distribution on fire can be understood, other categories of urban buildings must be examined in the way this study has examined the Landis Hospital. For example, the unreinforced masonry building is important in the eastern United States and its lack of a supporting framework will make the behavior of the floor structures different from what has been assumed in this study. Reinforced concrete wall panels must be treated.

LIST OF REFERENCES

1. Edmunds, J.E., C. K. Wiehle, and K. Kaplan, "Structural Debris Caused by Nuclear Blast," URS 639-4, Contract No. OCD-PS-64-19, URS Corporation, Burlingame, CA (October 1964).

2. Rotz, J. V., J. E. Edmunds, and K. Kaplan, "Effects of Fire on Structural Debris Produced by Nuclear Blast," URS 639-9, Contract No. OCD-PS-64-19, URS Corporation, Burlingame, CA (January 1965).

3. Rotz, J. V., J. E. Edmunds, and K. Kaplan, "Formation of Debris From Buildings and Their Contents by Blast and Fire Effects of Nuclear Weapons," URS 651-4, Contract No. B-70924 (4949A-20)-US, URS Corporation, Burlingame, CA (January 1966).

4. Rotz, J., Debris Model Research With Building Damage, Fire Spread, and Debris Predictions for Five-City Study, URS 651-8, Contract No. B-70924 (4949A-20)-US, URS Corporation, Burlingame, CA (March 1967).

5. Edmunds, J.E., "Structural Debris and Building Damage Prediction Methods," URS 686-5, URS Research Co., Burlingame, CA (June 1968).

6. Witt, E., "Blast Transport of Debris from Scale Model Buildings," Defense Nuclear Agency, Bell Telephone Laboratories, Inc., Engelwood NJ (January 1979).

7. Warren, R. E., "Debris Studies Compendium," U.S. Army Ballistic Missile Defense Systems Command, Bell Laboratories, Inc., Engelwood, NJ (September 1974).

8. Warren, R., "Tree and Automobile Debris/DIAL PACK Event," Defense Nuclear Agency, Bell Laboratories, Engelwood, NJ (August 1973).

9. Taylor, B., "Blast Effects of Atomic Weapons upon Curtain Walls and Partitions of Masonry and other Materials/Operation Upshot Knothole Project 3.29," Federal Civil Defense Administration (August 1956).

10. Gabrielsen, B. and C. Wilton, "Shock Tunnel Tests of Arched Wall Panels," URS Research Co. for Defense Civil Preparedness Agency (December 1974).

11. Gabrielsen, B., C. Wilton and K. Kaplan, "Response of Arching Walls and Debris from Interior Walls Caused by Blast Loading," URS Research Co. for the Defense Civil Preparedness Agency (February 1975).

12. Wilton, C. and B. Gabrielsen, "Shock Tunnel Tests of Preloaded and Arched Wall Panels," URS Research Co. for the Defense Civil Preparedness Agency, June 1973.

13. Wiehle, C. K., and J. L. Bockholt, "Existing Structures Evaluation, Part I: Walls," Office of Civil Defense, AD687 293, Stanford Research Institute, Menlo Park, CA (november 1968).

14. Wiehle, C. K., and J. L. Bockholt, "Existing Structures Evaluation, Part IV: Two-way Action Walls," Office of Civil Defense, AD 719 306, Stanford Research Institute, Menlo Park, CA (September 1970).

15. Wiehle, C. K., and J. L. Bockholt, "Blast Response of Five NFSS Bldgs," Office of Civil Defense, AD 738 547, Stanford Research Insitute, Menlo Park, CA (October 1971).

16. Wiehle, C. K., and J. L. Bockholt, "Dynamic Analysis of Reinforced Concrete Floor Systems," Defense Civil Preparedness Agency, AD768 206, Stanford Research Institute, Menlo Park (May 1973).

17. Wiehle, C. K., "All-Effects Shelter Survey System, Summary of Dynamic Analysis of 25 NFSS Buildings," for Defense Civil Preparedness Agency, Stanford Research Institute, Menlo Park, CA (March 1973).

18. Wiehle, C. K. "Summary of the Dynamic Analysis of the Exterior Walls and Floor Systems of 50 NFSS Buildings," Defense Civil Preparedness Agency, Stanford Research Institute, Menlo Park, CA (June 1974).

19. Beck, J.E., "Summary of Dynamic Analysis of Selected NSS Buildings," Federal Emergency Management Agency, SRI International, Menlo Park, CA (April 1980).

20. Rempel, J. R., "Debris Distribution as a Parameter in Blast/Fire Interaction," Federal Emergency Management Agency, SRI International, Menlo Park, CA (June 1980).

21. Warren, Robert E., Bell Laboratories (private communication, 1979).

22. Fletcher, E. R. and I. G. Bowen, "Blast-Induced Translational Effects," Annals of the New York Academy of Sciences, Vol. 152, Art. 1, pp. 378 - 402 (October 1968).

23. Fletcher, E. R. and I. G. Bown, "Blast-Induced Translational Effects," Defense Atomic Support Agency, DASA 1859, Lovelace Foundation for Medical Education and Research, Albuquerque, NM (November 1966).

24. Weast, R.C. and M. J. Astle, eds., "CRC Handbook of Chemistry and Physics," 61st edition, The Chemical Rubber Co., Cleveland, OH, 1981.

25. Rempel, J. and C. K. Wiehle, "Collateral Air Blast Damage," Defense Nuclear Agency, SRI International, Menlo Park, CA (April 1978).

26. Rempel, J. R., "Collateral Air Blast Damage," Defense Nuclear Agency, SRI International, Menlo Park, CA (July 1980).

27. Beck, James E., et al, "Single Degree of Freedom Evaluation," U.S. Air Force Weapons Laboratory, AFWL-TR-80-99, SRI International Menlo Park, CA (March 1981).

28. Wiehle, C. K., J. R. Rempel and J. E. Beck, "Middle North Series DICE THROW Event, Dynamic Response of Two Types of German House Construction," Defense Nuclear Agency, POR 6966, SRI International, Menlo Park, CA (October 1978).

29. Rempel, J. R., "Collateral Air Blast Damage," Defense Nuclear Agency, DNA 4948Z, SRI International, Menlo Park, CA (April 1979).

Appendix

CHARACTER OF THE SIMULATED AIRBLAST

Original location of the fragment is specified by a free-field overpressure along with weapon yield. (Height of burst is assumed zero in the work to date.) To convert this input value into range from ground zero (GZ), two methods have been used. The first makes use of the approximate relation,[A-1]

$$R = \left\{2A^2W/\left[2Ap_s + B^2 - \left((2Ap_s + B^2)^2 - 4A^2p_s^2\right)^{\frac{1}{2}}\right]\right\}^{1/3} \qquad \text{(A-1)}$$

in which side-on pressure p_s is measured in psi; radius R from GZ, in feet; $A = 3.152 \times 10^{12}$ and $B = 7.633 \times 10^6$; and W is in megatons. Recently, this expression for R has been evaluated only to obtain starting values in an iteration on the formula[A-2]:

$$p_s = \frac{10.47}{R_s^{1.22}} + \frac{2.9902}{R_s^{3.053}} - \frac{4.166}{1 + 0.6096\, R_s^{1.83}} - 0.2905 \qquad \text{(A-2)}$$

where R_s = scaled range, i.e., if W = weapon yield in megatons, then

$$R_s = R/10^4W^{1/3}$$

Unit of R_s is $kft/MT^{1/3}$. The differences between the predictions of these two methods are small, as shown in Table A-1. Neither formula is used outside the range of overpressure between 1 and 100 psi. Generalization of the implicit formula above to any height of burst is possible.[A-2]

With original range computed from given incident overpressure, DEBRIS at each subsequent time step converts distance travelled by the fragment since blast arrival into current range from GZ. If the direction

Table A-1. Comparison of Predictions of Pressure-Range Formula for W = 1 kt, HOB = 0.

Peak Overpressure p (psi)	Range R (ft)	
	Explicit formula	Iteration
10	1039.0	1031
20	735.4	726.5
30	608.8	601.0
40	535.2	528.4
50	485.6	479.5
60	449.3	443.8
70	421.2	416.2
80	398.6	394.0
90	379.8	375.6
100	364.0	360.0

cosine to GZ of the y-axis from the original position is c_y, R_o is original range, x_o and y_o are original coordinates, and x and y are current fragment coordinates, then current fragment range from GZ is written:

$$R^2 = (x - x_o)^2 + (y - y_o)^2 + R_o^2 - 2\cos(\pi - \alpha_1 + \alpha_2)R_o \cdot [(x - x_i)^2 + (y - y_o)^2]^{\frac{1}{2}}$$

$$\alpha_1 = \tan^{-1}[(x - x_o)/(y - y_o)]$$

$$\alpha_2 = \cos^{-1}(c_y) \qquad \text{(A-3)}$$

Although of most importance to debris translation is the character of the dynamic pressure that is responsible for quasi-steady drag of a free object, in some cases momentum imparted by the diffraction of the shock front around the fragment can be significant. When a wall is struck by blast, the diffraction episode is taken into account by computing the reflected pressure, clearing time, and back pressure caused by room-filling, if any exists. The wall response is computed in terms of displacement, velocity, and acceleration of an equivalent mass representing the wall fixed in its edge supports. After the wall is fragmented and is no longer supported, the diffraction episode is usually over and drag forces in the blast become responsible for translation of fragments. Other objects of interest become debris immediately upon blast arrival, e.g., furniture, automobiles, and the human body. In treating such objects, diffraction momentum must be separately calculated and entered into DEBRIS as initial conditions, i.e., as velocity at a certain time after blast arrival. Displacement during the diffraction episode is neglected.

Shock diffraction is a complicated phenomenon, but good estimates of its translatory effects upon initially free objects can be made with the help of simplified concepts. Essentially these amount to estimates of front and back pressures, the difference of which is the instantaneous net pressure. Consider a cube resting on the ground struck head-on by a blast wave of free-field static pressure, p_s. The peak pressure

against the front face, p_r, then becomes according to standard analysis

$$p_r = 2p_s(7P_o + 4p_s)/(7P_o + p_s) \qquad \text{(A-4)}$$

in which P_o = ambient pressure, 14.7 psi at sea level. Initially the back pressure is zero but after a time equal to shock transit time across the cube, back pressure begins to build up. During this same time, front face pressure is clearing. In fact to a first approximation the durations of these processes on opposite faces can be considered equal to each other and approximated by the standard formula:

$$t_c = 3S/c \qquad \text{(A-5)}$$

where S = clearing distance, i.e., one-half the cube edge ℓ, and c is either the sound speed in the reflected zone in front or in the ambient atmosphere behind the cube. Front and back pressure histories according to these very simple ideas are sketched in Figure A-1. The diffraction momentum, shown shaded in the figure, becomes the initial momentum for the object that starts moving at time $t = t_c + t_t$ where t_t is the transit time across the cube, i.e., $t_t = \ell/U$, where U = shock speed. As is evident in the figure the complex pressure clearing and buildup processes in front of and behind the cube are reduced to linear changes. In the case of a cube 1 ft on edge placed in the path of a 30-psi blast, initial momentum is estimated to be 187 ft-lb/s, which, for a cube weight of 65 lbs indicates a starting speed of approximately 2.9 ft/s at a time equal to 1.8 ms. Generally starting speeds of this amount are not important compared to the speeds gained during the drag phase.

In the few tests made so far, the effect of including shock diffraction has been to reduce or increase the total distance travelled by the initially free object, depending apparently on the original overpressure. At high overpressure (e.g., 50 psi), the diffraction episode in effect substitutes a relatively inefficient means of locomotion for drag pressure during a certain interval of time immediately after shock arrival. At low overpressure drag pressure declines dramatically and the diffraction of the shock may be a more effective means of accelera-

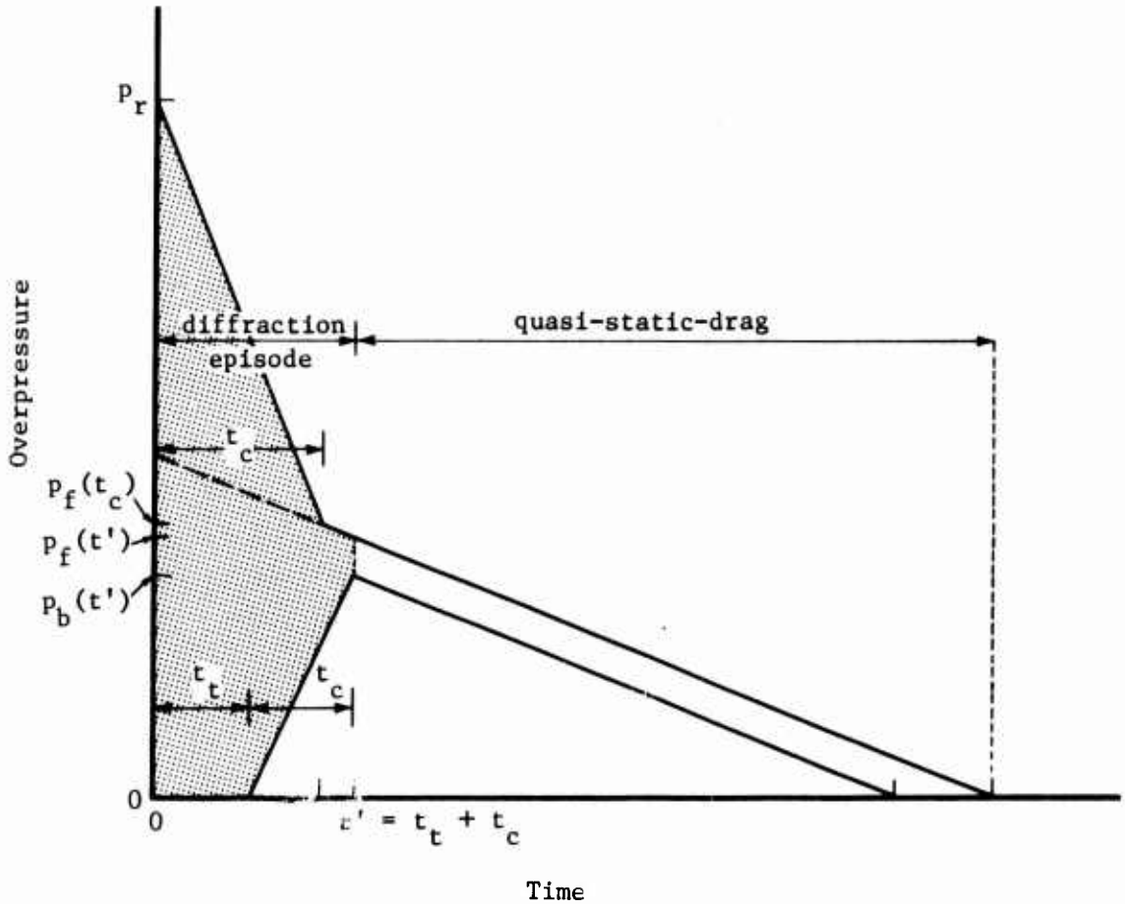

$$\text{Diff. Mom.} = \left(p_r - p_f(t_c)\right) \frac{3}{4} \frac{\ell}{c} + \frac{1}{2} \left(p_f(t_c) + p_f(t')\right) t' - p_b(t') \frac{3}{4} \frac{\ell}{c}$$

Figure A-1 Simplified Estimate of Diffraction Momentum.

ting the object. For example, the simulated concrete cube located originally at the 50-psi contour is transported approximately 6 percent less distance when it is started at 1.8 ms with a downrange speed of 4.8 ft/s. In contrast accelerating at 30 psi by diffraction increases distance traveled by approximately 6 percent, and at 15 psi, the simulated transport is increased 40 percent by diffraction. These results are suggestive only and some of the effect may in fact be caused by other differences in the calculations.

No cognizance has been taken of downward force of the blast against the ground springs through the object resting on the surface. Presumably were the surface perfect, the blast pressure would be effective in compressing the spring with or without the presence of the object and if the surface is slightly rough, the static air pressure would normally be present under the object.

To predict instantaneous dynamic pressure, q(t), in this research, two different empirical formulas have been used, which generally differ in their predictions by less than 10 percent. The first is based on simple curve fitting to the parameters in the equation[A-4]:

$$q(t) = Q_o \left(1 - \frac{t}{t_u^+}\right)^2 (d\ e^{-A} + (1 - d)\ e^{-B}) \qquad \text{(A-6)}$$

where Q_o is the peak incident dynamic pressure, i.e.

$$Q_o = 2.5\ p_s^2/(7P_o + p_s)$$

t_u^+ = duration of the positive dynamic pressure phase at current position

t = decay time of blast at current position

$A = \delta\ t/t_u^+$

and

$b = \phi\ t/t_u^+$

The parameters d, δ and ϕ are given as functions of static overpressure p_s in Table A-2. For the above formulation t_u^+ has also been treated as a numerical parameter and its values as a function of overpressure appear in Table A-2 also. Before it may be entered in the formula for q(t) however, t_u^+ must be scaled to the actual yield W (megatons):

$$t_u^+ = 10(t_u^+)_{tabular} W^{1/3} \tag{A-7}$$

The unit of q is the unit of p_s and p_o, but time t must be measured in seconds. From current fragment range, equation (A-2) supplies a value of incident peak overpressure with which to enter Table A-2. Blast decay time at current fragment position must be computed from shock travel time; at each time step, shock speed is computed from peak pressure at current position and divided into distance travelled during the time step. In this way shock travel time from the original position to each subsequent position of the fragment is available so that decay time at that location is simply the difference between current time and shock travel time. Thus all the quantities needed to evaluate q from equation (A-6) are available.

The second formulation of q(t), which is of more recent origin,[A-5,6,7] makes use of blast arrival time at the current blast location in order to determine the interval t_d during which the blast has decayed at the current fragment location, R. Corresponding to R, a value of peak free field peak overpressure is found as above, then by iteration a blast arrival time t_a is determined[A-5]:

$$p_s = 14843 \frac{(1 + .6715\ t_a + 0.004813\ t_a^2)}{(1 + 1.883\ t_a + 0.02161\ t_a^2)\ \ (0.0135 + t_a)} \tag{A-8}$$

As a starting value in this iteration t_a is approximated by[A-4]:

$$t_a = \left(\frac{p_s}{4}\right)^{-.906088} \tag{A-9}$$

Table A-2. Dynamic Pressure Waveshop Parameters as Functions of Static of Static Pressures.

P (psi)	2	3	4	5	6	7	8	9	10	15	20	25	30	40	50	60	70	80	90	100	150
d	0.86	0.87	0.88	0.88	0.89	0.89	0.89	0.90	0.90	0.90	0.90	0.92	0.94	0.95	0.95	0.95	0.95	0.93	0.88	0.86	0.68
δ	0.69	0.93	1.15	1.35	1.60	1.80	2.00	2.25	2.40	3.40	4.50	5.70	6.80	9.0	11.5	13.5	15.5	18.0	19.5	22.0	33.0
ϕ	8.4	10.7	12.8	14.5	16.0	17.5	18.8	20.0	21.5	27.0	33.0	37.0	41.0	49.0	56.0	63.0	70.0	75.0	82.0	88.0	113.0
t_u^+ (s)	0.355	0.355	0.315	0.300	0.285	0.280	0.270	0.265	0.255	0.230	0.245	0.265	0.275	0.285	0.290	0.290	0.290	0.285	0.280	0.275	0.265

If t_{ao} is the arrival time at the original position and t is the current problem time, then blast decay time at R is:

$$t_d = t_{ao} + t - t_a 10(2W)^{1/3} \qquad \text{(A-10)}$$

In the equation, the computed arrival time, t_a, has been scaled to equivalent yield W (megatons) of the surface burst.

The second formulation also makes use of an empirical expression for t_u^+ in terms of scaled range from a 1-KT surface burst:

$$t_u^+ = \left\{ \frac{(0.2455 - 0.0115\ R_s)}{(1 + 61.43\ R_s^6)} + \frac{(2.177\ R_s^3)}{(1 + 0.7567\ R_s^2) + (6.147\ R_s^3)} - 0.05546 \right\} 10(2W)^{1/3}$$

and

$$R_s = R/10(2W)^{1/3}$$

It is the ratio of t_d/t_u^+ that enters into the formula for q(t) as follows:

$$q(t) = Q_o' (R/R')^n \left[1 - \left(\frac{t_d}{t_u^+} \right)^2 \right] \qquad \text{(A-13)}$$

As before Q_o denotes the peak free-field dynamic pressure behind the shock front, but the primes make reference to the state at the current shock front. Hence,

$$Q_o' = \frac{2.5\ p_s'^2}{7P_o + p_s'} \qquad \text{(A-14)}$$

in which p_s' is computed from equation (A-8) above with arrival time equal to $t + t_{ao}$, scaled to 1-KT surface burst, i.e.:

$$t_a' = \frac{t + t_{ao}}{10(2W)^{1/3}} \qquad \text{(A-15)}$$

Once p_s' is found, the corresponding radius R' may be calculated from Equation (A-2) above.

The numerical term n is expressed in terms of current blast front radius R' scaled to 1 KT: i.e.,

$$n = 0.7917 + 11.04\ (R_s') + (14.37 + 6.291\ R_s')/(1 + 28.41\ R_s'^3)$$

and

$$R_s' = \frac{R'}{(W^{1/3})\ 10} \ .$$

At the present time the second formulation outlined above is not applicable to explosions not on the surface.

Sample plots of instantaneous dynamic pressure histories prepared according to the two different formulations set forth above are presented in Figure A-2. As can be seen, the differences are small. Peak static pressure is the parameter distinguishing the several plots; however, values of corresponding ranges are indicated in the figure.

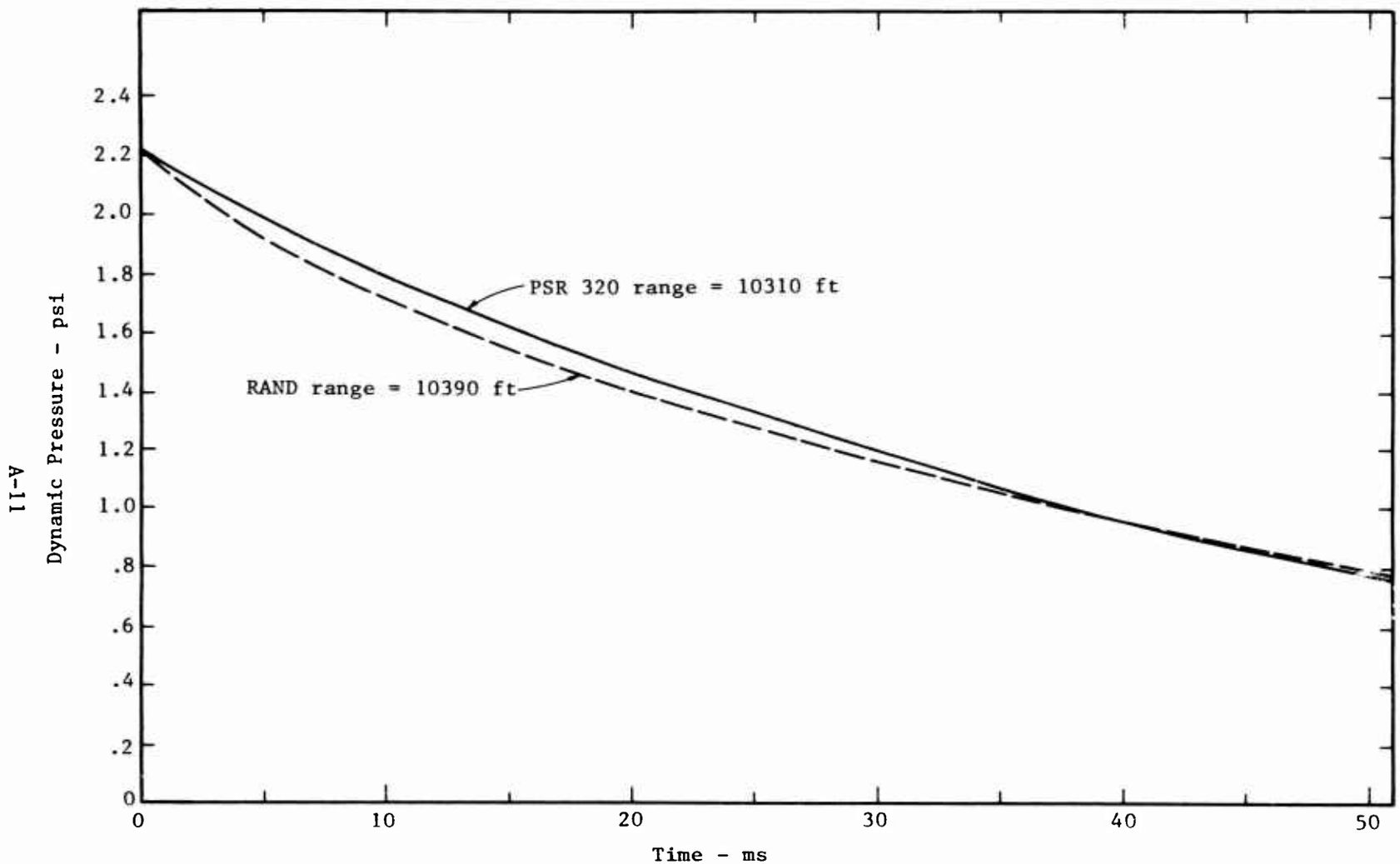

Figure A-2a. Comparison of Instantaneous Dynamic Pressure According to Two Different Emperical Formulations, P_{so} = 10 psi, (ranges correspond to W = 1MT, HOB = 0).

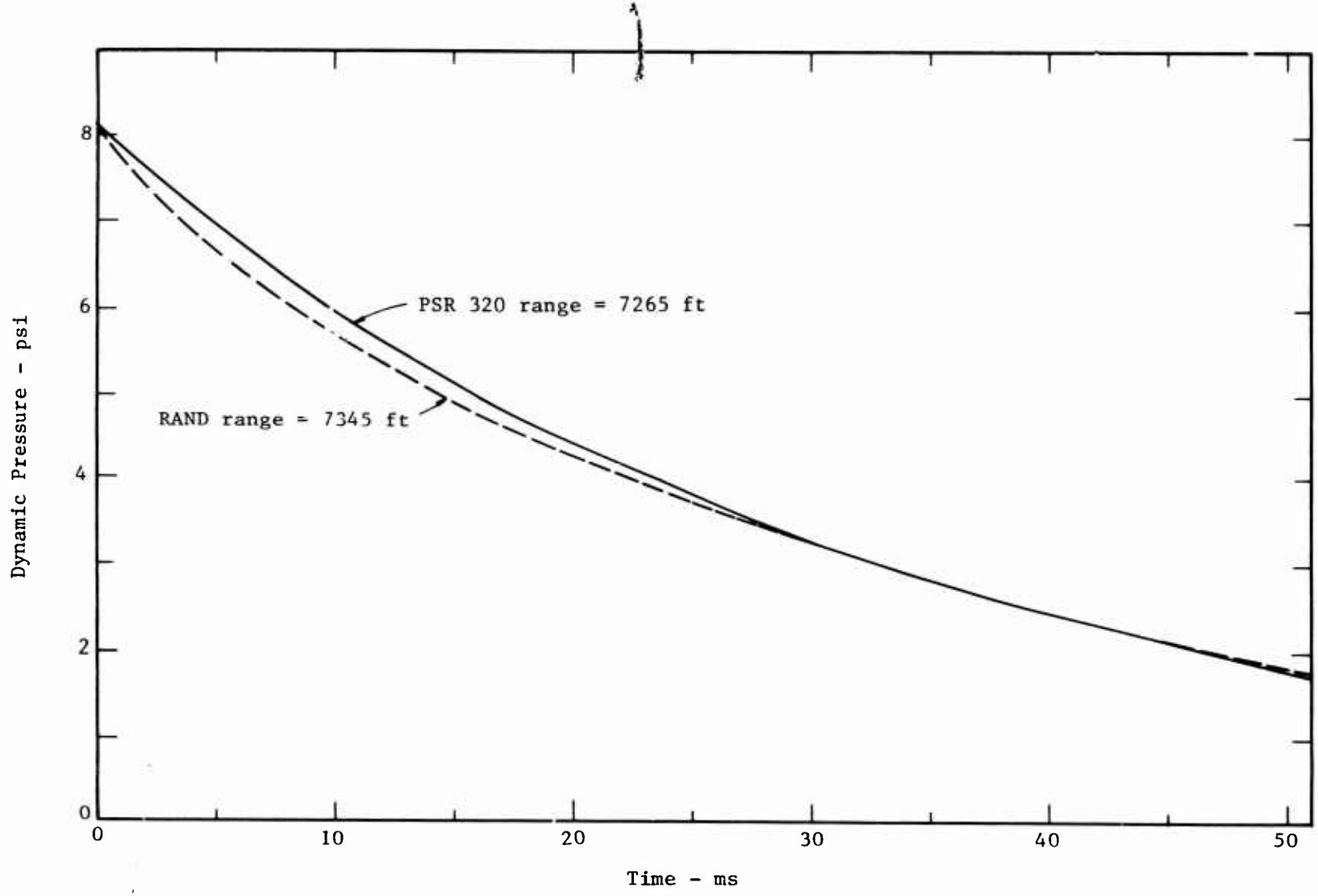

Figure A-2b. Comparison of Instantaneous Dynamic Pressure According to Two Different Emperical Formulations, P_{so} = 20 psi, (ranges correspond to W = 1 MT, HOB = 0).

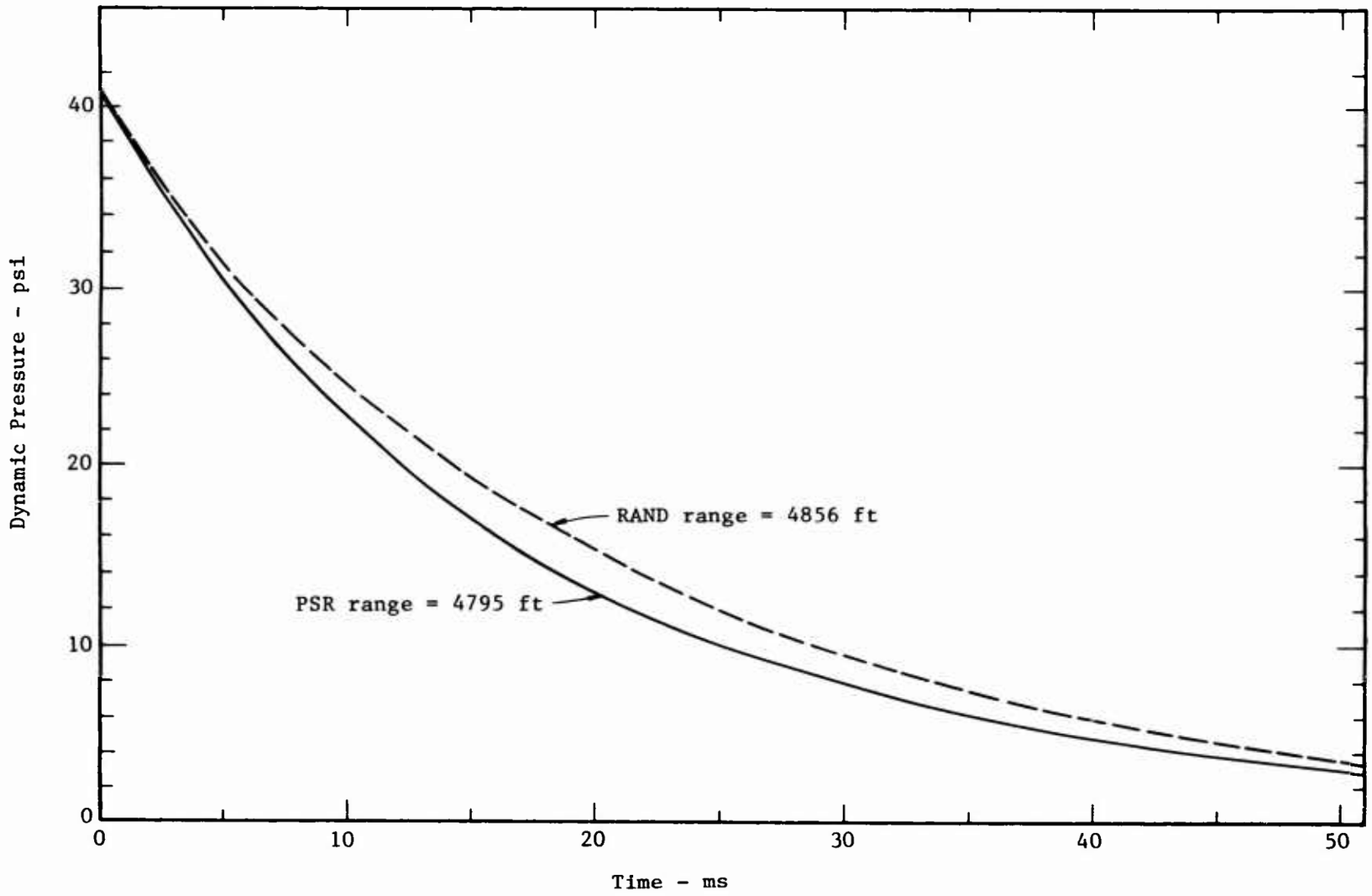

Figure A-2c. Comparison of Instantaneous Dynamic Pressure According to Two Different Emperical Formulations, P_{so} = 50 psi, (ranges correspond to W = 1 MT, HOB = 0).

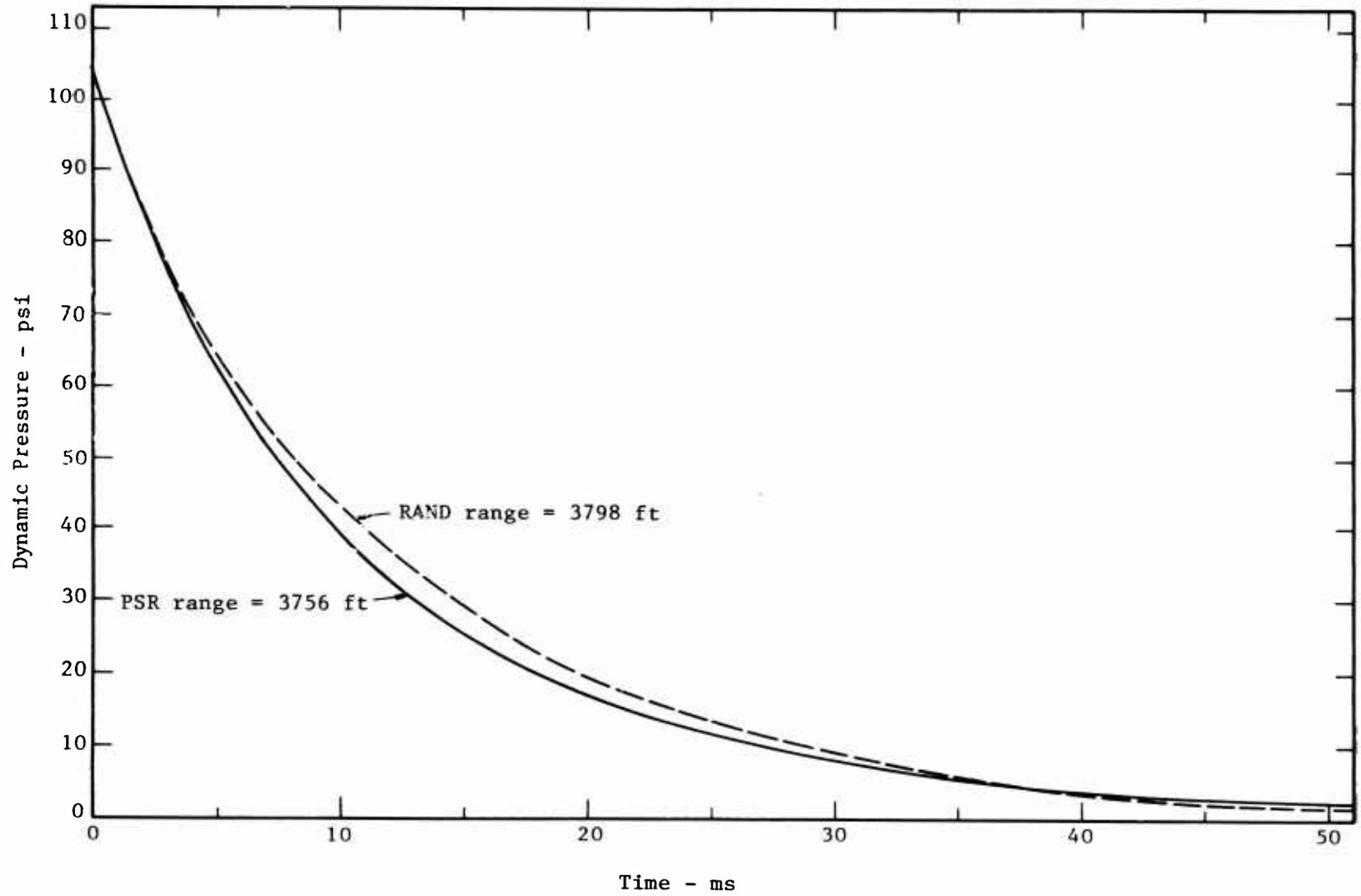

Figure A-2d. Comparison of Instantaneous Dynamic Pressure According to Two Different Emperical Formulations, p_{so} = 90 psi, (ranges correspond to W = 1 MT, HOB = 0).

APPENDIX REFERENCES

A-1. Beckham, Walter C., "Physical-Vulnerability Calculations for Nuclear Weapons Using DIA Green Book Methods," Lawrence Livermore Laboratory, January 1975 UCRL-51730.

A-2. Speicher, S. J. and H. L. Brode, "An Analytic Approximation for Peak Overpressure Versus Burst Height and Ground Range over an Ideal Surface," Pacific-Sierra Research Corp. for Defense Nuclear Agency, September 1980, PSR Note 336.

A-3. Glasstone, S. and P. J. Dolan, eds., "The Effects of Nuclear Weapons," U.S. Department of Defense and U.S. Department of Energy, Third edition, 1977.

A-4. Brode, H.L., "A Review of Nuclear Explosion Phenomena Pertinent to Protective Construction," RAND Corp, May 1964, R-425-PR.

A-5. Brode, H.L., "Height of Burst Effects at High Overpressures," Rand Corp. for Defense Atomic Support Agency, July 1970, DASA 2506.

A-6. "Analytic Approximation of Dynamic Pressure Versus Time," Pacific-Sierra Research Corp. for Defense Nuclear Agency, May 1980, PSR Note 320.

A-7. Brode, H. L., and S. J. Speicher, "Analytic Approximation for Dynamic Pressure Versus Time," Pacific-Sierra Research Corp. for Defense Nuclear Agency, May 1980, PSR Note 315.

MANDATORY STANDARD DISTRIBUTION LIST FOR RESEARCH REPORTS
(ALL PROJECTS)

(Number of Copies - One unless otherwise indicated)

Federal Emergency Management Agency 41
Office of Studies, Research & Development
ATTN: Administrative Officer
Washington, D.C. 20472

Assistant Secretary of the Army (R&D) 1
ATTN: Assistant for Research
Washington, D.C. 20301

Chief of Naval Research 1
Washington, D.C. 20306

Defense Technical Information Center 12
Cameron Station
Alexandria, Virginia 22314

Oak Ridge National Laboratory 1
ATTN: Librarian
P.O. Box X
Oak Ridge, Tennessee 37830

Mr. Phillip M. Smith 1
Associate Director,
Natural Resouces & Commercial Services
Office of Science and Technology Policy
Executive Office Bldg.
Washington, D.C. 20500

Los Alamos Scientific Laboratory 1
ATTN: Document Library
Los Alamos, N.M. 87544

The RAND Corporation 1
ATTN: Document Library
1700 Main Street
Santa Monica, CA 90401

AFWL/Civil Engineering Division
Kirtland Air Force Base
New Mexico 87117 — 1

Mr. Tom Kennedy
Defense Nuclear Agency
Washington, D.C. 20305 — 1

Pacific -Sierra Research Corp.
Attn: Harold L. Brode
1456 Cloverfield Blvd.
Santa Monica, CA 90904 — 1

Higgins, Auld & Associates Engineers
Attn: Cornelius J. Higgins
2601 Wyoming Blvd., Suite H-1
Albuquerque, New Mexico 87112 — 1

Center for Planning and Research, Inc.
2483 East Bayshore
Palo Alto, CA 94304 — 1

Mr. Kenneth Kaplan
Management Science Associates
P.O.Box 239
Los Altos, CA 94022 — 1

Stanley Martin
SRI International
Menlo Park, CA 94025 — 1

Laurence Pietrzak
Mission Research Corp.
735 State Street, P.O. Drawer 719
Santa Barbara, CA 93102 — 1

Fred Offensend
SRI International
Menlo Park, CA 94025 — 1

John Rockett
National Bureau of Standards
Center for Fire Research
Building 225, Room A17
Washington, D.C. 20234 — 1

Wilhelm Sjolin
Research Institute of National Defense
Forsvarets Forskningsanstalt
Stockholm 80, Sweden — 1

Dr. William F. Christian 1
Underwriters laboratories, Inc.
333 Pfingsten Road
Northbrook, Illinois 60062

Mr. W.L. Huff 1
USAE Waterways Experiment Station
Post Office Box 631
Vicksburg, Mississippi 39180

Mr. Richard Laurino 1
Center for Planning and Research
2483 East Bayshore
Palo Alto, California 94303

Mr. Joseph E. Minor 1
Texas Technological College
Lubbock, Texas 79408

Mr. Ashton M. Patterson 1
Canadian Defense Research Staff
2450 Massachusetts Ave., N.W.
Washington, D.C. 20008

Mr. Carl Wiehle 1
Defense Intelligence Agency
Attn: CKW DB-4C2
Washington, D.C. 20301

Dr. Steve J. Wiersma 1
Gas Research Institute
8600 W. Bryn Mawr Avenue
Chicago, IL 60631

Harvey G. Ryland 1
Ryland Research, Inc.
5266 Hollister Ave., Suite 324
Santa Barbara, CA 93111

Mr. Fred Sauer 1
Physics International Company
2700 Merced Street
San Leandro, CA 94577

The Dikewood Corporation 1
1008 Bradbury Drive, S.E.
University Research Park
Albuquerque, New Mexico 87112

Mr. J. Thomas Hughes 1
U.S. Fire Administration
Washington, D.C. 20230

Dr. Don Scheuch 1
430 Golden Oak Drive
Portola Valley, CA 94087

Dr. Geoffrey N. Berlin 1
National Fire Protection Association
470 Atlantic Avenue
Boston, Massachusetts 02210

Dr. Forman A. Williams 1
Department of the Aerospace
and Engineering Sciences
University of California San Diego
La Jolla, CA 03027

Mr. Leo A. Schmidt 1
Institute for Defense Analysis
Program Analysis Division
400 Army-Navy Drive
Arlington, VA 22202

Chief Joint Civil Defense 1
Support Group
Office, Chief of Engineers
Department of the Army
Attn: ENGMC-D
Washington, D.C. 20314

Director, U.S. Army Ballistic 1
Research Laboratory
Attn: Document Library
Aberdeen Proving Ground, MD 21005

Director, U.S. Army Engineer 1
Waterways Experiment Station
P.O. Box 611
Attn: Document Library
Vicksburgh, Mississippi 39180

Air Force Weapons Laboratory 1
Attn: SUL Technical Library
Kirtland Air Force Base
Albuquerque, New Mexico 87117

Civil Engineering Center/AF/PRECET 1
Wright Patterson Air Force Base
Ohio, 45433

Mr. Thomas Waterman 1
IITRI
10 W. 35th Street
Chicago, Illinois 60616

Emergency Technology Division 1
Oak Ridge National Laboratory
P.O.Box
Oak Ridge, Tennessee 37830
Attn: Librarian

Director 1
Lovelace Foundation
5200 Gibson Boulevard, S.E.
Albuquerque, New Mexico 87108

1

Department of Energy
Dept of Military Application
Washington, D.C. 20545

Technology & Management Consultants 1
330 Washington Street
Suite 613
Marina Del Rey, GA 90291

R&D Associates 1
Attn: Dr. Henry Cooper
1401 Wilson Blvd., Rosslyn, VA 22209

Director, Army Materials and 1
Mechanics Research Center
Attn: Technical Library
Watertown, Massachusetts 02172

Dr. Lewis V. Spencer 1
National Bureau of Standards
Room C313-Building 245
Washington, D.C. 20234

Mr. Samuel Kramer, Chief 1
Office of Federal Building
Technology
Center ofr Building Technology
National Bureau of Standards
Washington, D.C. 20234

Mr. William Parker 1
National Bureau of Standards
Room B66, Technology Bldg.
Washington, D.C. 20234

Mr. Thomas C. Goodale 1
SRI International
Menlo Park, CA 94025

Mr. H.L. Murphy 1
P.O.Box 1727
San Mateo, CA 94401

Mr. Walmer (Jerry) Strope 1
Center for Planning and Research, Inc.
5600 Columbia Pike
Baileys Crossroads, VA 22041

Mr. Don Sachs 1
Kaman Nuclear
Garden of the Gods Road
Colorado Springs, Colorado 80901

Prof. R.K. Pefley 1
University of Santa Clara
Santa Clara, CA 95053

Chief Robert G. Purington 1
Lawrence Livermore Laboratory
University of California
P.O.Box 808, L-519
Livermore, CA 94550

Mr. William Taylor 2
Ballistic Research Laboratories
Aberdeen Proving Grounds, MD 21005

Mr. Ronald Drzewoeclo 1
Calspan Corporation
P.O.Box 235
Buffalo, New York 15221

National Fire Protection Association 1
Library
470 Atlantic Avenue
Boston, Massachusetts 02210

Mr. Peter S. Hughes 1
Los Alamos Technical Associates, Inc.
P. O. Box 410
Los Alamos, New Mexico 87544

Fire Research Section
Department of Structural Research
Southwest Research Institute
8500 Culebra Road
San Antonia, Texas 78206 1

Factory Mutual Research Corp.
Attn: Dr. Raymond Friedman
1151 Boston-Providence Turnpike
Norwood, Massachusetts 02062 1

Mr. Edward L. Hill
Research Triangle Institute
Post Office Box 12194
Research Triangle Park, N.C. 27709 1

Mr. Arthur D. Caster
Chairman, Coordination Committee
on Civil Defense
American Society of Civil Engineers
2864 McFarlan Park Drive
Cincinnati, Ohio 45211 1

Mr. Norman J. Alvares
Lawrence Livermore Laboratory
Box 808, L-442
Livermore, CA 94550 1

Dr. Conrad V. Chester
Oak Ridge National Laboratory
P.O.Box X
Oak Ridge, Tennessee 37830 1

Mr. Marvin Drake
Scientific Applications, Inc.
P.O.Box 2351
1200 prospect Street
La Jolla, CA 92037 1

Professor A. Murty Kanury
Department of Aerospace and
Mechanical Engineering
University of Notre Dame
Notre Dame, Indiana 46556 1

Dr. Matthew G. Gibbons
5424 Lawton Avenue
Oakland, CA 94618 1

Naval Ship and Development Center 1
Attn: Mr. Tom Amrhein
Code 857
Washington, D.C. 20034

Command and Control Technical Center 1
Department of Defense
Room 2E312 Pentagon
Washington, D.C. 20301

Mr. A.P. Brackebusch 1
Forest Fire Research
Northern Forest Fire Laboratory
Missoula, Montana 59801

U.S. Forest Service 1
Attn: Dr. A Broido
P.O.Box 245
Berkeley, CA 94710

Dr. Ing P.G. Seeger 1
Forschungsstelle fur Brandschutztechnik
University of Karlsruhe (TH)
75 Karlsruhe 21
Postfach 63380
West Germany

Mr. Anatole Longinow 1
IIT Research Institute
10 West 35th Street
Chicago, Illinois 60616

Dr. Clarence R. Mehl 1
Division 1112
Sandia National Laboratories
Box 5800
Albuquerque, New Mexico 87185

Hudson Institute 1
Quaker Ridge Road
Croton-on-Hudson
New York, 10520

Richard Small 1
Pacific-Sierra Research Corp.
1456 Cloverfield Blvd.
Santa Monica, CA 90403

Raymond Alger
SRI International
Menlo Park, CA 94025 1

Geoffrey N. Berlin
National Fire Protection Association
470 Atlantic Avenue
Boston, Massachusetts 02210 1

Jana Backovsky
SRI International
Menlo Park, CA 94025 1

Tom Blake
Systems Science & Software
P.O.Box 1620
La Jolla, CA 92138 1

Craig Chandler, Director
Forest Fire & Atmospheric Science Res.
U.S. Forest Service
Department of Agriculture
Washington, D.C. 20250 1

Dr. John Cockayne
Senior Scientist
Science Applications, Inc.
1710 Goodridge Drive
P. O. Box 1303
McLean, VA 22101 1

Dick Foster
SRI International
1611 Kent Street
Arlington, VA 22209 1

Robert Fristrom
Applied Physics Lab/JHU
Johns Hopkins Road
Laurel, MD 20810 1

National Council & Radiation
Protection & Measurements
7910 Woodmont Avenue
Bethesda, MD 20014 1

Mr. John Rempel
Center for Planning and Research, Inc.
2483 E. Bayshore Road
Palo Alto, CA 94303 1

Mr. Irwin A. Benjamin 1
Building Research Division
National Bureau of Standards
Washington, D.C. 20234

Fire Research Library 1
National Bureau of Standards
Technology Building 225
Washington, D.C. 20234

U.S. Naval Civil Engineering Library 1
Attn: Document Library
Port Hueneme, CA 93041

Chief of Engineers 1
Department of the Army
Attn: ENGEME-RD
Washington, D.C. 20314

Mr. Howard McClennon, President 1
International Association of Fire
Fighters
815 16th Street, N.W.
Washington, D.C. 20006

The Information Center 1
Forest Fire Research Institute
331 Cooper Street
Ottawa Ontario
CANADA KIA 043

U.S. Army Training and Doctrine 1
Command
Fort Monroe
Hampton, VA 23651

U.S. Army Combined Arms Combat 2
Development Activity
Fort Leavensworth, KA 66027

Mr. Clay P. Butler 1
SRI International
Menlo Park, CA 94025

Dr. Francis E. Fendell 1
R1/1038
TRW
One Space Park
Redondo Beach, CA 90178

UNCLASSIFIED

DEBRIS DISTRIBUTION AS A PARAMETER IN THE BLAST/FIRE INTERACTION

by John R. Rempel

Improvements in the calculation of over-the-ground transport of solid objects by air blast have been made so that the DIAL PACK results are satisfactorily simulated with constant parameters over the range of incident pressures 15 to 100 psi. These calculations have then been combined with computational techniques for predicting unreinforced masonry wall collapse to derive an outline scenario for blast impact on an actual building at two incident overpressures, 1 and 30 psi.

September 1981
96 pages

Contract No. EMW-C-0311
FEMA Work Unit 2564G

UNCLASSIFIED

DEBRIS DISTRIBUTION AS A PARAMETER IN THE BLAST/FIRE INTERACTION

by John R. Rempel

Improvements in the calculation of over-the-ground transport of solid objects by air blast have been made so that the DIAL PACK results are satisfactorily simulated with constant parameters over the range of incident pressures 15 to 100 psi. These calculations have then been combined with computational techniques for predicting unreinforced masonry wall collapse to derive an outline scenario for blast impact on an actual building at two incident overpressures, 1 and 30 psi.

September 1981
96 pages

Contract No. EMW-C-0311
FEMA Work Unit 2564G

UNCLASSIFIED

DEBRIS DISTRIBUTION AS A PARAMETER IN THE BLAST/FIRE INTERACTION

by John R. Rempel

Improvements in the calculation of over-the-ground transport of solid objects by air blast have been made so that the DIAL PACK results are satisfactorily simulated with constant parameters over the range of incident pressures 15 to 100 psi. These calculations have then been combined with computational techniques for predicting unreinforced masonry wall collapse to derive an outline scenario for blast impact on an actual building at two incident overpressures, 1 and 30 psi.

September 1981
96 pages

Contract No. EMW-C-0311
FEMA Work Unit 2564G

UNCLASSIFIED

DEBRIS DISTRIBUTION AS A PARAMETER IN THE BLAST/FIRE INTERACTION

by John R. Rempel

Improvements in the calculation of over-the-ground transport of solid objects by air blast have been made so that the DIAL PACK results are satisfactorily simulated with constant parameters over the range of incident pressures 15 to 100 psi. These calculations have then been combined with computational techniques for predicting unreinforced masonry wall collapse to derive an outline scenario for blast impact on an actual building at two incident overpressures, 1 and 30 psi.

September 1981
96 pages

Contract No. EMW-C-0311
FEMA Work Unit 2564G